

Charles University in Prague
Faculty of Natural Science
Department of Analytical chemistry

**Analytical Characterization of the Surface Properties of Clay
Minerals**

—
A critical evaluation of the Cu-trien method for CEC determination

Thesis



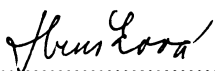
Prague 2008

Mgr. Michaela Hrušková

Declaration

I have prepared this Thesis independently, under the supervision by Prof. Ing. Karel Štulík, DrSc and RNDr. Tomáš Grygar, CSc. All the literature sources are properly cited. Neither the Thesis nor parts of it have been used to obtain the same or a different academic degree elsewhere.

In Prague..... 13 3 2008


.....
signature

List of Contents

1.	Preface	5
2.	Aims of the study.....	5
3.	Introduction	6
3.1.	Origin and interactions of clay minerals.....	6
3.2.	Definition of clay mineral.....	6
3.3.	Structure and properties of clay minerals.....	7
3.3.1.	Structure of layers.....	7
3.3.2.	Charge of layers.....	9
3.3.3.	Determination of charge	9
3.3.4.	Interlayer cations	13
3.4.	Classification of clay minerals	14
3.5.	Mixed-layered minerals.....	16
3.6.	Overview of clay minerals.....	16
3.7.	Use of clays and clay minerals	19
3.8.	Investigation of clayey materials.....	19
3.8.1.	Physical treatment of samples	19
3.8.2.	Chemical treatment of samples.....	20
3.8.3.	XRD analysis.....	21
3.8.3.1.	Quantitative analysis	27
3.8.4.	FTIR spectroscopy.....	37
3.8.4.1.	Infrared spectroscopy of clay minerals.....	39
3.8.5.	CEC determination	41
3.8.5.1.	Methods for CEC determination	42
3.8.5.2.	Cu ²⁺ -trien method.....	45
3.8.6.	Other methods for clay investigation	48
3.9.	Statistical methods, evaluation of results	51
3.9.1.	Data set characteristics	53
3.9.2.	Data distribution	55
3.9.3.	Statistic testing.....	57
4.	Experimental.....	63
4.1.	Samples.....	63
4.1.1.	Reference samples from Source Clays Repository.....	63
4.1.2.	Collected clays.....	65
4.2.	XRD analysis.....	66
4.2.1.	Equipment.....	66
4.2.2.	Specimen preparation	69
4.3.	FTIR spectroscopy.....	69
4.4.	CEC determination	69
4.4.1.	Copper trien method	70
4.4.2.	Ammonium acetate method.....	73
4.4.3.	Silver thiourea method.....	74
4.5.	Statistical methods, evaluation of results	75
5.	Results and Discussion.....	76
5.1.	Sample treatment	76
5.2.	Mineralogy of collected clays.....	77
5.2.1.	Characterization of bentonites	85

5.2.1.1.	X-ray diffraction.....	85
5.2.1.2.	FTIR spectroscopy.....	92
5.2.2.	Illite Füz sample characterization.....	95
5.2.3.	ME82 sample characterization	95
5.2.4.	Conclusion of collected clays characterization	99
5.3.	Homoionic Rokle samples characterization	100
5.4.	Cu-trien method.....	105
5.4.1.	Reference samples	105
5.4.2.	Homoionic DR samples.....	113
5.5.	Comparison of Cu-trien, ammonium acetate and AgTU method.....	122
5.6.	Application of Rietveld method	124
6.	Conclusions	128
7.	Literature	130
8.	Acknowledgements	141

1. Preface

In common life we pass clay minerals without noticing them. We should better say, we pass them without knowing what they are. Ages have passed and ochre is still a traditional pigment. Clay minerals appear in pottery, ceramics, cosmetic and pharmaceutical industry and are used in synthetic materials. They find use in metallurgy and in processing of other raw materials. They play an important role in agriculture and environmental protection (e.g., in radioactive waste disposal). Their application is evidently very wide and the demands of technologies and quality management lead us to evaluation of the quality of the clay raw materials.

Various new methods of analysis are tested and applied in order to gain information within short time, non-destructively¹ and at the lowest possible cost. The analytical methods selected must then be adapted to satisfy the requirements of geochemical analysis. Collaboration among various scientific disciplines is now necessary to solve the problems and to open new views of the world.

2. Aims of the study

The surface structure of clay materials and its properties are closely bound to the character of their inner structure, its chemical composition and crystallinity. The interactions of expandable clay minerals with their surroundings – exchange of cations and sorption of organic molecules – have been well known for a long time. They are best quantitatively described using the concept termed the Cation Exchange Capacity (CEC). The older methods for determination of CEC are time consuming and thus are not suitable for analysis of large sets of samples. New, simpler methods are being developed to rapidly obtain reliable results.

In 1997, Bergaya and Vayer reported a new, fast method for determination of CEC using the copper-II complex with polyamines.² The method was recognized and further developed by Meier and Kahr in 1999.³ The first evaluation of this Cu-trien procedure and its reliability, using a colorimetric detection of the complex in the supernatant, was performed in 2005 by Amman.⁴

Nevertheless, there are still some questions left unresolved:

- What is the reliability of the Cu-trien method when using atomic absorption/emission spectroscopy?
- How much the results differ between AAS/AES and colorimetry?
- Are the results affected by the composition of the stock solution, by the way of its addition and by the sample preparation procedure?
- Does the type of the interlayer cation influence the results?
- How much the results differ from those obtained by the classical NH_4^+HAc method?

This study is aimed at answering these questions, establishing the properties of the Cu-trien method, defining its limitations and evaluating its suitability for analyses of clay minerals.

3. Introduction

3.1. Origin and interactions of clay minerals

Clay minerals are formed by weathering of parent rocks under various conditions. Their particles can be formed in two ways as a consequence of hydrolysis:

- nucleation and growth
- recrystallization

The type of the parent rock and the intensity of weathering influence the structure of newly formed material. The structure is further influenced by outer factors, such as temperature and pressure. Clay minerals adapt their structures to the outside conditions and change their properties accordingly. This reconstitution is called diagenesis. The diagenesis usually creates several minerals - transitional zones of different mineral compositions (see, e.g., the description of zones in postmagmatic alteration, Kawano 1991⁵).

In general, the climatic dependence of mineral structure serves as an indicator of climate in the past (paleoclimatic record) and the clay minerals are used as paleo-thermometers. The diagenesis indicates the conditions during deposition of a material (burial diagenesis). For example, kaolinite and dickite and their transition minerals from the kaoline group have been used to work out the history of petroleum basins.⁶ Clay minerals may influence the formation of accompanying minerals.⁷ On the other hand, clay minerals are influenced by living organisms like plants, fungi or insects.⁸

3.2. Definition of clay mineral

Before presenting the structures of individual clay minerals, their general definition should be provided, based on the standardized structural terms:

- The plane, formed by atoms
- The sheet, consisting of linked tetrahedra or octahedra
- The layer, composed of sheets (1:1 or 2:1); layers may be separated by interlayer material (cations, hydrated cations, organic molecules, hydroxide octahedral groups and sheets)
- The unit structure, assembled of the layer and interlayer material

Note: The plane, sheet and layer refer to increasingly thicker arrangements.⁹

The term, clay mineral, refers to phyllosilicate minerals and to minerals which impart plasticity to clays and which harden upon drying or firing.¹⁰ Phyllosilicates contain continuous two-dimensional tetrahedral sheets of composition T_2O_5 (T = Si, Al, Be...) with tetrahedra linked by sharing three corners of each, and with the fourth corner pointing in any direction. The tetrahedral sheets are linked in the unit structure to octahedral sheets, or to groups of coordinated or individual cations. (Brindley & Pedro 1972, reported in Summary of Recommendations of the AIPEA Nomenclature Committee⁹)

The term, clay mineral, is often confused with the term, clay. According to AIPEA (Association internationale pour l'étude des argyles - International Association for the

study of clays), clays are defined as naturally occurring materials composed primarily of fine-grained minerals, which are generally plastic if sufficiently damp and which harden when dried or fired. They may contain associated phases that do not impart plasticity and organic matter.¹⁰ AIPEA differentiates the minerals present in the clays into the categories of clay minerals and accompanying minerals.¹¹ The criteria of the particle size and the surface area, as proposed by Moore¹² have not been found suitable for the mineral classification scheme.¹³

3.3. Structure and properties of clay minerals

It is clear from the definition by Brindley and Pedro that the structure consists of two basic sheets.

3.3.1. Structure of layers

A tetrahedral sheet is ideally formed by tetrahedra of oxygen atoms with silicon in the central position, connected through basal oxygens to form a sheet. The structure of a tetrahedral sheet is depicted in Fig. 3.1. In this arrangement, the sheet has no overall electric charge. In natural materials a non-equivalent substitution of silicon by Al^{3+} commonly occurs and other ions can also enter this position (Fe^{3+} , Ge^{4+}). The substitution by Fe^{3+} is less common. The remaining oxygen, which does not link tetrahedra, is called apical and it links tetrahedral sheets to octahedral ones.

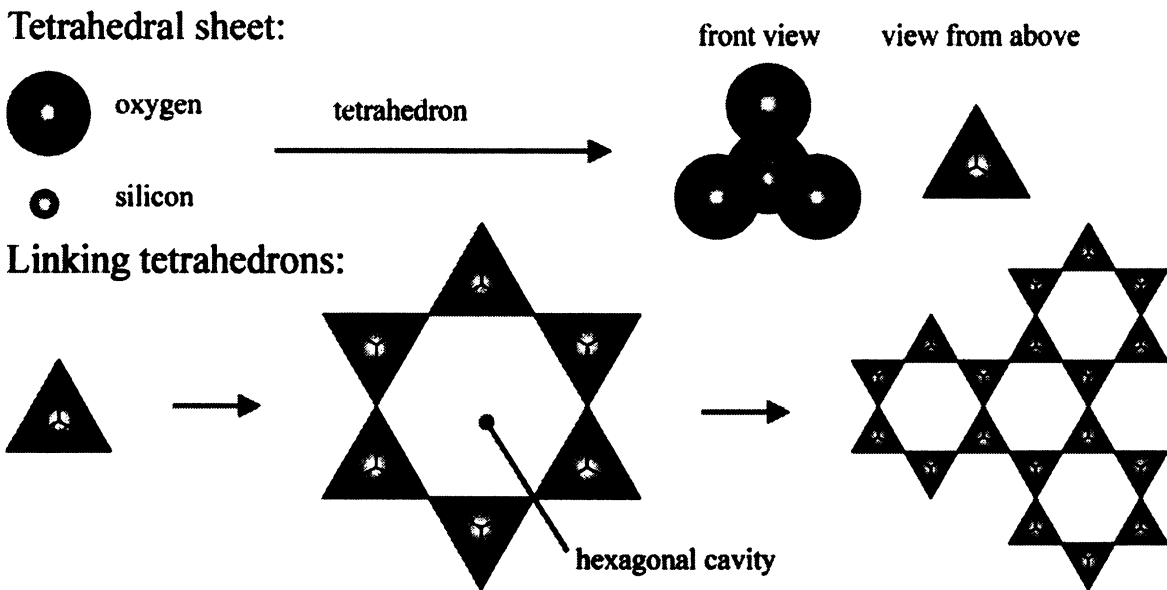


Fig. 3.1 - Structure of a tetrahedral sheet

An octahedral sheet is formed by octahedra where the apices are occupied by $-O$ and $-OH$ groups and the central position by Al^{3+} , Fe^{3+} , Fe^{2+} , Mg^{2+} or Mn^{2+} (other elements are also possible).¹¹ An octahedral sheet can be formed in two ways. When all the positions are occupied by a divalent cation, such as Mg^{2+} , the sheet is called trioctahedral. When the two thirds of the positions are occupied by a trivalent cation,

such as Al^{3+} , the sheet is called dioctahedral. The structure of an octahedral sheet can be seen in Fig. 3.2.

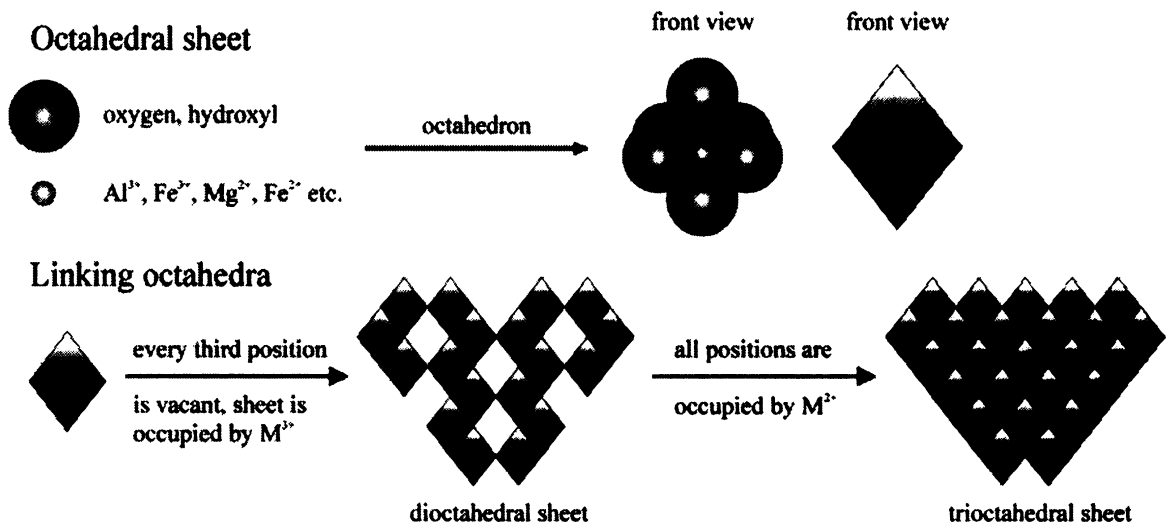


Fig. 3.2 - Structure of an octahedral sheet

A layer of a clay mineral is formed by connecting these two sheets. When an octahedral sheet is connected with only one tetrahedral sheet, then the 1:1 minerals are formed. When the octahedral sheet is packed in-between two tetrahedral sheets, the 1:2 layer is formed. The sheet linking is shown in Fig. 3.3

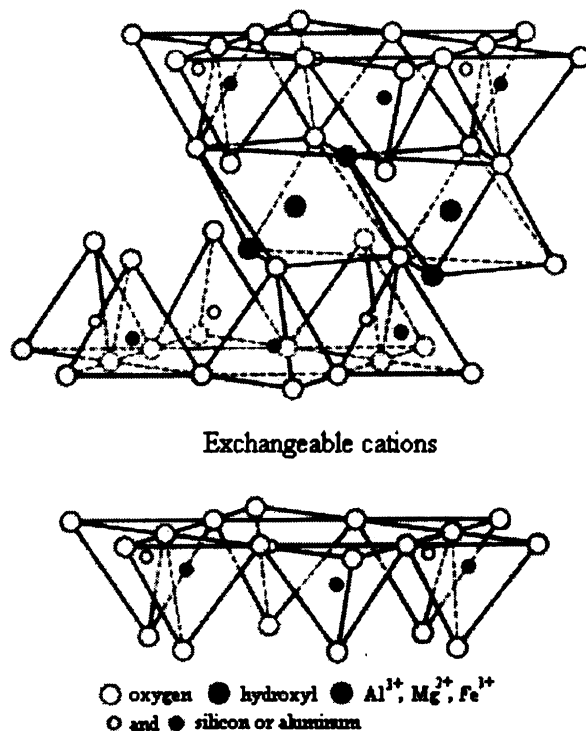


Fig. 3.3 - Formation of a layer, linking of sheets

3.3.2. Charge of layers

Permanent charge

The structure mentioned above describes an ideal state when no non-equivalent substitution appears. This case is, in fact, very rare and substitution of a higher-charged cation by a lower-charged one leads to a negative overall charge on the structure. The permanent charges thus result from isomorphic substitutions and defects in the octahedral and tetrahedral sheets. The most common non-equivalent substitutions involve:

- substitution of Si^{4+} by Al^{3+} in tetrahedral sheets and
- substitution of Al^{3+} by Mg^{2+} , Fe^{3+} by Fe^{2+} etc in octahedral sheets.

The charge is then localized on the appropriate substituted sheet. Substitutions on both the sheets are also common. The extent of substitution is not limited. Structures with one prevailing octahedral cation possess mineralogical names. Minerals with structures in between two named structures are commonly named according to the more similar structure. The charge imbalance has to be neutralized. It is attained by inserting interlayer cations in-between layers. The strength of the interaction between the cation and the layer depends on the charge localization and the type of the compensating cation. Under certain conditions, the permanent charge can be neutralized by inserting a small cation into the structure.

Variable charge

Another part of the total charge on the layer is called variable charge. This charge originates from defects of the structure (the charge on the crystal edges) and the pH which causes protonation and deprotonation of outer $-\text{O}$ and $-\text{OH}$ groups.¹⁴

The total charge

The sum of the permanent charge (dependent on the non-equivalent substitution) and the variable charge (dependent on defects and the pH) is called total charge. For smectites, the variable charge varies from 10 to 30% of the total cation exchange ability.¹⁵ The capacity of mineral for retaining cations, the cation exchange capacity (CEC), then results from the attractive forces generated by these charges located on the structure.

3.3.3. Determination of charge

The homogeneous distribution of layer charge over the crystal is only an ideal assumption and, concerning montmorillonites, the charge density varies from layer to layer. The following methods are used to determine the layer charge:

Calculation of mineral structural formulae from the results of chemical analysis

In this way it is difficult to obtain reliable data. The calculation depends on the following assumptions:

- the chemical analysis is performed on a sample of a single mineral
- the chemical analysis is reliable

- silicon cations exist only in tetrahedral sheets, aluminium cations occupy the rest of the tetrahedral sites, if Si and Al cations are insufficient to fill all the tetrahedral sites, the remaining ones are occupied by iron cations
- other cations are assigned to octahedral sheets and/or to the interlayer space
- at least one type of site (tetrahedral or octahedral) is fully occupied

The calculation can be performed in two ways. The first one depends on the assumption that the O network is perfect and fully compensated by central atoms. The other one assumes that the central atoms occupy all of the tetrahedral and octahedral positions in the unit cell. The structural formulae method gives the total charge of the layers. It is not significantly influenced by a 10% layer silicate admixture. The presence of free oxides causes problems. The formulae can also be derived from acid dissolution (ADT) in combination with spectroscopic methods. The ADT is not suitable for mixtures of layered silicates, non swelling dioctahedral layered silicates and mixed-layered minerals.¹⁶

The alkylammonium method

The method is based on intracrystalline reactions with primary n-alkylammonium salts (C: 6, 7, 8...18). The exchange is quantitative and may require a pre-treatment of samples, e.g., the removal of organic matter and free oxides. According to the interlayer cation density and the alkylammonium chain length, ions arrange into different structures (Fig. 3.4).

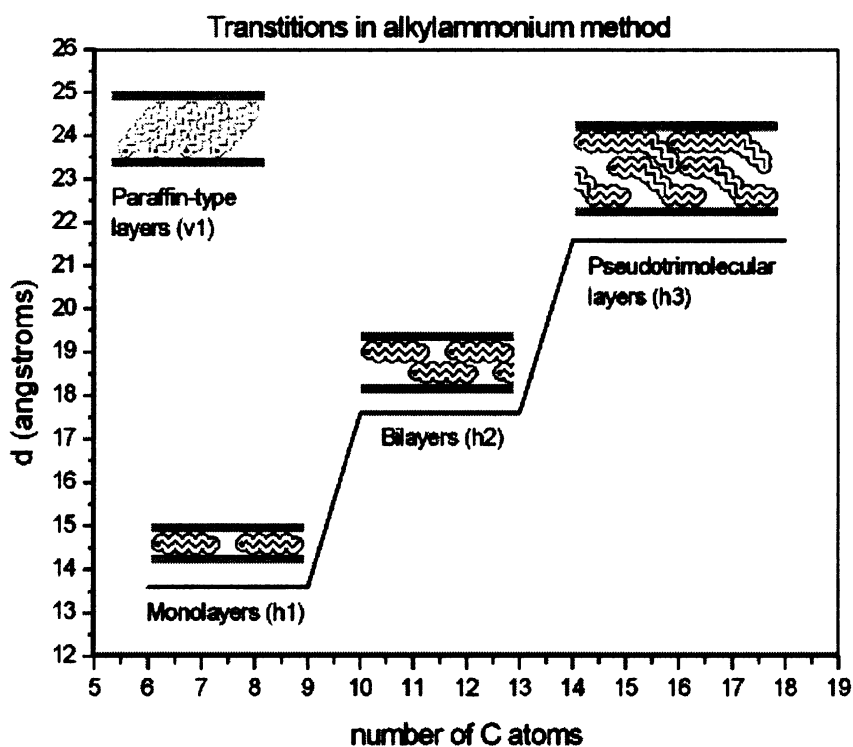


Fig. 3.4 - Increase in the basal spacing in relation to the arrangement of alkylammonium ions in the interlayer space

The structures with flat chains (h1 – h3) are formed when the cation density is smaller than 0.5. For most smectites, the transition from h1 to h2 is not sharp and mixtures of h1

and h2 layers are present in the samples. The start of the transition is related to the highest and the end to the lowest interlayer cation density. The h2 to h3 transition is related to the highest surface charge density of the silicate layer. The paraffin-type is characteristic for highly charged vermiculites, with a layer charge of at least 0.75 eq/(Si,Al)₄O₁₀, where the tilt angle is related to the layer charge.¹⁷ The position of 001 diffraction is not influenced by the solvent used during the intercalation.¹⁸ The correction for the Lorentz and polarization factors, together with curve-fitting, significantly improves the reliability of the determination.¹⁹ The use of an internal (Ag-behenate) standard also allows for a correction of 001 diffraction at low angles by interpolation.²⁰ This method can determine the layer charge of several 2:1 clay minerals in a mixture and the charge distribution can be calculated from the basal spacing in the transition range.¹⁵

Note: The comparison of the structural formulae and the alkylammonium methods concludes that the former estimates the total charge and the latter the permanent charge. Tetrahedral and octahedral charges are highly sensitive to contamination and wrong assumptions concerning the structural formulae. The alkylammonium method exhibits uncertainties about the particle size effect; the packing densities of interlayer alkylammonium cations and the configuration of the structure in the mono-bilayer transition (see Fig. 3.5, the standard interpretation operates with a mixture of monolayers and bilayers, for an island-like structure, where the interlayer volume is largely filled up, the permanent charge is underestimated). A comparison of the results shows substantial underestimating/overestimating of high/low-charged smectites by the alkylammonium method.^{21,22}

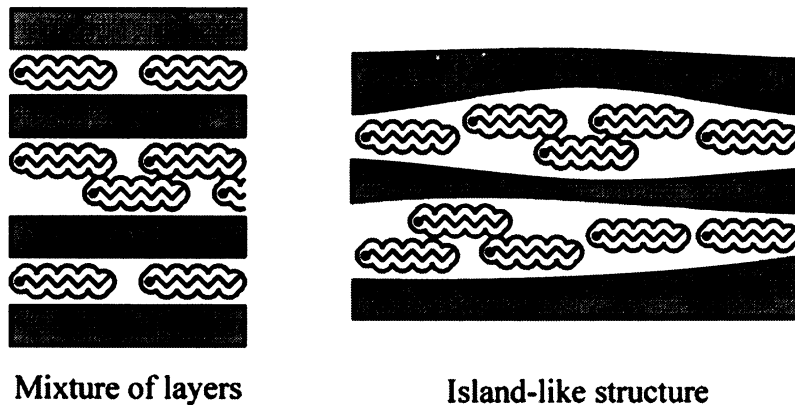


Fig. 3.5 - Possible configurations of an intercalated smectite

Observation of intracrystalline reactions

The K⁺ saturated ethylene-glycol solvated samples can be used to estimate the layer charge and the charge distribution by fitting the XRD oriented sample pattern. The pattern is modelled as a combination of 3 different structures with charge -0.39 (001 basal spacing 17.1 Å), -0.42 (001 b. spacing 13.5 Å) and -0.53 for low-charge and -0.76 for high-charge (001 b. spacing 9.98 Å).²³ The tetrahedral and octahedral charge can be distinguished by Li⁺ fixation.¹⁴

Dye aggregation

The organic dyes have a high affinity to smectites. They can adsorb in a higher extent than required by CEC (cation-exchange capacity) and form aggregates due to non-coulombic interactions.^{24,25} Methylene blue (MB) was found to be a probe molecule reacting to the surface properties by aggregation even with very small loadings. Monomers, dimers and aggregates can be observed in the VIS spectra (Fig.3.6, Table 3.1).²⁶ The aggregation process is controlled by the layer charge. Therefore, the amount of each species qualitatively reflects the layer charge distribution.²⁷ The MB aggregation is also significantly influenced by the tetrahedral/octahedral charge ratio²⁸ and cation present in the interlayer space.²⁹ Other dyes, forming aggregates with different optical properties than isolated dye cation, can be successfully applied in the layer charge investigation.^{30,31,32}

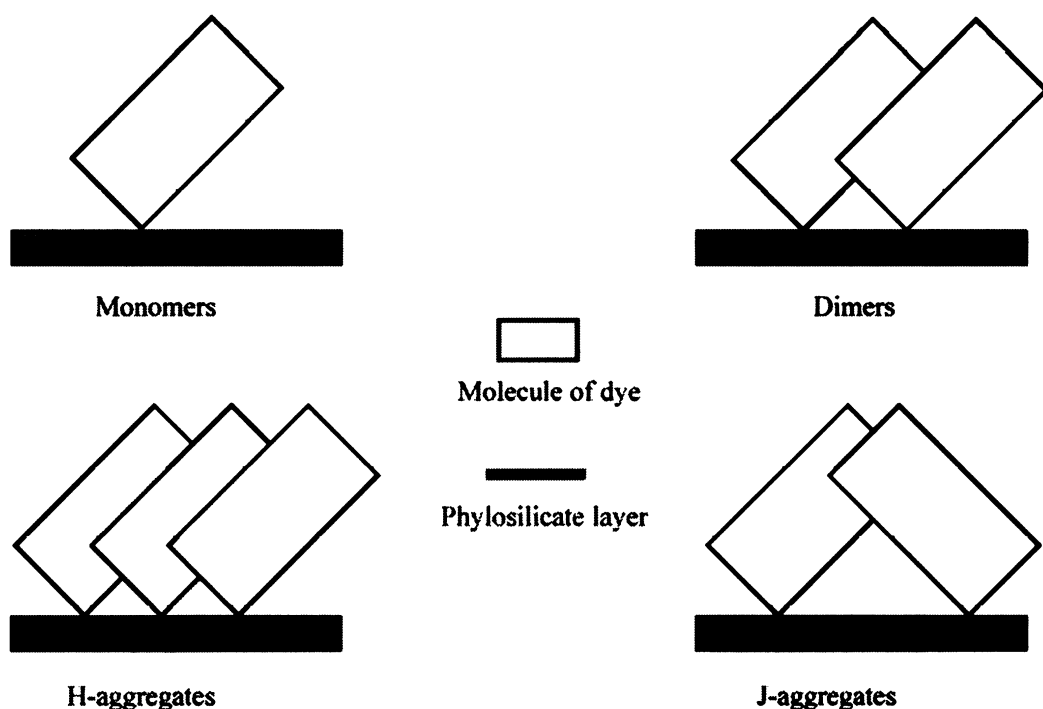


Fig. 3.6 - Possible arrangements of a dye molecule on the phyllosilicate layer

Table 3.1 - Positions of the absorption band according to the dye aggregate

Species	Absorption band (λ , nm)
H-aggregate	570-590
H-dimer	600
Monomer	650-675
J-aggregate, acidified	770

CEC (cation-exchange capacity) determination

It displays the total charge under the given conditions (the temperature, pH and the index cation chosen for displacement of the natural interlayer cations). The interlayer

cations and CEC are discussed below. The overview of the methods is given in Section 3.8.5.

3.3.4. Interlayer cations

Interlayer cations compensate for the non-equivalent substitutions and the pH dependent variable charge. Their sum is called cation-exchange capacity (CEC) and it represents the total charge present in the structure. (Note: However, there is no linear correlation of CEC with the layer charge determined from structural formulae calculations. A better correlation was found compared with layer charge determined by alkylammonium method. CEC values recalculated from layer charge obtained by this method are 20 - 30% lower than obtained experimentally^{33,34})

The type of interlayer cation significantly influences the properties of a clay mineral.³⁵ The interlayer cation rules the hydration of the interlayer space. Hydration runs via interstratified hydrated states and the opening of layers occurs at a defined relative pressure in relation to the hydration energy of the interlayer cation. The Li- and Na-montmorillonites show limitless "osmotic" swelling. K- and Rb-montmorillonite tend to aggregate layers and Cs-montmorillonite remain in quasi-crystals during the whole process of water adsorption. Hydration of larger cations involves lower number of water molecules per cation and thus a lower content of water in the interlayer space.³⁶ The Ca- and Mg- montmorillonites are characteristic by the presence of two water layers in the interlayer space over an extensive range of relative humidity. Dehydration is also driven by the interlayer cation. The larger the cation, the lower is its solvation energy and its tendency to retain water molecules.³⁷

The interlayer cations can be extracted from the clay mineral by another cation, which is called index cations. The experimental data indicate that many exchange reactions are significantly irreversible and display hysteresis. There is no hysteresis during homovalent exchanges of divalent cations. However, when the exchange reaction involves ions of different valences, hysteresis occurs and can be explained as follows:

- The swelling hysteresis concerns the content of water in the interlayer space. The K^+ , NH_4^+ and Cs^+ ions expand the interlayer space during the swelling to 14-15 Å, divalent cations to 19 Å. The Na^+ and Li^+ expand the interlayer space limitlessly. Hysteresis may be expected whenever there is a change in the interlayer space during the exchange.
- The other source of hysteresis comes from the formation of quasi-crystals. Much of the apparent irreversibility is a consequence of imperfection of the dispersion (flocculation). This process is influenced by the nature of the adsorbed ion, the electrolyte concentration, and the type of the clay and its concentration. The air drying of a smectite suspension also increases the average size of quasi-crystals.³⁸ The prediction of backward scanning curves is not possible due this feature.³⁹

Note: Hysteresis has also been found during the water sorption/desorption from the vapor and liquid phases on Na-montmorillonite and its desorption. The differences in the relative humidity and the degree of order in the stacking of the clay layer have been

observed and explained by differences in the state of the material before hydration and after dehydration. During hydration, the interlayer cation is hydrated at the appropriate vapour pressure; it is extracted from the cavity, leading to relaxation of the mineral structure and liberation of the strain energy. Hydration increases the order in the layer. Desorption of water molecules proceeds in the opposite direction but the degree of order is not entirely degraded.⁴⁰

Exchange processes occurring in the vicinity of a single clay particle can be described by the Stern-Gouy double-layer model. The interlayer cations are held by electrostatic attraction in hydrated form next to the negatively charged clay particle surface (a homogeneous charge distribution is assumed). The attraction force is balanced with outward molecular diffusion. This model has been successfully applied to modeling and confirmed experimentally.⁴¹ The exchange reactions can also be characterized in terms of the free energies (ΔG°_{ex}), the cation selectivity and fixation resulting from interplay of the attractive forces of the hydration shell and the clay surface. The cation selectivity is a function of the layer charge (the distribution of cations between high- and low-charge interlayers shows cation segregation). The hydration energy and the water-molecule shell are important for the resultant molarity of the interlayer space. The cation size is important for approaching the site of negative charge.⁴² The selectivity has also been predicted from the Hard and Soft Acid and Base (HSAB) model where a hard acid (e.g., Li^+ , Na^+ , K^+ , Rb^+ or Cs^+) prefers coordination with a hard base (e.g. OH^- , H_2O) and a soft acid (e.g., Ag^+ , Tl^+) with a soft base (e.g. the thiol group). The charge location also influences the surface basicity. Coordination of water to O groups is stronger when the charge is localized in the tetrahedral sheet than when it is present in the octahedral sheet. Under a constant temperature, pressure and ionic strength, the alkali cation selectivity can be quantitatively predicted from the tetrahedral and octahedral charges of the clay mineral and the absolute electronegativity and softness of the exchangeable cation.⁴³ The adsorption of an interlayer cation is complicated when the pH varies and complexes are formed with other ligands present in the suspension.^{44,45}

It follows from these considerations that the cation exchange capacity must be determined using a homovalent ion exchange reaction with a cation whose affinity to the clay mineral surface is higher than that of the cations originally present in the mineral.

3.4. Classification of clay minerals

Clay minerals are classified according to their structure and charge present on the layer.

1:1 clay minerals

The 1:1 minerals possess a small or no charge. The imbalance is compensated by substitution in an accompanying sheet. The 1:1 minerals are further classified in terms of the character of the octahedral sheet. The kaolin group is formed by dioctahedral minerals ($\text{Al}_4\text{Si}_4\text{O}_{10}(\text{OH})_8$) and the group of serpentine is formed by trioctahedral minerals ($\text{Mg}_6\text{Si}_4\text{O}_{10}(\text{OH})_8$). Examples of these minerals are listed in Table 3.4 (pp. 17-18).

2:1 clay minerals

The layer charge is important for classification of 2:1 minerals. The charge is expressed per the formula unit: $T_4O_{10}(OH)_2$ and equals the sum of the tetrahedral and octahedral sheet charges. The groups of 2:1 minerals are given in Tables 3.2, 3.3 and 3.4 (pp. 17-18).

Table 3.2 - Classification of 2:1 clay minerals into groups according to the layer charge

Group	Charge per formula unit (e)
Talc and phyllosilicate	0
Smectite	0.2-0.6
Vermiculite	0.6 – 0.9
Mica (illite and glauconite)	0.9 – 1.0
True mica*	1.0

* These are present in macro forms (not in the clay size fraction) and serve as structural and chemical models for 2:1 minerals

It is impossible to distinguish between a medium charged smectite and vermiculite (layer charge per half unit cell is 0.6) and the samples are suggested to be called smectite-vermiculite intermediates.⁴⁶ The difference between hectorite (tetrahedral charge) and montmorillonite (octahedral charge) is also problematic; application of a test distinguishing the charge location (see the Green-Kelly test, Section 3.8.3) is doubtful.⁴⁷

Table 3.3 - Detailed classification of 2:1 clay minerals according to the layer charge¹⁵

Mineral	Layer charge per half unit cell $[O_{10}(OH)_2]$	Interlayer CEC ($cmol_c kg^{-1}$)
Hectorite (smectite)	0.20-0.25	50-65
Montmorillonite (smectite)	0.25-0.40	70-110
Vermiculite	0.50-0.80	130-210
Illite (hydromica)	0.60-0.90	160-230
Biotite (mica)	~1.00	~220
Muscovite (mica)	~1.00	~260

Chlorites

These minerals are not classified according to the layer charge. These 2:1 minerals differ in the occupation of interlayer space. The compensating element is an octahedral net with a positive charge expressed by the formula: $[(R^{2+}, R^{3+})_3(OH)_6]^+$. Chlorites are classified according to the type of octahedral sheets. The majority of chlorites contain trioctahedral sheet in both layer and interlayer sheet. There is only one mineral with both

dioctahedral sheets (donbassite). Chlorites with dioctahedral layer and trioctahedral interlayer sheet are known, however, a structure with a trioctahedral layer and a dioctahedral interlayer sheet has never been observed.

Sepiolite and palygorskite

The last group of clay minerals is formed by sepiolite and palygorskite. The structures of these minerals differ from the others. Tetrahedral sheets are periodically inversed, the connected octahedral sheet appears alternately above and below the tetrahedral sheet plane and the adjacent modulated (periodically inversed) tetrahedral sheet is connected. The layers formed in this manner produce net of channels in the structure.

3.5. Mixed-layered minerals

Physical mixtures of various clay minerals occur most often. Deposits of pure (one-phase) clay mineral are very rare. Admixtures of minerals other than clay minerals, e.g., quartz, feldspars, rutile (anatase), siderite, calcite, dolomite, magnesite, iron oxides, gypsum, gibbsite etc. are common. Mixed-layered minerals are not physical mixtures of layered silicates but intergrown layers of different clay minerals forming crystallites. The layers may be stacked in a random, partially regular or a regular manner. The degree of ordering is described by R – *Reichweite* which represents the probability of finding layer A after layer B in the structure. If the stacking is random, then $R = 0$, when it is regular, then $R = 1$. The values $R = 2$ or 3 can be encountered when ordering is tracked in relation to one layer (e.g. $R = 2$: ABBABBABB..., $R = 3$: ABBBABBABBB...).

Regularly stacked layers with $R = 1$ form superstructures with characteristic sets of 00l basal reflection in XRD powder diffractograms. A mixed-layered mineral has the privilege of its own name only when it fulfills perfect interstratification in XRD patterns.⁴⁸ These minerals involve, e.g.:

- rectorite 1:1 paragonite:smectite
- tosudite 1:1 dioctahedral chlorite:smectite
- aliettite 1:1 talc:saponite

The irregularly stratified minerals are important markers of their environment during their formation or burial period. The mixed-layered mineral formed from layers of illite and smectite – commonly written I/S – is reported as a paleothermometer, because of its temperature sensitivity.

3.6. Overview of clay minerals

An overview of clay minerals can be found in Table 3.4 (created according to Bailey 1980⁹ and corrected as in Guggenheim et al. 1997⁴⁹). Some minerals can appear in more than one space group, depending on its polytype (the character of layer stacking disorder).

Table 3.4 - overview of clay minerals

Structure	Charge per (T ₄ O ₁₀ (OH) ₂)	Group	Subgroup	Octahedral sheet	Mineral species (e.g.)	Charged sheet	Space group	Colour
1:1	no	kaolin-serpentine	kaolin	dioctahedral	kaolinite (Al ³⁺)		P1	white
			serpentine	trioctahedral	berthierine (Fe ²⁺) odinite (Fe ³⁺ , Al ³⁺ , Mg ²⁺ , Fe ²⁺)		Cc Cm Cm	white, yellowish, redish, greenish green green
2:1	no	phyrophyllite-talc	pyrophyllite	dioctahedral	phyrophyllite (Al ³⁺)		P1(-)	brown, gray
			talc	trioctahedral	talc (Mg ²⁺)		C2/c C2/m C2/m	gray/silver white green
0.2 - 0.6		smectite	dioctahedral smectite	dioctahedral	beidellite (Al ³⁺) nontronite (Fe ³⁺) montmorillonite (Al ³⁺ , Mg ²⁺)	T T O	C2/m C2/m C2/m	white green white, yellow, greenish, brownish
			trioctahedral smectite	trioctahedral	saponite (Mg ²⁺ /Fe ²⁺) hectorite (Mg ²⁺ /Li ⁺)	T and O O	C2/m C2/m	white, yellowish, redish, greenish white
0.6 - 0.9		vermiculite	dioctahedral vermiculite	dioctahedral	microscopic vermiculite		C2/m	colourless, green, gray, yellow
			trioctahedral vermiculite	trioctahedral	macroscopic and microscopic vermiculite		C2/m	colourless, green, gray, yellow
0.9 - 1.0		illite (hydromica)	dioctahedral mica	dioctahedral	illite (Al ³⁺ , Mg ²⁺ , Fe ²⁺) glauconite (Fe ³⁺ , Al ³⁺ , Mg ²⁺)	T and O T and O	C2/m C2/m	white blue green, green
			trioctahedral mica	trioctahedral	muscovite (Al ³⁺ , Fe ³⁺ , interlayer c.: K ⁺) paragonite (Al ³⁺ , Fe ³⁺ , interlayer c.: Na ⁺)	O O	C2/m C2/c	white white, yellow

			trioctahedral	trioctahedral	biotite (Fe ²⁺ , Mg ²⁺)	T	C2/m	dark brown, yellow, white
		trioctahedral mica			phlogopite (Mg ²⁺)	T	C2/m	brown, gray, yellow
					annite (Fe ²⁺)	T	C2/m	reddish brown, black
		dioctahedral	dioctahedral (both)		donbassite (Al ³⁺ , int.l.Al ³⁺)		C2/m	white, yellowish, greenish
		di-trioctahedral	dioctahedral sheet, trioctahedral interlayer sheet		cookeite (Al ³⁺ /Mg ²⁺)		P2 ₁ /a	white, green, brown
	variable				sudoite (Al ³⁺ /Li ⁺)		C2/m	white
					clinochlore (Mg ²⁺ /Fe ²⁺)		C2/m	green, white
					chamosite (Fe ²⁺ /Mg ²⁺ /Fe ³⁺)		C2/m	gray, brown, green
					nimite (Ni ²⁺ /Mg ²⁺ /Fe ²⁺)		C2/m	yellow green
					pennantite (Mn ²⁺ /Al ³⁺)		C2/m	orange red, reddish brown
	variable	sepiolite	trioctahedral		sepiolite (Mg ²⁺)		Pnan	white, gray
		palygorskite	trioctahedral		palygorskite (Mg ²⁺ /Al ³⁺)		P2/a	white, gray

T – tetrahedral

O – octahedral

3.7. Use of clays and clay minerals

The clay minerals are widely used in building and foundry industry, in the production of ceramic, cosmetic, pharmaceutical, rubber and plastic materials, in agriculture (e.g., influencing the mobility of herbicides^{50,51}) directed toward medical applications, in environmental protection, etc. The applications are lucidly summarized by Konta.⁵²

The environmental application has recently been extensively investigated. The clay minerals are used as such or are chemically modified. Sorption of heavy metals on various clay minerals has been studied. The predominant sorption process on bentonite is cation exchange. Organic matter present in the clay causes various complexation reactions.⁵³ Chemical modification enhances the sorption, e.g., acid activation increasing porosity.⁵⁴ Modification of the interlayer space opens new possibilities. Pillaring of the interlayer space by poly(oxo zirconium) or tetrabutyl-ammonium did not bring an improvement in the Cu^{2+} sorption⁵⁵ but enhanced sorption of Zn^{2+} through surface complexation (poly(oxo zirconium) modification). The high affinity to Zn^{2+} is also exhibited by Al-pillared bentonites.⁵⁶ The mobility of heavy metals in bentonites is also governed by the pH and the nature of the organic chelating ligands present.^{57,58} The sorption processes have successfully been modelled using computing techniques.⁵⁹

One of the consequent logical applications is the use of clays in radioactive waste repositories. The liquid low level radioactive waste is immobilized by cementation where kaolin enhances immobilization.⁶⁰ The topic of bentonite barriers in nuclear waste deposits is widely reviewed by Madsen⁶¹ with respect to physico-chemical factors influencing the barrier. Further factors have also been investigated, e.g., the influence of radiation on bentonite⁶², evolution of gas phase and formation of cracks and bubbles in the barrier⁶³, or interactions between the host rock and bentonite⁶⁴.

A new widely investigated area of clay mineral application is polymer/layered silicate nanocomposites.⁶⁵ The topic of biodegradable nanocomposites is reviewed well by Okamoto.⁶⁶

3.8. Investigation of clayey materials

3.8.1. Physical treatment of samples

- Disaggregating sample: milling is the most common way of disaggregating samples. Care must be taken during the milling not to break the sample, as demonstrated on the intensity of 001 diffraction of the XRD pattern. A 6 min. milling causes a significant diminishing of diffraction, cation-exchange capacity and specific surface area.⁶⁷ The time of milling should not exceed 10 min.⁶⁸ The gentle manual disaggregation by impact in mortar is preferred.⁶
- Size separation: It is performed by sedimentation of a salt-free sample or after a chemical removal of admixtures (see below). The sedimentation rate in relation to the particle size is described by the Stokes law (formulated for spherical particles), see Eqs. 3.1 and 3.2.

$$V_T = g \cdot (d_p - d_l) \cdot D^2 / 18\eta \quad (3.1)$$

V_T – terminal velocity
 g – force of gravity
 d_p – particle density
 d_l – liquid density
 D – particle diameter
 η – viscosity of liquid

$$t = 18 \cdot \eta \cdot h / g \cdot (d_p - d_l) \cdot D^2 \quad (3.2)$$

t – time (s)
 h – the particle trajectory (cm)

The settling force may be increased by centrifugation, thus significantly shortening the time of clay-fraction preparation. For typical conditions of centrifugation see Table 3.5. The separation may also be based on the shape of the particles. Weiszbürg et. al had separated quartz (3D grains) from 2D platy minerals by centrifugation in a high-viscosity medium.⁶⁹

Table 3.5 - Examples of the centrifugation conditions for particle size separation⁶

Particle diameter (μm)	Specific gravity of particles	Centrifuge speed (RPM)	Time (min.)
5	2.65	300	3.3
2	2.65	750	3.3
0.2	2.50	2400	35.4

data for 20 °C, 15 cm distance from centrifuge axis to meniscus, 10 cm suspension depth, 1 cm of sediment on the cuvette bottom

3.8.2. Chemical treatment of samples

Chemical sample pretreatment is only performed when necessary, taking care to avoid significant changes in the sample.

- Carbonate removal: The carbonates commonly function as buffers in samples.⁷⁰ The dissolution rates are slightly affected by the CO₂ pressure and salinity⁷¹, but they do not depend on the sample crystallinity or origin.^{72,73} Carbonates are removed using sodium acetate-acetic acid solution buffers at pH 5. Heating is necessary to remove dolomite. Other way of removal is use of 0.3 M solution (or a lower concentration) of acetic acid applied directly to the sample when carbonate itself functions as the buffer.
- Sulfate removal: The dissolution of gypsum in water follows nonlinear dissolution kinetics when the transport constant of molecular diffusion is similar to the rate constant of dissolution.⁷⁴ The dissolution is mainly controlled by the water flow velocity.⁷⁵ Gypsum or anhydrite is removed from clay samples according to Bodine and Fernald⁷⁶ by dissolution in 0.2 M solution of sodium salt of ethylenediaminetetraacetic acid (EDTA) with a pH of 11, adjusted by sodium hydroxide. The supernatant is removed until the reaction of sulfates with a 0.1 M BaCl₂ solution is negative.

- Iron oxides removal: It is performed only when absolutely necessary. The dithionite-citrate-bicarbonate method (DCB) designed by Mehra and Jackson⁷⁷ is commonly used when the sample is dispersed in a citrate-bicarbonate buffer and solid Na-dithionite powder is added. The reaction is carried out at 70 °C. The application causes reconstitution of the octahedral sheet of nontronites forming supercells, trioctahedral Fe²⁺ domains and a loss of hydroxyls.^{78,79} The IR spectrum is significantly changed, re-oxidation is incomplete⁸⁰, magnetic⁸¹ and other properties are also changed. Other methods with different reduction extent have been developed (using hydrazine, sodium sulfide, sodium hydrosulfide or benzidine, etc., as the reduction agents).⁸² The reduction of iron oxides also affects mixed-layered clay minerals and chlorites.
- Organic matter removal: It is performed to avoid its influence on XRD patterns, leading to broadening of X-ray diffractions because of intercalation of smectites and an increase in the background⁸³ what complicates identification of clay minerals. The original procedure proposed by Jackson and using hydrogen peroxide was replaced by sodium hypochlorite agent⁸⁴ and recently by buffered solution of sodium peroxodisulphate.⁸⁵
- Amorphous inorganic material removal: These admixtures generate errors mainly in the establishment of the chemical formulae. Digestion with dilute Na₂CO₃ is used and heating is performed only during the last digestion step.⁸⁶ Note: This procedure has also been recommended as a step preceding the removal of iron oxides, to free the iron oxides from amorphous coating of the sample grains.⁸⁷
- Preparation of homoionic forms: This is readily performed by soaking the sample with a 1M solution of the chloride of a suitable monovalent cation (e.g.: NaCl, LiCl) or a 0.1 M solution of a divalent cation chloride (e.g.: CaCl₂, MgCl₂). The equilibrium of the cation between the solution and the solid phase must be re-established on changing the supernatant. The process is finished by washing out or by dialysis using distilled water or its mixture with ethanol.⁶

3.8.3. XRD analysis

X-ray diffraction (XRD) is the most common method in study of clay-sized minerals. The XRD method is based on scattering of X-rays on the spatial structure of crystals. The X-ray wavelength and the crystal cell dimensions are approximately the same (10⁻¹⁰ m). This process can be understood as a reflection on the set of atomic planes. In 1912 W.L. Bragg worked out Bragg's law which sums up the condition for constructive interference of diffracted beams. The situation is described on Fig. 3.7. The constructive interference is reached when beam 1 meets beam 2 after diffraction in phase. The additional distance of beam 2 than has to equal the product of a whole number and the wavelength.

We can formulate the condition as: $\Delta l = |CB| + |BD| = n \cdot \lambda$ (3.3)

When inter-planar distance is: $d = |AB|$ (3.4)

The situation in ABC triangle is described by:
$$\sin \theta = \frac{|CB|}{|AB|} = \frac{\Delta l}{2 \cdot d} \quad (3.5)$$

The additional distance is:
$$\Delta l = 2 \cdot d \cdot \sin \Theta = n \cdot \lambda \quad (3.6)$$

which is the diffraction condition and Bragg's law.

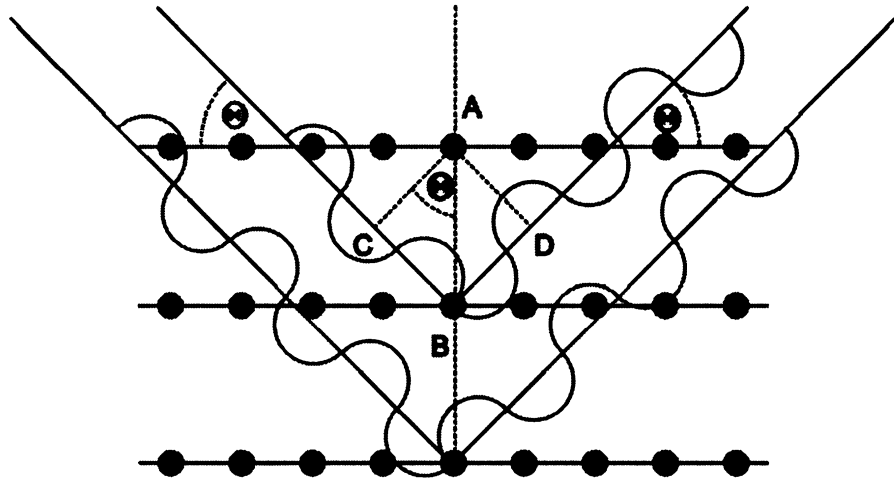


Fig. 3.7 - Reflection on the set of atomic planes

Von Laue characterized the diffraction conditions in the 3D space and the approximation has further been extended. Every atom has a different number of electrons where scattering of X-rays takes place. The ability to scatter X-rays is called the scattering efficiency of atom, f (it depends on the number of electron in an electron shell). The scattering related to the arrangement of atoms in the unit cell, its scattering efficiency, is called the structure factor, F . The kinematic theory describes diffraction using these properties of atoms and unit cells. The theory of diffraction has further developed as a dynamic theory. In reality, the diffraction width reaches an interval of $\approx 2\theta$ values and not only a single angle position. This is caused by the alignment of device, imperfections in the crystal order, the size of diffracting particles, mixed layering or interstratifications of different kinds of clay minerals which form a crystallite. As the consequence of their structure arrangement, clay minerals have plate-like morphology and perfect 001 cleavage.

The source of X-ray radiation is an X-ray tube: the tungsten filament is the source of electrons which are accelerated by voltage (15 – 60 kV) and fly through vacuum to strike a metal target. Continuous radiation is formed by deceleration these electrons in the vicinity of atoms of the target (repulsion by electron shells). The short-wavelength limit is a reciprocal function of the voltage and is independent of the type of the target material. Characteristic radiation is formed after impact of an accelerated electron on the target atom. The accelerated electron releases an inner shell electron and the vacancy is filled up by an electron dropping from a higher shell. This drop is coupled with simultaneous emission of excess energy in the form of radiation (Fig. 3.8, notation of spectral lines included).⁸⁸ Characteristic radiation is dependent on the electron shell

arrangement and thus on the type of atom. To produce the characteristic radiation, the impact electron must have a sufficient energy (voltages of the order of kV). About 98% of the whole energy is changed to heat and only a small part appears as X-ray photons, hence the X-ray tube system must be cooled. The use of a monochromatic beam simplifies the analysis of crystalline materials. Single-crystal monochromators or β -filters are used (the filter material is one or two atomic numbers lower element than the target material and filters $K\beta$ characteristic radiation). The $K\alpha_1$ and $K\alpha_2$ are not separable and the resultant radiation is a 1:1 mixture of these lines. It is called $K\alpha$ and used for calculations.

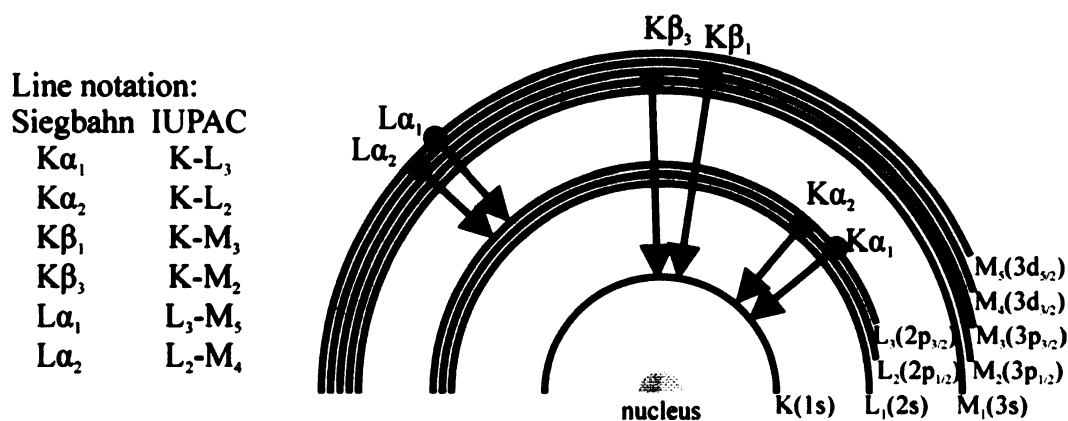


Fig. 3.8 - The characteristic radiation evolution and line notation

The radiation is collimated by Soller, divergence, receiving and anti-scatter slits. The signal is then detected using film, proportional, Geiger or scintillation counters and solid-state semiconductor detectors.

Specimen preparation

The specimens are prepared with respect to the aim of study. Random oriented specimens are used for mineralogical and semi-quantitative characterization. Their investigation also enables the observing of 060 diffraction describing the octahedral sheet constitution. There are several techniques for the preparation of random oriented specimens:

- Front loading: The material is loaded to the sample holder directly. The sample cavity is filled to the height of the sample holder. An access of the sample must be removed. The sample surface can further be roughened with coarse paper.
- Back loading: The material is loaded to the ring of the sample holder to the height of the ring. The powder is lightly pressed and the sample access is removed. The bottom platform is clipped to the ring and the specimen is turned up.
- Side loading: The procedure requires sample holder with a channel in the side wall, glass slide (frosted glass or glass rough on a microscopic scale) and binding clips. The glass is assembled to the sample holder using clips and the sample is loaded through the channel. The sample is lightly tapped and the glass is removed.

- RTS technique (Razor Tapped Surface Technique): The sample is loaded to an Al rectangular plate with 50.2×32.2×1.6 mm dimensions and 20.0×18.0×1.6 mm window. The powder mound is chopped in random directions using a razor blade. The access of sample is removed by chopping from centre to side and by blowing across the specimen.⁸⁹
- Freeze-drying: This technique requires special instrumentation. A suspension of the sample is dried in a freeze-dryer and further compacted.

The effectiveness of the random specimen preparation is shown in Fig. 3.9.

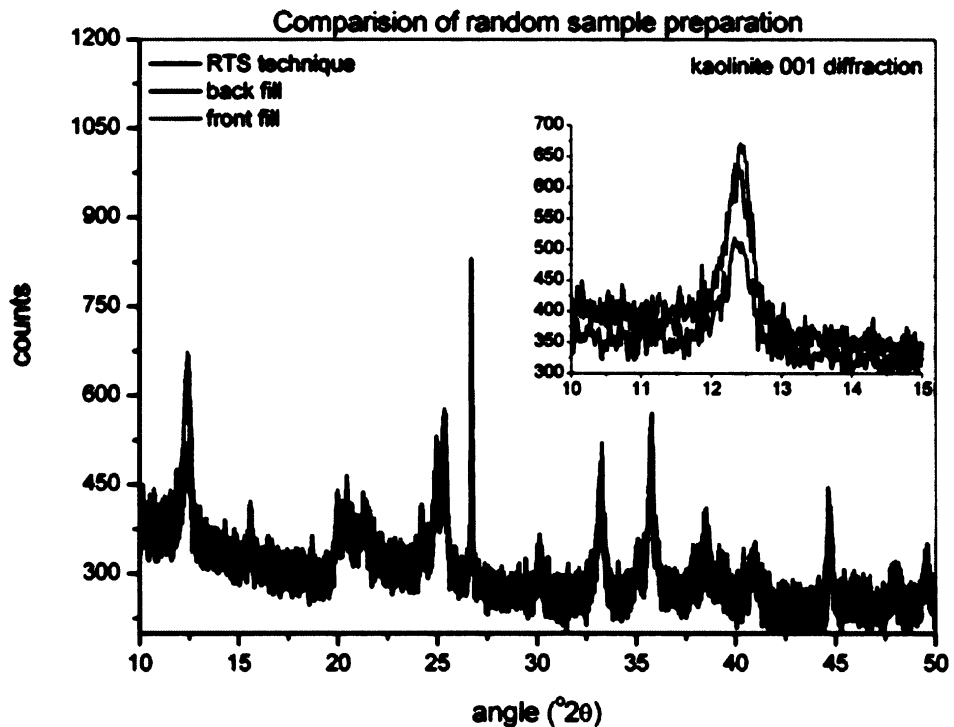


Fig. 3.9 - Comparison of random specimen preparation techniques. Ochre sample, CuK α radiation

Oriented specimens highlight the basal diffractions and make the observation of interlayer space behaviour easier. Specimens are commonly further treated during the tests.

The techniques for preparation of oriented specimens:

- Glass slides: The sample suspension is prepared from approximately 1 g of the sample and 10 mL of distilled water, the ratio of solid to liquid parts is dependent on the ability to form the suspension. The suspension is then transferred onto a glass slide using a pipette or Pasteur pipette. The glass slide is covered and the sample is allowed to dry at ambient temperature. The preparation procedure is also shown in Fig 3.10.
- Smear slides: The sample suspension is centrifuged to obtain a paste (or the powdered sample is mixed with 2 or 3 drops of a dispersing solution) which is then smeared across a labelled slide. This technique leads to a good orientation of the particles and a very good sample thickness.

- Porous ceramics specimens: They require special instrumentation and specimen support. The construction of the device used for the sample preparation in this work is shown in Fig. 3.11. The process of sample preparation is evident from Fig. 3.12, attaining a good particle orientation by filtration under a decreased pressure. The specimen is washed with water and placed into a dessicator filled with a solution of ammonium nitrate to dry slowly under controlled humidity.

Note: the height of the ceramic plate support may vary and the XRD pattern may suffer from sample displacement which can be corrected to the position of plate diffraction (see Table 3.6).

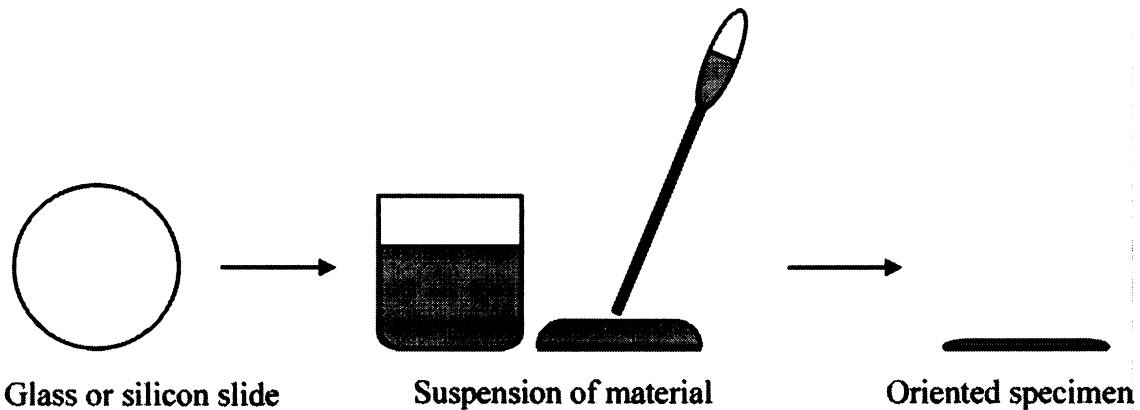


Fig. 3.10 - Preparation of oriented specimen from suspension

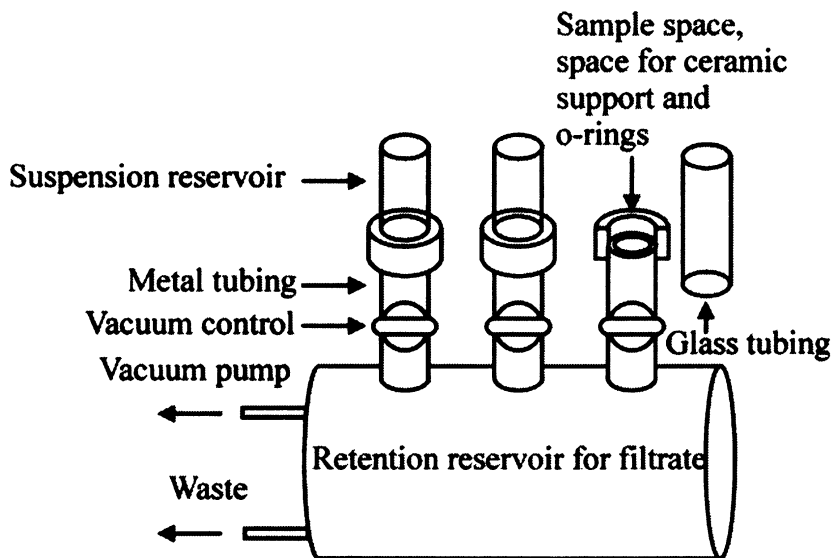


Fig. 3.11 - A device for preparation of oriented samples using a ceramic support and a low pressure (designed and manufactured by the Faculty of Mining, Geology and Petroleum Engineering, University of Zagreb)

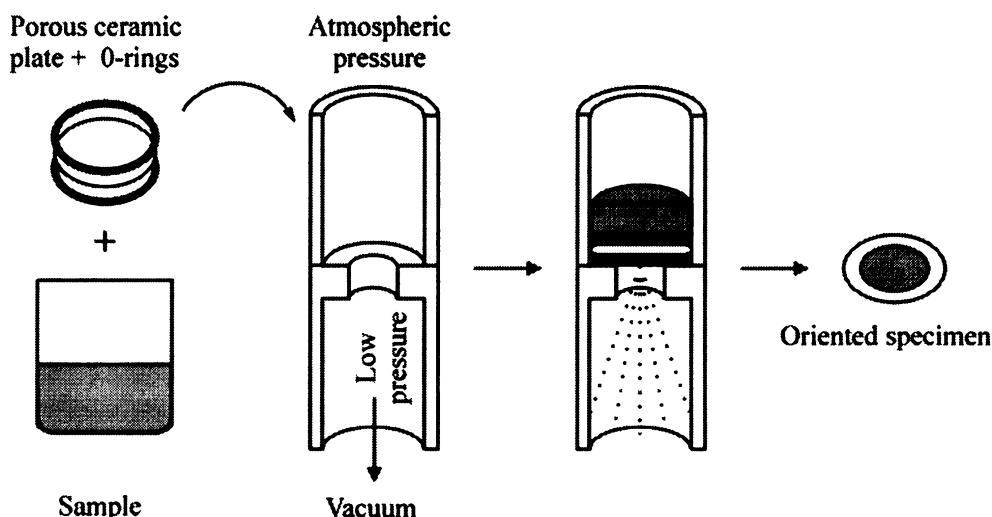


Fig. 3.12 - The procedure for the preparation of oriented samples using a ceramic support

Table 3.6 - An overview of the strongest diffractions on a ceramic plate support

Diffraction position ($^{\circ}2\theta$)	Intensity
25.60	1500
35.16	2500
37.77	1000
43.37	3000
52.54	1500
57.52	3000
66.54	1500
68.20	2000

Tests performed on oriented specimens

- Ethylene-Glycol (EG) expandability test: The specimen is exposed to ethylene-glycol vapours generated at 60 °C for 8 hours. The saturation influences the position of 00l diffractions and reveals the presence of expandable interlayer spaces characteristic for smectites (001 basal diffraction shifts from 15 Å to 17 Å concerning Ca-form) or mixed-layered structures containing smectitic layers (the shift is dependent on the proportion of expandable layers and the degree of ordering).
- Green-Kelly test: It is based on the Hofmann-Klemen effect when heating of a lithium saturated sample to 300°C (for 24 hours) causes migration of Li^+ to the site of charge imbalance. The proper position of Li^+ in the structure is still discussed and recent results point to the space around apical oxygens.⁹⁰ Nevertheless, montmorillonite is the only expandable clay mineral remaining collapsed after the heating treatment and saturation with EG leads to no

re-expansion. Therefore, the Green-Kelly test is used to distinguish montmorillonite from other smectites.

- Dimethylsulfoxide (DMSO) saturation: It is performed using porous-ceramics oriented specimen. The sample is placed onto a Petri dish embedded with filter paper soaked in DMSO. The dish is covered, exposed to a temperature of 70 °C for 24 hours and then stored at ambient temperature for further 24 hours.⁹¹ The temperature of DMSO vapour generation is 100 °C.⁹²
- Heating procedures: The samples are heated to 300 or 550 °C for 2 hours. A slow cooling rate is essential for glass slide oriented specimens. Heating produces a collapse of expandable layers. On the other hand, it also points to layers which are incapable of collapsing (e.g. chlorites), removes diffraction of minerals which are only stable at low temperatures and become amorphous during heating (kaolinite).

The XRD analysis is an essential method for investigation of clay minerals and it now represents the routine method for sample characterization.

3.8.3.1. Quantitative analysis

Variety of samples requires the use of various methods for quantitative analysis. The data collection is a crucial step in quantitative analysis. The diffractometer has to be well-aligned, calibrated and must not exhibit zero-point error (shifts d -values). There are also demands on the sample preparation:

1. The sample must be longer than the spread of the incident beam at the lowest diffraction angles (see Fig. 3.13, the sample length and the angular divergence of the beam have to be controlled).
2. The sample must appear infinitely thick at the highest diffraction angles.
3. The sample must be mounted so that the incident and diffracted beams impact/reflect under the same angle (for all the diffraction angles used).
4. There must be no particle-size gradient throughout the sample (the particles of various minerals should be of the same dimensions avoiding mineral separation and diminishing preferred orientation).

The diffraction intensity is proportional to the volume of the sample irradiated. It is recommended to avoid the use of low-angle reflections ($<10^\circ 2\theta$).

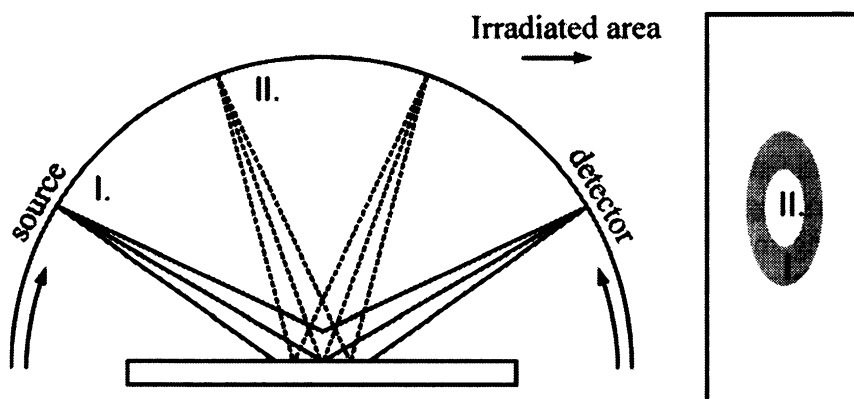


Fig. 3.13 - The spread of the incident beam in relation to the diffraction angle

Rietveld method:

This method was originally developed for refinement of crystal structures using neutron powder diffraction. Nowadays, it is commonly applied to X-ray diffraction data (also to clay minerals). Several Rietveld codes have been reported.⁹³ This method does not require measurement of calibration data or the use of an internal standard. Rietveld method provides additional information on the precise cell parameters. Application of the Rietveld method to clay minerals is limited because of their disordered nature.

The XRD data have to:

- Exhibit only Bragg diffractions (the preferred orientation has to be avoided).
- The structure factor must not vary across a reflection. Substitutional disorder is very common, the diffraction pattern is not significantly affected (structure factor F is unaffected by Al/Si substitution whereas Al-Mg/Fe substitution affects F through a change in number of electrons present on the scattering atom). Substitutional disorder brings micro-strain and reflections are broadened. Decreasing particle size also broadens all the reflections with non-zero l Miller index.
- The sample must not possess any layer-stacking disorder, or turbostratic stacking (Fig.3.14). Moreover, the preferred orientation causes the intensities measured to decrease nonlinearly with increasing diffraction angle.
- The amorphous phase, if present, cannot be modelled (some programs include it in the background).

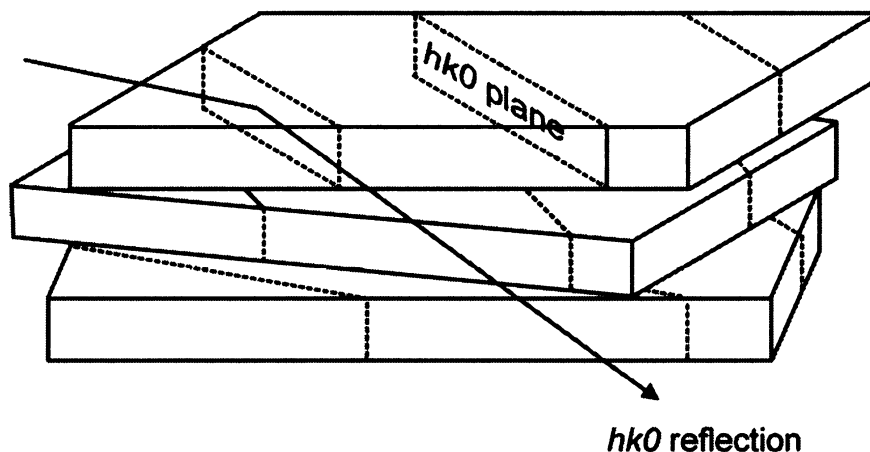


Fig. 3.14 - Effect of turbostratic disorder on the reflection on $hk0$ plane

Note: Turbostratic stacking, or the absence of any significant long-range order in the Z direction, occurs essentially in all smectites, most vermiculites and many other layer silicates resulting in the loss of most diffraction information. The diffraction patterns mainly contain broadened $00l$ reflections and two-dimensional diffraction bands. The Rietveld method cannot model broad, asymmetric bands correctly and completely.

The data are digitally refined. The use of all the lines minimizes the uncertainty in the derived weight fractions. Point-by-point fitting refines the R parameter (the sum of the weighted, squared differences between observed and calculated intensities):

$$R = \sum_i w_i |y_i(o) - y_i(c)|^2 \quad (3.7)$$

$y_i(o)$ – observed intensity at the i point
 $y_i(c)$ – calculated intensity at the i point
 w_i – weight assigned to the intensity

The calculation is performed using starting models of the mineral structures present in the sample (construction of the motive – atoms, their positions, and the space group which generates whole structure). The starting models have to be reasonably accurate. Large numbers of refined structures have been published and are accessible (e.g., on-line at American mineralogist crystal structure database: <http://ruff.geo.arizona.edu/AMS/amcsd.php>, or WWW-MINCRYST, Crystallographic and Crystallochemical Database for Mineral and their Structural Analogues: <http://database.iem.ac.ru/mincryst/index.php>).

Model structures are fitted to yield optimum agreement between observed and calculated data (moreover the real structures of phases are obtained). The calculated intensity at each point is determined by summing up the contributions from the background and all the neighbouring Bragg reflections:

$$y_i(c) = S \sum_k (p_k L_k |F_k| G(\Delta\theta_{ik}) P_k) + y_{ib}(c) \quad (3.8)$$

$y_i(c)$ – calculated intensity at the i point
 S – phase-specific scale factor
 p_k – multiplicity factor
 L_k – Lorentz and polarization factor for the k^{th} reflection

F_k – structure factor for an individual reflection of a particular phase
 $G(\Delta\theta_{ik})$ – reflection profile function,
 θ_{ik} – Bragg angle for the k -th reflection
 P_k – preferred orientation function,
 $y_{ib}(c)$ – refined background

Preferred orientation is treated by correcting G :

$$G = \exp(-G_1 \alpha^2) \quad (3.9)$$

α – the acute angle between the normal to crystallites and the scattering vector
 G_1 – refinable parameter (measure of half width of the Gaussian distribution of the normals about the preferred orientation direction)

The G correction modified by Toraya and Marumo:

$$G = G_2 + (1 - G_2) \exp(-G_1 \alpha^2) \quad (3.10)$$

α – the acute angle between the normal to crystallites and the scattering vector
 G_1 – refinable parameter (measure of half width of the Gaussian distribution of the normals about the preferred orientation direction)
 G_2 – (refinable) fraction of oriented crystallites

Preferred orientation correction using the March function:

$$G = (r^2 \cos^2 \alpha + r^{-1} \sin^2 \alpha)^{-3/2} \quad (3.11)$$

α – the acute angle between the normal to crystallites and the scattering vector
 r – adjustable coefficient related to the degree of preferred orientation

Eqs. 3.9 and 3.10 are only successfully used in the case of weak preferred orientation. The March function works for all preferred orientations of plate-like materials and for rod-like materials with low degrees of preferred orientation. It has a valid theoretical basis related to the mechanism producing preferred orientations and it has a single variable parameter.⁹⁴

The quantitative analysis is based on the fact, that the refined scale factor for each crystalline phase is related to the amount of the material present in the mixture. The integrated intensity of the beam diffracted by a randomly oriented infinitely thick polycrystalline sample in a flat-plate geometry utilizing a diffracted-beam monochromator is defined for a particular reflection by equation:

$$I_{hkl} = \left\{ \frac{I_0 A \lambda^3}{32\pi r} \left(\frac{\mu_0}{4\pi} \right)^2 \left(\frac{e^4}{m^2} \right) \left(\frac{1}{2\mu} \right) \left(\frac{1}{V^2} \right) x \left[|F|^2 p \frac{1 + \cos^2 2\theta \cos^2 2\theta_m}{\sin^2 \theta \cos \theta} \right] e^{-2m} \right\}_{hkl} \quad (3.12)$$

hkl – related to the Bragg reflection hkl

I – integrated intensity per unit length of diffraction line (joules sec⁻¹ m⁻¹)

I_0 – intensity of incident beam (joules sec⁻¹ m⁻²)

A – cross-sectional area of incident beam (m²)

λ – wavelength of incident beam (m)

r – radius of diffractometer circle (m)

μ_0 – $4\pi \times 10^{-7}$ m kg C⁻², magnetic constant (equal to the vacuum permeability)

e – charge on electron (C)

m – mass of electron (kg)

V – volume of unit cell (m³)

F – structure factor

p – multiplicity factor

θ – Bragg angle

e^{-2m} – temperature factor

μ – linear absorption coefficient (m⁻¹)

$2\theta_m$ – refers to the diffraction angle of diffracted-beam monochromator crystal

Eq. 3.12 can be divided into two parts:

$$K = \left(\frac{I_0 A \lambda^3}{32\pi r} \right) \left(\frac{\mu_0}{4\pi} \right)^2 \left(\frac{e^4}{m^2} \right) \quad (3.13)$$

$$R_{hkl} = \left(\frac{1}{V^2} \right) \left[|F|^2 p \left(\frac{1 + \cos^2 2\theta \cos^2 2\theta_m}{\sin^2 \theta \cos \theta} \right) e^{-2m} \right]_{hkl} \quad (3.14)$$

The K value holds for a constant intensity of the incident beam and constant cross-sectional area, under constant measuring conditions. The R_{hkl} value varies. Eq. 3.12 can be re-written in the form:

$$I_{hkl} = K \left(\frac{1}{2\mu} \right) R_{hkl} \quad (3.15)$$

In a mixture of phases, the intensity of hkl reflection from α phase is given by:

$$I_{\alpha,hkl} = C_{\alpha} K \left(\frac{1}{2\mu_m} \right) R_{\alpha,hkl} \quad (3.16)$$

C_{α} – volume fraction of the α phase
 μ_m – linear absorption coefficient of the mixture (m^{-1})

This formula can be re-written for weight fraction expression (W_{α}):

$$I_{\alpha,hkl} = \left(\frac{W_{\alpha}}{\rho_{\alpha}} \right) K \left(\frac{\rho_m}{2\mu_m} \right) R_{\alpha,hkl} \quad (3.17)$$

ρ_{α} – is the density of phase α
 ρ_m – is the density of the mixture

The scale factor featuring in Eq. 3.8 can be written, using Eq. 3.13 in the form:

$$S = \frac{K}{V^2 \mu} \quad (3.18)$$

V – volume of unit cell (m^3)
 μ – linear absorption coefficient (m^{-1})

for one phase in the mixture:

$$S_{\alpha} = \frac{C_{\alpha} K}{V_{\alpha}^2 \mu_m} \quad (3.19)$$

C_{α} – volume fraction of the α phase
 V_{α} – unit cell volume of α phase (m^3)
 μ_m – linear absorption coefficient of the mixture (m^{-1})

with the weight fraction expression:

$$S_{\alpha} = \frac{W_{\alpha} K}{\rho_{\alpha} V_{\alpha}^2 \mu^*} \quad (3.20)$$

μ^* – mass absorption coefficient of the sample (absorption per gram per square centimetre of sample)

W_{α} – weight fraction of α phase
 ρ_{α} – the density of phase α
 V_{α} – unit cell volume of α phase (m^3)

The K value and the sample mass absorption coefficient are difficult to determine. Therefore, the analysis of an unknown sample is performed using constrain of the unit sum of the weight fractions:

$$W_{\alpha} + W_{\beta} + W_{\gamma} + W_{\delta} + \dots = 1 \quad (3.21)$$

For the weight fraction of the i^{th} component:

$$W_i = \frac{S_i \rho_i V_i^2}{\sum_j S_j \rho_j V_j^2} \quad (3.22)$$

Another approach to the Rietveld analysis is the addition of a known weight fraction of a crystalline internal standard to the unknown sample. Now the W_α is known and K/μ^* can be determined:

$$C = \frac{K}{\mu^*} = \frac{S_\alpha \rho_\alpha V_\alpha^2}{W_\alpha} \quad (3.23)$$

This parameter can then be used to determine the weight fractions of other phases:

$$W_i = \frac{S_i \rho_i V_i^2}{C} \quad (3.24)$$

W_i – weight fraction of i phase

S_i – refinable scale factor of i phase

ρ_i – the density of phase i calculated from the composition and cell parameters of i phase

C – determined using internal standard

This method is not constrained by assumption of the unit sum of the weight fractions. The total weight fraction of any amorphous components (or component not included in the calculation) can thus be determined if the amorphous phase can be fitted with the Rietveld background polynomial and its content is significant (5-10%). Its content is the difference of the sum of all the weight fractions calculated and 1.0.^{95,96}

Matrix-flushing method:

The matrix-flushing method has been developed by F.H. Chung in 1974 deriving a simple relationship between the intensity of the diffracted beam and the content of the diffracting compound in a mixture.⁹⁷ The quantification is based on the use of a flushing agent. The standards for measurement of reference intensities are needed (they have to possess the same crystal perfection as the investigated compounds in the mixture). The equation is derived below.

The diffracted beam intensity is given by

$$I_i = K_i \frac{X_i / \rho_i}{\sum_i \mu_i X_i} = K_i \frac{X_i / \rho_i}{\mu_i} \quad (3.25)$$

I_i – intensity of diffracted beam by a selected hkl plane of component i

K_i – constant related to geometry of diffractometer and the nature of i component

X_i – weight fraction of component i

ρ_i – density of component i

μ_i – mass absorption coefficient of pure component i

μ_i – mass absorption coefficient of the mixture

The ratio of intensity of compound in the mixture and pure compound is:

$$\frac{I_i}{I_i^0} = X_i \frac{\mu_i}{\mu_i} \quad (3.26)$$

I_i^0 – intensity of the strongest line of diffracted beam by a selected hkl plane of pure compound I (constant from the same diffractometer)

The equation must be pruned of the mass absorption coefficients. This is performed using a so-called flushing agent for which:

$$\frac{I_f}{I_f^0} = X_f \frac{\mu_f}{\mu_i} \quad (3.27)$$

Then it holds that

$$\frac{\frac{I_i}{I_i^0}}{\frac{I_f}{I_f^0}} = \frac{X_i \frac{\mu_i}{\mu_i}}{X_f \frac{\mu_f}{\mu_i}} = \left(\frac{I_i}{I_f} \right) \left(\frac{I_f^0}{I_i^0} \right) = \left(\frac{X_i}{X_f} \right) \left(\frac{\mu_i}{\mu_f} \right) \quad (3.28)$$

When standardizing all the components to corundum through the reference intensities derived from the one-to-one weight ratio mixture:

$$\left(\frac{I_i}{I_c} \right) \left(\frac{I_c^0}{I_i^0} \right) = 1 \cdot \left(\frac{\mu_i}{\mu_c} \right) \quad (3.29)$$

and substituting an intensity ratio of 1:1 mixture by the constant:

$$\frac{I_i}{I_c} = k_i \quad (3.30)$$

then Eq. 3.29 for the compound and flushing agent becomes:

$$\frac{I_c^0}{I_i^0} = \left(\frac{1}{k_i} \right) \left(\frac{\mu_i}{\mu_c} \right) \quad (3.31a)$$

and:

$$\frac{I_c^0}{I_f^0} = \left(\frac{1}{k_f} \right) \left(\frac{\mu_f}{\mu_c} \right) \quad (3.31b)$$

and its quotient becomes:

$$\frac{\frac{I_c^0}{I_i^0}}{\frac{I_c^0}{I_f^0}} = \frac{\left(\frac{1}{k_i} \right) \left(\frac{\mu_i}{\mu_c} \right)}{\left(\frac{1}{k_f} \right) \left(\frac{\mu_f}{\mu_c} \right)} = \frac{I_f^0}{I_i^0} = \left(\frac{k_f}{k_i} \right) \left(\frac{\mu_i}{\mu_f} \right) \quad (3.32)$$

The Eq. 3.28 then becomes:

$$\left(\frac{I_i}{I_f} \right) \left(\frac{k_f}{k_i} \right) \left(\frac{\mu_i}{\mu_f} \right) = \left(\frac{X_i}{X_f} \right) \left(\frac{\mu_i}{\mu_f} \right) \quad (3.33a)$$

$$\left(\frac{I_i}{I_f} \right) \left(\frac{k_f}{k_i} \right) = \left(\frac{X_i}{X_f} \right) \quad (3.33b)$$

$$\left(\frac{I_i}{I_f}\right)\left(\frac{k_f}{k_i}\right) \cdot X_f = X_i \quad (3.33c)$$

The last derived equation is a simple relationship between the intensity and the concentration. Any pure compound which is not a component of the sample can be used as the flushing agent. When corundum is chosen as the flushing agent, $k_f = k_c = 1$, Eq. 3.33c becomes:

$$\frac{X_c}{k_i} \left(\frac{I_i}{I_c}\right) = X_i \quad (3.34)$$

Intensity ratios from the same scan are used for multi-component analysis and the amorphous content can be determined calculating the difference between the component content and unity. For binary mixtures and auto-flushing effect is present (one compound is the flushing agent for the second one). The auto-flushing theory has been extended to multi-component mixtures by adiabatic principle of auto-flushing. The extension omits the possibility of amorphous phase and unidentified phase presence.⁹⁸

The reference intensities have to be:

1. recorded using the same diffractometer under the same instrumental conditions.
2. the material used to determine the reference intensity must have the same level of perfection of the crystal structure
3. the optimum particle size and sample homogeneity have to be ensured
4. preferred orientation has to be avoided

Note: when the strongest diffraction is unresolved the second strongest diffraction can be recalculated and used as reference intensity etc.

Quantification using the peak intensity ratio:

The main difficulties in quantitative mineral analysis are related to variable chemical composition and variable structures (including swelling layers, interstratifications or disorder). Selection of analytical reflection measured on a random sample offers a chance to avoid sensitivity to the chemical and structural variations. The grinding and homogenization procedures have to be controlled. The method is derived from internal standard technique to eliminate the sample mass absorption coefficient.

The weight fraction of mineral x in the mixture is:

$$X_x = \frac{I_x \mu_m^*}{K_x} \quad (3.35)$$

X_x – weight fraction of mineral x

I_x – intensity of chosen diffraction of mineral x

μ_m^* – mass absorption coefficient of the mixture

K_x – constant for a chosen reflection of mineral x and given experimental settings

If the mixture contains an internal standard s than ratio of their weight fractions is:

$$\frac{X_x}{X_s} = \frac{K_s \cdot I_x}{K_x \cdot I_s} \quad (3.36)$$

X_s – weight fraction of standard s

I_s – intensity of chosen diffraction of standard s

K_s – constant for a chosen reflection of standard s and given experimental settings

If the standard and the mineral are mixed in a binary mixture of known composition, the intensities of the selected pair of reflections can be measured and mineral intensity factor (MIF) can be calculated:

$$MIF = \frac{K_x}{K_s} = \frac{I_x \cdot X_s}{I_s \cdot X_x} \quad (3.37)$$

The MIF value is constant for the chosen mineral and standard at given experimental conditions (because the intensity is interrelated to the content). The value is independent of the mineral or standard amount (when sample is finely ground and microabsorption is eliminated). In general:

$$MIF = \frac{I_x \cdot X_s}{I_s \cdot X_x} \quad (3.38)$$

$$X_x = \frac{I_x \cdot X_s}{I_s \cdot MIF} \quad (3.39)$$

The MIF values are determined from mixtures of known minerals and standard compositions. An unknown mixture is investigated by adding a known amount of a standard. The weight percentages of the standard and the mineral x are:

$$X_s = \frac{m_s}{m + m_s} \cdot 100 = \frac{m_s}{M} \cdot 100 \quad (3.40)$$

$$X_x = \frac{m_x}{m + m_s} \cdot 100 = \frac{m_x}{M} \cdot 100 \quad (3.41)$$

m_s – weight of added standard s

m_x – weight of mineral x in the mixture

m – weight of original mixture

M – weight of mixture after addition of standard

and the weight percentage of mineral x is calculated from Eqs. 3.39 and 3.40:

$$X_x = \frac{I_x \cdot m_s \cdot 100}{I_s \cdot (m + m_s) \cdot MIF} = \frac{I_x \cdot m_s \cdot 100}{I_s \cdot M \cdot MIF} \quad (3.42)$$

If a narrow angle range is investigated, the influence of the preferred orientation is neglected and the standard deviation of the tilt angle of the crystallites about the mean crystallite orientation is assumed to be the same for all the minerals. Line overlap may reduce the number of measurable lines. The analysis is accompanied by MIF

determinations using standards of minerals present in the mixture and the internal standard. The following sample preparation is recommended:

- use of a lowered laboratory splitter
- grinding by McCrone Miconizing mill (5 min grinding of 3g sample in 4 ml of methanol)
- 10 wt.% zincite internal standard for mixture quantification and 20 wt.% for *MIF* determination, addition prior to grinding (ZnO)
- side loading, packing by vortex or vigorous tapping
- the integrated intensity measurement using EVA software

A linear relationship X_x/I_x is possible only if there is a completely random orientation. Among the mineral diffractions, the *0k0* diffractions seem to be the best analytical diffractions of the mineral because of its low sensitivity to polytypism and defects (for *060* diffractions the 59 – 64 °2θ, 5s per 0.01 °2θ regime is recommended). The presence of amorphous phase can be determined from the difference of the sum of weight fractions of minerals from unity.⁹⁹

XRD-pattern stripping:

The method was introduced by Batchelder and Cressey in 1998. The XRD-patterns are obtained using curved Position Sensitive Detector (PSD, consisting of 4096 channels in 120 °2θ, which is a channel per 0.03 °2θ). The measurements are performed in reflection, fixed beam-sample-detector geometry (5° angle with incident beam), and the diffracted intensities are collected at all angles simultaneously around the 120° arc. The irradiated area is constant for each experiment. The data acquisition time is 10 min per sample. The mixture and separate clay minerals standards have to be measured. The preferred orientation has to be avoided.

The quantification itself is performed by sequential stripping of mineral standards XRD-patterns using ENRAF-GUFI software until the residual pattern indicates no phases remained. The single standard pattern is superimposed upon the multiphase pattern, proportionally reduced to meet the best match of counts and subtracted. The optimal-fit scaling fraction represents the clay mineral volume proportion in the sample (if one unknown mineral is present, its content can be determined after subtraction of all the remaining minerals, determining their contents, and calculating the sum of proportions to unity). The order of minerals stripping is indifferent. The accuracy of determination is related to match with the standard pattern. Mixtures of non-clay minerals have to be further manipulated applying absorption correction factors.¹⁰⁰

Summary:

All the methods presented, the quantification of clay minerals require standards of clay minerals (whether the crystal structures concerning Rietveld method or real clay minerals for deriving reference intensities or *MIF* values or gaining XRD patterns for the subtraction). Finding a standard matching the clay mineral present in a natural mixture is always the crucial step which limits the reliability of quantification.

3.8.4. FTIR spectroscopy

Infrared spectroscopy is a rapid and non-destructive method. The incident radiation is distinguished into:

- near-infrared region (NIR, $\tilde{\nu} = 12000 - 4000 \text{ cm}^{-1}$)
- mid-infrared region (MIR, $\tilde{\nu} = 4000 - 400 \text{ cm}^{-1}$)
- far-infrared region (FIR, $\tilde{\nu} = 400 - 50 \text{ cm}^{-1}$)

Note: the basic relations in spectroscopy are:

$$c = \lambda \cdot \nu \quad (3.43)$$

$$\tilde{\nu} = \frac{1}{\lambda} \quad (3.44)$$

$$E = h \cdot \nu = \frac{h \cdot c}{\lambda} = h \cdot c \cdot \tilde{\nu} \quad (3.45)$$

c – velocity of light
($2.9979 \times 10^{10} \text{ cm} \cdot \text{s}^{-1}$)

λ – wavelength (commonly in nm)

ν – frequency (s^{-1})

$\tilde{\nu}$ – wavenumber (commonly cm^{-1})

h – Planck's constant ($6.6262 \times 10^{-34} \text{ J s}$)

E – energy

Absorption of the radiation causes transitions between rotational and vibrational levels of molecules (excitation to higher energy levels). The classification of the vibrational quantum states exploits the symmetry of vibrating groups. The vibrations are further classified as stretching (symbol ν , a higher energy needed), bending (symbol δ , a lower energy needed) and out-of-plane (symbol γ). Stretching vibrations are characterized by changing bond lengths, bending vibrations cause changes in bond angles while bond lengths are preserved. The out-of-plane vibration is caused by oscillation of the atom above the plane defined by at least three neighbouring atoms. The stretching vibrations are further classified in terms of the symmetry of movement. The bending vibrations are further distinguished as scissoring, rocking, wagging or twisting. These are fundamental vibrations. Features of much lower intensity present in the sample spectrum are combination bands and overtones. Combination bands are obtained by adding or subtracting frequencies of one or more fundamental vibrations. Overtones are multiples (2 or 3 times) of fundamental vibrations. Note: not all of the vibration modes can be active in the IR. The selection rules define the modes present in the spectra. Only the transitions involving a change in the dipole moment of the vibrating atomic group or molecule is active in IR spectra.

To cause transition between discrete energy levels, only the radiation of proper energy can be absorbed. The relation between the energy absorbed and the frequency of light needed to satisfy the transition is expressed by Bohr's law:

$$E'' - E' = \Delta E = h \cdot \nu \quad (3.46)$$

E'' – energy of higher excited state

E' – energy of ground state or lower excited state

ΔE – energy difference of the transition

h – Planck's constant ($6.6262 \times 10^{-34} \text{ J s}$)

ν – frequency of light absorbed

The de-excitation follows the same law and the frequency of the emitted light can be calculated.

The polychromatic infrared light is generated in globar (silicon carbide rod, electrically heated to 1000 – 1650 °C) or other IR source (halogen lamp etc.). In the emission technique the sample itself is the source of IR radiation. The energy of light is modulated by a grid monochromator, nowadays by an interferometer (FTIR – Fourier transformed infrared spectrometer). Beam is passed through the sample and transmitted/reflected beam reaches detector and is analyzed. The decrease in the incident beam intensity after interaction with the sample is characterized by the transmittance or absorbance¹⁰¹:

$$T = \left(\frac{I}{I_0} \right) \quad (3.47)$$

$$A = -\log \left(\frac{I}{I_0} \right) = -\log T \quad (3.48)$$

T - transmittance

I_0 – intensity of incident beam

I – intensity of beam after absorption interaction

A – absorbance

The absorption of radiation by the sample is related to the quantity of the absorbing species by the Lambert-Beer law:

$$A = \varepsilon \cdot c \cdot l \quad (3.49)$$

ε – molar absorption coefficient ($\text{dm}^3 \cdot \text{mol}^{-1} \cdot \text{cm}^{-1}$)

c – concentration of the species ($\text{mol} \cdot \text{dm}^{-3}$)

l – length of absorbing environment, sample thickness (cm)

The Fourier-transform instrumentation provided infrared spectroscopy with improved frequency accuracy, signal-to-noise ratio and high data acquisition speed. The range of the techniques in the IR region has been extended involving¹⁰²:

- Transmission methods (KBr-pellet and self-supporting film samples)
- Diffuse reflectance (DRIFT, it requires small or no sample preparation, matt surface and it is suitable for organic composites analysis)
- Attenuated total reflectance (ATR, suitable for pastes ensuring maximum contact with the ATR crystal)
- Specular reflectance (applied to polished samples)
- Emission spectroscopy (radiation is emitted by the sample heated on a platinum stage. It is the most sensitive method among IR techniques, and it enables, e.g.: observation of clay mineral dehydration in-situ)
- Infrared microscopy (mapping surfaces of flat samples)
- Remote fibre optic spectrometry

The choice of method is related to the physical form of the sample and information needed. The most common is the transmission technique with KBr pressed discs (200 mg of KBr and 2-3 mg of sample in OH- stretching region, 0.6 mg in OH- bending region). Digital data can further be handled, employing standards or baseline subtraction, maximum assignment, deconvolution (fitting with different distribution functions), Kramers-Krönig transformation (relation of real and imaginary parts of

response function), application of Kubelka-Munk equation (recalculation of reflection spectra to absorption spectra) or principal component analysis (for statistical evaluation of data).

3.8.4.1. Infrared spectroscopy of clay minerals

Infrared spectroscopy reveals short-distance arrangement of structure. Distinguishing between physical mixture of clay minerals and mixed-layered minerals is not possible and investigation of mixtures is complicated. Identification of mineral/s is performed using the Atlas of Infrared Spectra or by search for and assignment of characteristic vibrations (functional atomic groups are treated as independent oscillators and the vibration energy is calculated).

Infrared spectra of clay minerals are divided into:

- 1300 – 400 cm^{-1} region with OH bending and Si-O stretching vibrations
- 3750 – 3500 cm^{-1} region with OH stretching vibrations
- 4400 – 7100 cm^{-1} region with overtones and combination vibrations

The spectra also contain water-molecule vibrations. Water is present in two different states: as solvation shells of cations and external water. A broad asymmetric stretching vibration is present at 3620-3640 cm^{-1} , the symmetric stretching vibration occurs at 3560-3580 cm^{-1} and the bending mode is present at 1630 cm^{-1} . The position is influenced by the character of the interlayer cation and the charge location in the mineral structure. The position of the H-O-H (3400 cm^{-1}) vibration decreases in dependence on the interlayer cation, in the order: K^+ , Na^+ , Ca^{2+} , Mg^{2+} . The interlayer cation also modifies the intensity of vibration. The strength of H-bonding to clay mineral surface is stronger with closer location of non-equivalent substitution (tetrahedral substitution creates stronger H-bonding than octahedral substitution). Water molecules on the smectite surface have a preferred orientation.¹⁰³ Water vibrations can be eliminated by heating to 150 °C overnight.

Characteristic bands of clay minerals are rare. Kaolinite is characterized by in-phase symmetric OH stretching vibration at 3695 cm^{-1} . Nontronite is distinguishable from other smectites by the presence of Fe-Fe-OH bending vibration at 817 cm^{-1} , together with 676 cm^{-1} Fe-O out of plane. An overview of vibrations of clay minerals is given in Table 3.7. The OH stretching region shows vibrations related to the chemical composition of octahedral sites (the chemistry of octahedral sheet of mineral can be investigated under the conditions of single phase sample). The IR spectra slightly change with changing interlayer cation and water content.¹⁰⁴ Clay mineral spectra can be complicated by vibrations of admixtures (e.g, Si-O stretching vibration of amorphous silica at 1083 cm^{-1})

Application of FTIR to clay investigation

FTIR is a useful tool for investigation of the chemistry of layers. It enables observation of structure changes, e.g.:

- acid activation, proton attack of OH- groups which causes dehydration and dissolution of the octahedral sheet, three-dimensional protonated amorphous silica is formed (influence on OH- and Si-O vibrations).¹⁰⁵

Table 3.7 - Overview of clay mineral vibrational modes

OH stretching region			Si-O bending region			OH-bending region			Si-O-M bending vibration		
Position (cm ⁻¹)	Assignment	Mineral	Position (cm ⁻¹)	Assignment	Mineral	Position (cm ⁻¹)	Assignment	Mineral	Position (cm ⁻¹)	Assignment	Mineral
3703	A1A1OH	D	1125	Si-O ^{apical oxygen}		936	A1A1OH	D	520	Si-O-Al _{octa}	
3700	MgMgLiOH		1030	Si-O	M	935	A1A1LiOH		470	Si-O-Si	
3683	AlMgOH		1019	Si-O	N	916	A1A1OH	M	470	Si-O-Mg	
3680	MgMgMgOH		1012	Si-O	H	914	A1A1OH	K	428	Si-O-Si	
3670	AlMgLiOH		1009	Si-O	S	890	FeFeOH				
3669	A1A1OH	K				886	AlFeOH	M			
3653	out-of-plane	K				855	MgAlLiOH				
3643	A1A1LiOH					844	AlMgOH	M			
3620	A1A1OH					817	FeFeOH	N			
3603	AlMgOH					810	MgFeLiOH				
3596	AlFeOH					800	MgMgOH				
3587	AlFeOH					786	FeMgOH				
3567	FeFeOH					660	MgMgMgOH	S			
3565	FeMgOH					655	MgMgMgOH	H			
D – dickite		H – hectorite			K – kaolinite			M – montmorillonite			
N – nontronite		S – saponite									

- fixing of small cations and their position within the structure (observation of new band formation, perturbation of Si-O and OH- vibrations).^{106,107}
- observation of dehydration processes of interlayer cations (H-O-H vibration, OH- vibration of clay mineral).^{108,109}

The investigation recently shifted to the NIR region where small structural changes are observable by monitoring overtones.¹¹⁰

3.8.5. CEC determination

The cation-exchange capacity is a very important property of clay minerals. It plays the main role in their interactions with the environment. The magnitude of CEC depends on non-equivalent substitutions and structural defects, the ambient conditions, such as the temperature, pH and interacting cationic species, are also significant. Not all the interlayer cations can be exchanged (e.g., when electrostatic interaction is too intense, the cation cannot be extracted, like potassium in mica). Tightly bound interlayer cations can be extracted using special treatment.¹¹¹ All the methods for CEC determination are based on exchange of natural cations with index cations (see the flowchart in Fig. 3.15). The influence of hysteresis on the exchange reaction was discussed in Chapter 3.3.4. Therefore, the index cation has to be:

1. properly exchanged
2. or have a higher affinity to the clay mineral

The first approach usually involves more than one saturation step and it is time consuming. The second approach has given rise to a plenty of new, fast, one-step methods which, in fact, have not been explored in detail.

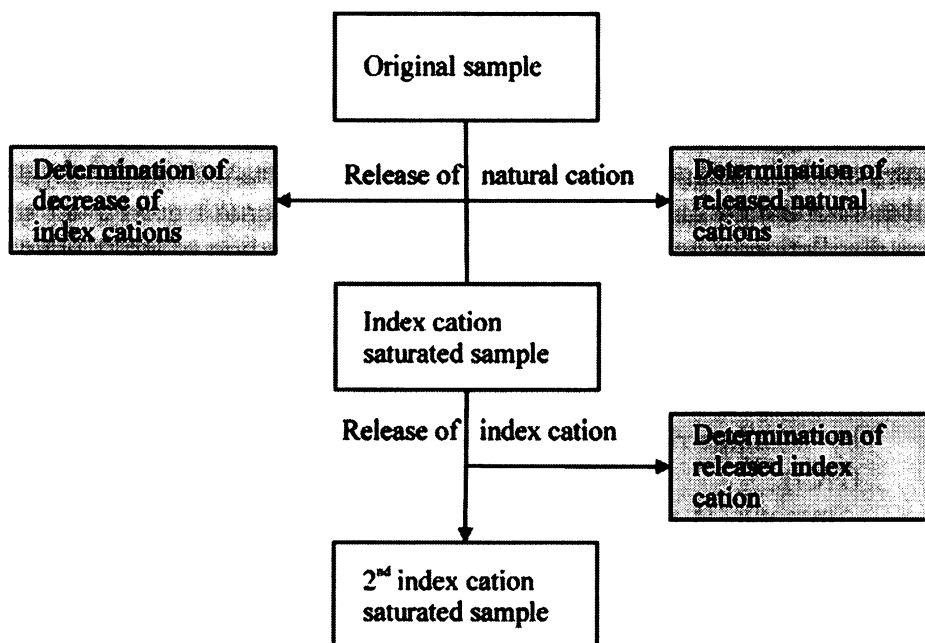


Fig. 3.15 - Flowchart of CEC determination procedure. Gray boxes mark the position of measurement and analytical evaluation of CEC

The choice of the index cation is not restricted to inorganic ions. The binding coefficients of organic dyes (methylene blue, crystal violet, acriflavin) to montmorillonite are actually six orders of magnitude higher than those of inorganic cations (Na^+ , Cd^{2+} , Cs^+). The adsorption depends on the type of dye, its amount added and the solution ionic strength.¹¹² Organic cations are, in addition, bound through non-coulombic interactions. The sorption of dyes exceeds CEC due to aggregation effects.¹¹³ The adsorption of a particular inorganic cation is dependent on its concentration and on the ligand present in the coordination sphere. The strength of coordination is important (e.g.: Ca^{2+} has a greater binding affinity than Mg^{2+} , due to the weaker H_2O coordination sphere and the formation of bridges between adjacent layers). Divalent cations can be sorbed as monovalent species (M^{2+}X^+)⁺ which enhances CEC by up to 20 - 30%.^{114,115,116}

The CEC is also influenced by soluble admixtures, such as carbonates. The reliability of the results can be evaluated using *Carbonate- and Sulphate Field Model (CSF model)* where CEC is determined using two solid/liquid ratios of clay and index cation solution. If both the results are the same within the experimental error, the CEC value is correct.¹¹⁷

3.8.5.1. Methods for CEC determination

NH_4^+ index cation:

The ammonium cation is the traditional index cation. The ammonium acetate method was introduced by Mackenzie in 1951 and it is recognized as the standard procedure.¹¹⁸ The method has been several times unsuccessfully modified to fit calcareous samples. Its application in this case is restricted by dissolution of calcium carbonates and competition of Ca^{2+} for the exchange sites.¹¹⁹ Identical CEC results are obtained when replacing ammonium acetate by ammonium chloride.¹²⁰ The CEC can be determined in many ways:

- as the sum of exchangeable bases released on percolation with ammonium acetate
- from percolation of ammonium sample with sodium acetate and determination of the adsorbed Na^+
- from distillation of ammonium sample and determination of ammonia evolved¹²¹

A wide variety of analytical methods can be used:

- Titration:
 - Residual ammonia (after homoionic form preparation) can be determined by alkalimetric titration with a 0.2 M solution of hydrochloric acid (HCl).¹²²
 - Ammonia is released from homoionic sample by alkali hydroxide and trapped in a boric acid solution. The trapping agent is titrated with 0.01 M sulfuric acid (H_2SO_4) to the pH corresponding to boric acid solution. AAS revealed problems with calcareous samples where an addition of ammonium acetate caused dissolution of CaCO_3 .¹²³
- Ion-selective electrode potentiometry: Fresh calibration solutions have to be prepared prior to each new set of experiments. Other dissolved species do not interfere (except for volatile amines). Ammonia is released from dispersed

samples by 10 M sodium hydroxide (NaOH) and measured with an NH_4^+ -ion-selective electrode.^{124,125}

- Spectrometry: the NH_4^+ content is determined from the colouration of the complex with a phenol.¹²⁶

H^+ index cation:

The homoionic form can be prepared using a strong acid resin, e.g.: sulfonic type, in H^+ cycle. The soil reacts with the exchanger and its cations are replaced by protons. The CEC can be evaluated by potentiometric titration with barium hydroxide in the presence of barium chloride.¹²⁷ Note: other alkali hydroxides can also be used for titration of H^+ .¹²⁸ The CEC of a matrix in the H^+ cycle can also be determined by constant current coulometry (H^+ is exchanged by K^+ and the protons released are titrated with electrogenerated OH^- ions).¹²⁹

Ba^{2+} index cation:

Barium was proposed as the index cation by Mehlich in 1948. Saturation with barium is performed with a barium chloride solution in three steps. Barium is consecutively released by magnesium chloride or magnesium sulphate (second index cation). Barium samples can also be investigated using conductometric titration (using sulphates) or ISE potentiometric titration. The potentiometric results tend to be higher than those of conductometric titrations. Among the ISE measurements, the CEC depends on the second index cation used (the best results have been obtained with Mg^{2+}).¹³⁰

Ag^+ index cation:

Ammonium acetate and barium chloride methods are suspected to overestimate the value of effective cation exchange capacity (ECEC, measured in unbuffered solutions), because they involve high pH values and high electrolyte concentrations. The Ag-thiourea complex, introduced by Chhabra et al. in 1975, effectively displaces natural cations at a relatively low ionic strength. The ECEC is determined after a single extraction from Ag^+ consumption by atomic absorption spectroscopy. The complex has a much larger adsorption affinity to soils and clays than commonly occurring cations. The results have been found to be in a good agreement with the NH_4Ac method.^{131,132} The latest modification of the method employs a new stock solution preparation in order to obtain a more stable agent and two washing steps with deionized water to reduce overestimation due to weak physical bonding of access Ag-thiourea complex.¹³³ The pre-treatment of the stock solution by Ca^{2+} saturation (equilibration with calcite grains) leads to reliable information on CEC and the composition of natural exchangeable cations avoiding additional carbonates dissolution.¹³⁴

Sr^{2+} index cation:

The sorption of radioactive elements can also be used for CEC determination. Francis proposed the sorption of Sr^{85} .¹³⁵ The method has later been modified for sandy samples.¹³⁶ Strontium is also an effective ion displacer because of its high selectivity for clay surfaces. The CEC can also be determined from the Sr^{2+} exchange observed by atomic absorption.¹³⁷

Ni²⁺ index cation:

The nickel index cation is sorbed by clays in the form of its violet complex with ethylenediamine. The CEC is calculated from the content of the cations present in the supernatant after the exchange (determination by AAS/AES). This is a one-step procedure and the pH is controlled to prevent calcareous admixtures dissolution.¹³⁸

Co²⁺ index cation:

The octahedrally coordinated complex with hexamine trichloride is formed. One-step saturation is sufficient to replace natural interlayer cations. The cobalt consumption is determined by AAS or absorption spectrometry (colliding with dissolved organic matter). Filtration causes retention of the complex on filter paper. The complex solution causes dissolution of carbonates (positively related to addition).^{139,140} The results of the spectrometric method have been compared with those of the barium chloride and ammonium acetate procedures and found to be equivalent to the barium chloride method, but different from the ammonium acetate method.¹⁴¹ CEC can also be determined using Co-hexaqua complex prepared by simple dilution of cobalt sulphate (CoSO₄×7H₂O). The Co²⁺ concentration in the filtrate is determined by UV/Vis spectrometry. The results are in a good agreement with those of the ammonium acetate method.¹⁴²

Methylene blue (MB):

Methylene blue is one of frequently used organic dyes. It replaces interlayer cations irreversibly. Pre-treatment of clay with Na⁺ leads to an increase in the CEC explained by a better dispersion. The influence of the interlayer cation is significant.¹⁴³ Increasing ionic strength causes a drop in the MB sorption while the effect of the pH is insignificant.¹⁴⁴ Contradictory information has been published on the thermodynamic nature of the exchange and on the relationship between adsorption and temperature.^{145,146} The size of clay particles also influences the extent of sorption. The larger the particles are, the higher degree of aggregation is gained.¹⁴⁷ The adsorption to clay surface is instantaneous but nonuniform. Aggregates are formed causing an increase in the CEC. In addition, the sorption is influenced by the experimental conditions, such as the clay concentration, type of the clay and time of the suspension equilibration.¹⁴⁸ Reproducible results are only obtained for optimum dispersion, clay:water ratio and an appropriate initial methylene blue content. The MB spot-test can be used as a quality control.¹⁴⁹ (MB filter paper spot-test: sample is dispersed and 0.01M methylene blue solution is added in 0.5 ml aliquots. After each addition and 0.5 min swirling, one drop of the suspension is placed on a filter paper. The titration ends when faint blue ring or halo surrounds the dyed solids retained on paper)¹⁵⁰

Cationic surfactants:

Hexydecylpyridinium chloride cationic surfactant or benzyltriethyl ammonium chloride (BTEA) can be used for CEC determination. In the first case, the access of agent was detected by surface tension measurements.¹⁵¹ In the second case, the residual surfactant was detected by organic carbon analyzer. The application of organic molecules for determination of CEC is wide; nevertheless, larger organic molecules overestimate CEC by enhanced sorption.¹⁵²

The exchange of native cations can be performed by multi-step saturation in a mechanical extractor¹⁵³ or the untreated sample can be leached in a column.¹⁵⁴ Moreover, inorganic and organic index cations can be determined simultaneously. ICPEES detects both these species without interferences.¹⁵⁵

3.8.5.2. Cu^{2+} -trien method

The cupric ion is sorbed on clay surfaces in two steps. In the first step, the Cu^{2+} consumption is attributed to interlayer cation- Cu^{2+} ion exchange. The second step is a combination of ion exchange and adsorption by aluminol groups (silanol groups do not adsorb Cu^{2+}).¹⁵⁶ Therefore, cupric ion alone is not useful for CEC determination. Trien, tetren and penten are selective Cu^{2+} titrants and form complexes which are stable for weeks. The selectivity of ligand to cupric ion can be enhanced by the presence of EDTA as the masking agent for other ions. Spectrophotometric determination of the violet-blue complex formed is substantially increased by halides, in the $\text{F}^- < \text{Cl}^- < \text{Br}^- < \text{I}^-$ order.¹⁵⁷

Cu^{2+} -dien (ethylenediamine, 1,2-diaminoethane, $\text{NH}_2\text{CH}_2\text{CH}_2\text{NH}_2$, EDA) method for CEC was introduced by Bergaya and Vayer in 1997. It involves Cu^{2+} -ethylenediamine ($\text{Cu}(\text{EDA})_2^{2+}$) 1:2 complex which is stoichiometrically stable within a pH 6 – 8 range. The complex has a square planar configuration with a 40 \AA^2 area and it is strongly stabilized in clays. The method has been reported as fast and single step, with possible AAS or UV-Vis spectroscopy detection. The copper complex is claimed to displace even heavy metals and the reaction is irreversible. The CEC accuracy has been reported as $\pm 5\%$ of $\text{CEC} \geq 100 \text{ meq}/100\text{g}$ and $\pm 10\%$ for CEC around $20 \text{ meq}/100\text{g}$. The results have been found to be in a good agreement with those of the Kjeldahl method (ammonium acetate method). A 0.05 M stock solution of 1:2 complex is prepared from 1 M CuCl_2 and 1 M ethylenediamine. The exchange runs for 30 min (5 min was found to be sufficient to reach complete displacement of original ions). No washing step of the solid phase is required. Desired 50-100% access of $\text{Cu}(\text{EDA})_2^{2+}$ enables colorimetric determination. Other proposed methods are iodometry and AAS.²

Meier and Kahr investigated other two complexes. The complex with triethylenetetramine is discussed below. The exchange reaction was performed with higher concentration (0.01 M) stock solution prepared from CuSO_4 and trien (N,N'-bis(2-aminoethyl)-1,2-ethanediamine, $\text{NH}_2\text{CH}_2\text{CH}_2(\text{NHCH}_2\text{CH}_2)_2\text{NH}_2$, TETA). The equilibration time was 3 minutes and absorbance of supernatant was measured for residual complex. The absorbance maximum is present at 580 nm and linearity of Lambert-Beer law was found in $10^{-4} - 10^{-2} \text{ M}$ concentration range. Slight variation in absorbance was found in relation to the pH and the maximum position did not vary in the presence of other ions at low concentration. Buffered experiments were performed and gave similar results. In comparison with the ammonium acetate CEC, the results were slightly higher. The authors disputed reliability of atomic absorption spectroscopy and its sufficiency for CEC determination.³

A breakthrough work on testing the copper-polyamines CEC determination was performed by Amman et al. in 2005. The Cu-dien and Cu-trien complexes were investigated. The high affinity of cationic complexes to clay was explained by preferred sorption of organic complexes on inorganic cations. Stock solutions were prepared from CuSO_4 and a proper polyamine, resulting in a 0.01 M complex solution. The absorption maximum of Cu(EDA)_2^{2+} lies at 584 nm and that of Cu(TETA) at 577 nm. The 30 min. reaction was followed by photometric determination. The differences among parallel measurements (3 parallels) were found to be 4% or better, in relation to the type of clay. No influence of sample preparation was found (CEC values resulting from addition of stock solution to dry and dispersed samples were identical). The influence of pH on the absorption coefficients of both complexes were investigated by buffering the supernatant solution before absorbance measurement (pH = 8). The absorption coefficient of Cu-dien was found to be more pH sensitive than that of Cu-trien. In general, the buffer modestly increases the absorption coefficients of both the complexes. The results were in good agreement with those obtained by the ammonium acetate method. The CEC of Source Clays from The Source Clays Repository were discussed because of distinctly higher CEC values which might be caused by different drying conditions. Ammann recommends photometric determination and addition of tris(hydroxymethyl)aminomethane buffer as a standard procedure.⁴

The comparison of CEC using copper-polyamine complex with ammonium acetate CEC, obtained by the above authors, is given in Table 3.8.

Table 3.8 - Variation in CEC, comparison of ammonium acetate and copper-polyamine methods

Author	Sample	CEC		Diference (%)
		NH ₄ OAc (mmol/100g)	CEC Cu (mmol/100g)	
Meier and Kahr (1999)	Bentonite SAz-1	120.0	122.0	1.6
	Bentonite Volclay	81.9	84.5	3.1
	Bentonite MX-80	71.5	75.5	5.3
	Bentonite Montigel	62.0	63.9	3.0
	K-bentonite B39	53.0	60.1	11.8
	K-bentonite B31/32	42.0	46.1	8.9
	K-bentonite M40	29.0	31.4	7.6
	Illite MC	19.0	20.0	5.0
	Illite S	16.0	19.0	15.8
	China Clay (kaolinite)	3.8	6.4	40.6
Ammann et al. (2005)	Beidellite B2		113.0	
	Beidellite B18/4	116.9	120.0	2.6
	Bentonite Cameron	58.6	61.5	4.7
	Bentonite Cream	67.9	70.7	4.0
	Bentonite de Maio	84.4	84.5	0.1
	Hectorite H3	40.6	45.7	11.2
	Kaoline KGa-1	1.7	1.5	-13.3
	Na-montmorillonite			
	Kunipia A	102.3	102.8	0.5
	Bentonite M3		101.8	
	Bentonite M26		67.9	
	Bentonite Camp Berteau			
	M34		87.7	
	Bentonite M39		86.7	
	Bentonite M40a	88.4	89.0	0.7
	SWy-1		73.4	
	STx-1	71.0	71.8	1.1
	Bentonite M46		91.2	
	Bentonite M47	95.2	98.4	3.3
	Bentonite M48	95.0	94.5	-0.5
	Ca-bentonite M50	100.1	102.2	2.1
	Bentonite Otay	83.2	92.4	10.0
	Bentonite oxidizable blue	61.0	65.1	6.3
	Bentonite Polkville	84.8	85.2	0.5
	Bentonite Schwaiba		87.3	
	Bentonite Upton	69.9	74.9	6.7

3.8.6. Other methods for clay investigation

Electron microscopy

Impact of an electron on a sample can result in various processes (Fig. 3.16).

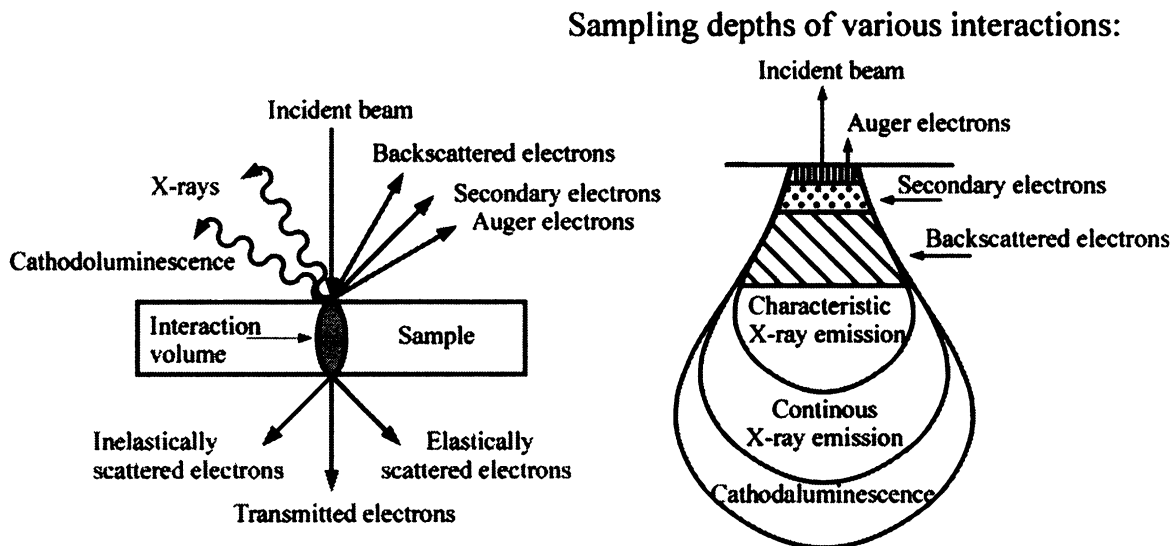


Fig. 3.16 - Results of electron interaction with a sample

- Backscattered electrons are formed on atoms nearly normal to the incident beam. Number of backscattered electrons is directly related to the atomic number of the target atom. Backscattered electrons are used for surface element distribution analysis.
- Secondary electrons are produced by ionization and have a low kinetic energy related to the atomic orbital the electron was loosed from. Only the atoms near the surface emit secondary electrons. Changes in topography (larger than sampling depth) change the yield of secondary electrons enabling topography exploration.
- Auger electrons are formed after emission of secondary electrons when vacancies are filled by drop of an electron from a lower energy shell (more distant from the nucleus). The drop leads to energy surplus and this is released by emission of a new – Auger – electron. The electron energy is unique for each element. Auger electron energy analysis informs on the specimen composition.
- X-rays are produced when secondary electron vacancies are filled by drops of lower energy electrons and the surplus in energy is released in the form of X-ray radiation. Released radiation is unique for each element. X-ray emission analysis informs on specimen composition.
- Cathodoluminescence occurs when high-energy electrons return to ground state with simultaneous light emission.
- Transmitted electrons pass through specimen without interaction, in proportion to the sample thickness.

- Elastically scattered electrons (without energy loss) are deflected by the specimen from incident beam path, according to Bragg's law. The observed diffraction pattern (spots) informs on the crystal orientation, atomic arrangement or the phases present.
- Inelastically scattered electrons pass through the specimen with a loss of energy. Energy loss is related to the elements which interacted with the passing electron. It is characteristic for the element and its bonding state. Inelastically scattered electrons inform on the composition and bonding state (i.e., the oxidation state). Inelastic scattering is also related to the atomic spacing in the specimen resulting in the presence of light and dark lines (Kikuchi Bands).

The source of electrons is a tungsten filament, LaB₆ or a field emission gun. The whole electron pathway has to be evacuated to avoid interaction with gas and other molecules (though low-pressure devices are developed recently). The beam is accelerated and focused in the system of electromagnetic lenses to reach the sample. According to the interaction observed, several electron microscopies are distinguished:

- TEM – transmission electron microscopy
- SEM – scanning electron microscopy
- REM – reflection electron microscopy
- STEM – scanning transmission electron microscopy

Electron microscopy is mainly used for morphological observation and chemical composition determination. Concerning the clay minerals, it is of lower importance. All smectites exhibit sponge-like morphology and wide variation in chemical composition which makes identification by electron microscopy impossible.^{158,159}

Thermal analysis

Thermal analysis is based on observation of processes taking part during programmed sample heating. The temperature is usually programmed as a linear function of time. When no thermal effect is present, the difference in the sample and the standard temperatures equals zero (zero line). Chemical changes are thermodynamically classified into endothermic and exothermic processes. The change in the sample temperature is directly related to the process taking part in its volume. The methods of thermal analysis are:

- DTA (differential thermal analysis) observes differences in thermal behaviour of the sample and a standard (usually corundum – Al₂O₃). During the endo/exothermic processes, the difference in the sample-standard temperatures is not null. Endothermic processes are registered under the zero line and exothermic ones above it. Every thermally active mineral exhibits one or more thermal effects present in a characteristic temperature interval. Observing the character, number and location of thermal effects enables identification of minerals (in comparison with etalons or the literature).
- DTG (differential thermal gravimetry) describes thermal processes from quantitative point of view. The sample weight is observed as the function of heating. Thermo-balances measure sample weight continuously through the heating program. Thermal gravimetry (TG) and differential thermal gravimetry (DTG) provide the same amount of information. Nevertheless, differential

thermal gravimetry enables a better resolution of neighbouring thermal processes.

The furnace space is heated electrically. Common temperature limits are 1000 °C (or 1200°C) for classical thermal analysis and 1500 °C (resp. 1600 °C) for the high-temperature version. Clay minerals mainly exhibit dehydration and dehydroxylation endotherms and exotherms connected with structural rearrangements. Kaolinite dehydroxylates in 550–570 °C interval and structural changes are pronounced in 970-980 °C interval. Smectites dehydrate in 130-170 °C interval (first solvating shell is released). The second dehydration step is at 210 °C when the second hydration shell is extracted and divalent cations are left unsolvated. Dehydroxylation is found within 680 - 700 °C interval.⁶⁸

Mössbauer spectroscopy

Atom nucleus is built by nucleons arranged in distinct energy levels. The energy levels are influenced by the atom environment causing changes in the energy levels or their splitting. Nucleons can be excited to higher energy levels by absorption of gamma rays and their deexcitation leads to emission of radiation. Free nucleus recoils during absorption/emission due to momentum conservation. Therefore, the emitted gamma ray has a lower energy than the nuclear transition and resonance of another identical nucleus is impossible. Mössbauer discovered (in 1958) that, when atoms are fixed within a solid matrix, the recoil and Doppler broadening (due to thermal motion) are eliminated and the resonance transition is possible. The recoil can further be lowered by cooling the sample to 77 K (liquid nitrogen temperature) or to 4 K (liquid helium temperature).

The quality of Mössbauer spectra is related to the average lifetime of the excited state (the resolution) and the relative number of recoil-free events (the signal strength). The Mössbauer effect is only detected in isotopes with very low excited states. Spectra are commonly measured for ⁵⁷Fe iron isotope which has a 2.14 % natural abundance. The probing gamma-ray source has to be a radioactive atom decomposing to an excited isotope detected by Mössbauer spectroscopy (⁵⁷Co for ⁵⁷Fe detection). Modulation of radiation is achieved by Doppler effect when the radioactive source oscillates with respect to sample at a velocity of a few mm/s. The spectrum is recorded as the transmission counts in relation to the source motion (mm/s, related to the radiation energy). Use of transmitted gamma-rays restricts the sample thickness.

The energy levels of an atom are modified by the environment in three ways:

- Isomer shift: the interaction of nucleus with electron shell influences the nuclear energy levels. The alteration is characterized by the isomer shift (for ⁵⁷Fe quoted relatively to alpha-iron at room temperature). The isomer shift causes a shift of the whole spectrum. It is useful for determining the valency state, ligand bonding states, electron shielding and the electron-drawing power of electronegative groups.
- Quadrupole splitting rises from the presence of an asymmetric electric field (the nucleus is exposed to an electric field gradient). The gradient splits the nuclear energy level of the excited state and the spectra exhibit double peaks of identical

intensity. Quadrupole splitting is sensitive to the oxidation state, the coordination number and symmetry of the surrounding environment.

- Magnetic splitting arises from the presence of a magnetic field (Zeeman splitting). The ^{57}Fe energy level of the excited state is split into a quartet and the fundamental state into a doublet. The spectrum exhibits a sextet. The separation is related to induction of a field.

Application of Mössbauer spectroscopy to clay mineral investigation is often complicated by the presence of admixtures, lower contents of iron in clay mineral (kaolinite), poor magnetic ordering and the presence of preferred orientation causing unequal doublet line intensities. Clay minerals rich in iron are glauconite, celadonite or nontronite. Mössbauer spectroscopy is useful tool for iron oxides investigation. The spectra can be fitted in several manners. The “minimal” model fits only as many Lorentz profile functions as necessary and its result is considered consistent and serviceable. The spectra can also be fitted on the basis of information obtained from other methods additionally used (e.g.: FTIR).^{160,161,68}

Nuclear magnetic resonance (NMR)

NMR observes transitions between energy levels of the nucleus in a strong magnetic field. Nuclei are oriented according to the magnetic field applied while the sample rotates. The Zeeman effect splits the energy of the excited state. The energy needed for transition is in the range of radio-electromagnetic radiation. The nucleus is shielded by electrons which are in interaction with the surrounding ligands. The chemical shift describes the extent of electron shielding ability in relation to a standard where the atom is bound in a symmetric environment (standards involve, e.g.: $(\text{CH}_3)_4\text{Si}$ for ^{29}Si and $\text{Al}(\text{H}_2\text{O})_6\text{Cl}_3$ for ^{27}Al), therefore, the nearby arrangement can be detected. Atoms with even numbers of protons and neutrons are NMR invisible. Atoms with odd numbers of protons and neutrons have complicated NMR spectra. Thus only the elements other than these are investigated. Concerning clay minerals, NMR of silicon and alumina are investigated (^{29}Si , ^{27}Al). Nevertheless, the NMR spectra of solid matrices, compared with liquid samples, are enriched by new features (dipolar interaction, quadrupole interaction and anisotropy of chemical shift). The new method for investigation of solid phases is MAS NMR (Magic-Angle Spinning Nuclear Magnetic Resonance).

3.9. Statistical methods, evaluation of results

Information on the sample composition or properties is obtained by measurement. Even if the sample is homogeneous, replicate measurements lead to different results. The result is composed of information and noise and is subject to an error of measurement.

The errors are:

- random: they cannot be determined in advance, occur randomly and are described by some distribution function.
- systematic: they are commonly functions of time and shift all the results in the same manner (to higher or lower values). They can be identified when the data are compared with the same data set obtained using a different measuring method and/or a different instrument.

- gross: this occurs when one or more results significantly differ from the rest and is caused by instrumental and/or human failures during the experimental work. Gross errors must be avoided.

A determination is considered to be accurate, when the systematic error is below a permissible value and precise when the random error does not exceed the permitted level. Acceptably accurate and precise results are called reliable and the reliability is generally enhanced by increasing the number of parallel measurements and by comparison of the sample measurements with those on reliable standard materials.

Model of measurement:

Experimental data are statistically evaluated using a suitable model of measurement, see Table 3.9).

Table 3.9 - Models of measurement

Model	Expression	Note
Additive	$x_i = \mu + \varepsilon_i$ (3.50)	omits sample variability, random errors can be positive or negative
Multiplicative	$x_i = \mu \cdot \exp(\varepsilon_i)$ (3.51)	results of measurement are positive only, scattering grows in respect to measured x_i
With systematic error	$x_i = \mu + \varepsilon_i + a$ (3.52)	systematic error cannot be determined if x_i is measured at only one μ level

x_i – is observation of i-th measurement
 μ – location (correct observation)
 ε_i – random error
 a – constant (systematic error)

Data exploration (concerning the additive model)

Before any statistical testing is performed, it has to be assured that the data are:

1. Sufficient
2. Independent
3. Homogeneous (results are of the same distribution)
4. All the results have the equal chance of being chosen

The minimal size of a data set can be determined in many ways. For example, to reach a desired relative error,

$$n_{\min} = \frac{g_2(x) - 1}{4\delta^2(s)} + 1 \quad (3.53)$$

n_{\min} – minimal size of the data set

$g_2(x)$ – shape (sharpness) of the set distribution

$\delta(s)$ – relative error (standard deviation, commonly $\delta(s)=0.1, 10\%$)

The minimal size of a data set for normal distribution (the most commonly used) is above 50 measurements. Replicate measurements commonly performed are insufficient.

“Independent data” requirement is commonly violated by measuring device instability, setting of measurement, sample volumes, temperature, contamination of the chemicals or by restrained sample choice. Dependent data identification is performed using autocorrelation coefficient of the first order.

Outliers are data which are subject to a gross error. They have negative influence on evaluation and therefore they have to be identified and excluded.

Graphical exploration is performed by:

1. Diagram of dispersion is a one dimensional graph where the results are shown on the x-axis. The graph points to data grouping and suspected outliers.
2. Box plot is graphical representation of robust characteristics of data set (data are ranked according to their value, specific positions dividing the set according to the percentage content of the results are called quantiles). A box plot is a rectangle containing 50% of the results (data lying between 25 and 75% quantiles, means between lower and upper quantile). The rectangle height equals \sqrt{n} . Median (50% quantile) is marked as the vertical line dividing the quartile rectangle. The lower and upper inner borders (B_L and B_U) are marked out of the quartile box as horizontal lines ended by short vertical lines and are calculated as:

$$B_L = \tilde{x}_{0.25} - 1.5 (\tilde{x}_{0.75} - \tilde{x}_{0.25}) \quad (3.54)$$

$$B_U = \tilde{x}_{0.75} + 1.5 (\tilde{x}_{0.75} - \tilde{x}_{0.25}) \quad (3.55)$$

$\tilde{x}_{0.25}$ – lower quartile (border of 25% quantile)

$\tilde{x}_{0.75}$ – upper quartile (border of 75% quantile)

Data lying out of the upper and lower inner borders are suspected to be outliers and are marked as circles. Box plots also indicate the symmetry or declination of data set and outliers.

Note: graphical indication of outliers can also be performed by graph of quantiles, symmetry, half-sums and other.

3.9.1. Data set characteristics

Each random selection (data set fulfilling the conditions noted above) is characterized by location, scale (data dispersion), and data distribution. An additional information is the shape of distribution. These are the selection characteristics. The way the data are distributed around location is described by distribution function $f(x, \theta)$ concerning continuous random variable or by probability function $p(x, \theta)$ for discrete variable. The θ is the vector of parameters formed from the location, scale and shape. The aim is to determine appropriate estimates of the parameters. The criteria of estimation quality are:

- Consistence: The estimate is consistent when the probability of data being distinct from the real value is arbitrary small, equal to 1 (valid for sufficiently sized selections).
- Impartiality: Location of a given set with n members is equal to the estimate.
- Efficiency: The estimate is efficient when the dispersion around the location is minimal among all the other estimates.

Point estimates of location and scale

Point estimates are prescribed mathematically and result in the most probable observation of the location and scale. Application of the proper location estimate is driven by distribution of the data set (e.g.: the same precision of the estimate using median for normal distribution, 1.6 more measurements have to be performed than using selection average). Some point estimates of location and scale are shown in Tables 3.10 and 3.11.

Table 3.10 - Location estimate

Location estimate	Equation	Note
Selection average	$\bar{x} = \frac{1}{n} \sum_{i=1}^n x_i$ (3.56)	so called first general moment
Modus	$\hat{x}_M = \max(x_1, x_2, \dots, x_n)$ (3.57)	maximum on distribution function
Selection median	odd membered selection: $\tilde{x}_{0.5} = x_k, k = (n+1)/2$ (3.58)	robust guess of location
	even membered selection: $\tilde{x}_{0.5} = (x_k + x_{k+1}), k = (n)/2$ (3.59)	
Half-sum	$x_p = (x_1 + x_n)/2$ (3.60)	average of maximum and minimum
n – number of measurements		x_i – i th measurement

Table 3.11 - Scale estimate

Scale estimate	Equation	Note
Selection variance	$s^2 = \frac{1}{n-1} \sum_{i=1}^n (x_i - \bar{x})^2$ (3.61)	so called second central moment
Variance	$\hat{\sigma}^2 = \frac{1}{n} \sum_{i=1}^n (x_i - \mu)^2$ (3.62)	Square root of variance is standard deviation
Average absolute deviation	$d = \frac{\sqrt{\pi}}{\sqrt{2}} \left(\frac{1}{n} \sum_{i=1}^n x_i - \mu \right)$ (3.63)	
n – number of measurements		\bar{x} - selection average
x_i – i^{th} measurement		μ – location

Interval estimates of location and scale:

Interval estimates offer more information. The position of a parameter is marked by two values L_1 and L_2 which are borders of a confidence interval. It shows with the selected probability $(1-\alpha)$ the interval where the real observation is located ($P(L_1 < \theta < L_2) = 1-\alpha$). Parameter α is called the level of significance.

The confidence intervals are:

- narrower with wider selection (growing n)
- narrower with smaller variance of selection
- wider with higher statistic certainty ($1-\alpha$) chosen

Confidence interval of normal distribution can be calculated:

$$\bar{x} - 2 \frac{\sigma}{\sqrt{n}} \leq \mu \leq \bar{x} + 2 \frac{\sigma}{\sqrt{n}} \quad (3.64)$$

\bar{x} - selection average

σ - standard deviation

n - number of measurements

μ - location

3.9.2. Data distribution

Identification of data distribution

Histogram is the oldest tool for evaluation of the distribution. The data are ranked according to their value. The X-axis of graph is linearly divided. The number of results lying in each interval is marked on the y-axis in the form of columns. The quality of histogram depends on the X-axis interval width. (note: data distribution can be evaluated by many other methods, such as quantile-quantile graph, rankite graph, Poisson's graph etc.)

Types of distribution

Poisson distribution is most often found during observation of a rare phenomenon (e.g.: in particle counters). The probability function is defined by:

$$p(x, \lambda) = \frac{\lambda^x \cdot e^{-\lambda}}{x!} \quad (3.65)$$

x - discrete random variable

λ - characterize central value and variance.

The best estimate of the central value is:

$$\hat{\lambda} = \frac{\sum_{x=1}^k n_x \cdot x}{n} \quad (3.66)$$

n - number of measurements

x - result of measurement

n_x - number of realisation of result x

The variance is calculated:

$$D(\hat{\lambda}) = \lambda/n \quad (3.67)$$

Normal distribution is the most common model of random continuous variable distribution. Additive model of measurement is considered and the result is composed of information and random independent errors. The normal distribution function is:

$$f(x) = \frac{1}{\sqrt{2\pi\sigma^2}} \cdot \exp\left\{-\frac{(x-\mu)^2}{2\sigma^2}\right\} \quad (3.68)$$

x – variable, $-\infty < x < \infty$

μ – location

σ^2 – variance

The best estimate of the location of normal distribution is the set average, \bar{x} and of scale is the set variance, s^2 .

Rectangular distribution is the simplest distribution of variable which appears in a selected interval ($a-h \leq x \leq a+h$). The distribution function is:

$$f(x) = \frac{1}{2h}, a-h \leq x \leq a+h \quad (3.69)$$

The best estimate of location is half-sum x_p and the estimate of scale is:

$$\hat{h}_0 = \frac{(n+1)}{(n-1)} \cdot \frac{(x_{\max} - x_{\min})}{2} \quad (3.70)$$

n – number of measurements

x_{\max} – maximal observation

x_{\min} – minimal observation

Other distributions are e.g.: Laplace, exponential, log-normal etc. Note: if the data are of other than normal distribution, the evaluation is complicated. The data can be transformed to lower the variance and improve symmetry. To interpret the results of analysis performed with transformed data, a backward transformation has to be found.

Confirmation of data normality:

The majority of statistical evaluation procedures requires random independent data of normal distribution. Normality of distribution can be tested (tests are less sensitive than diagnostic graphs).

Shapiro-Wilk test: for 3-50 membered set the mathematical expression of test statistics is:

$$W = \frac{\left[\sum_{i=1}^n a_i \cdot x_{(i)} \right]^2}{\sum_{i=1}^n (x_i - \bar{x})^2} \quad (3.71)$$

a_i – is related to rank statistics of expected normal distribution (table values)

If W is lower than critical $W_{1-\alpha}$ quantile the normality hypothesis is rejected.

Kolmogorov-Smirnov (KS) test is used to decide if the set originates from a population with a specific distribution. The KS test can be applied only to continuous distributions and tends to be more sensitive near the center than at the tails of the distribution. Testing requires full specification (location, scale, shape). The test statistic is:

$$D = \max_{1 \leq i \leq N} \left(F(Y_i) - \frac{i-1}{N}, \frac{i}{N} - F(Y_i) \right) \quad (3.72)$$

F – is theoretical cumulative distribution of tested distribution

If D is higher than the critical table value, then the distribution identity is rejected.¹⁶²

3.9.3. Statistic testing

Statistic hypothesis is presumption on probability distribution of one or more random variables.

Statistic hypothesis test is a procedure which prescribes the decision on a statistic hypothesis. Testing procedure contains null hypothesis H_0 and alternative hypothesis H_A formulating the goal of testing. Alternative hypothesis is accepted when null hypothesis is rejected. The equation called test statistic is constructed to decide on null hypothesis validity. If the result falls into acceptance region, null hypothesis is accepted. If the result falls into a critical region, the null hypothesis is rejected and an alternative hypothesis is accepted.

Level of significance: The probability of rejecting null hypothesis is called level of significance - α . It is commonly expressed as $100 \cdot \alpha\%$ level of significance (commonly 0.5).

The testing procedure is:

1. Formulation of null hypothesis and alternative hypothesis
2. Choice of significance level α
3. Selection of test statistic
4. Determination of critical region
5. Random selection, calculation of test statistic
6. Decision on hypothesis

Rejection of a valid null hypothesis creates error of the first kind. Acceptation of invalid null hypothesis creates error of the second kind. Generally, when null hypothesis is not rejected on $\alpha=0.5$, there is no significant difference between the theoretical and selected parameter. When the null hypothesis is rejected on $\alpha=0.1$, the difference between the theoretical and selected parameter is statistically different. When null hypothesis is rejected on $\alpha=0.5$ but not on $\alpha=0.1$, the test did not provide sufficient information for decision.

Testing selection parameters

Hypothesis on selection location and scale is commonly tested while normal distribution is assumed. A common goal in analytical chemistry is comparison (e.g.: of two instrumental methods or laboratories, of two materials, etc.). In this case similarity of distributions and parameters of location and scale is tested. Conformity of two

selections (X, Y) location is performed using Student's t-test where $H_0: \mu_x = \mu_y$, and $H_A: \mu_x \neq \mu_y$. In the case of different dispersion ($\sigma_x^2 \neq \sigma_y^2$) and when the data are measured with different precision, the test statistic is:

$$T_2 = \frac{|\bar{x} - \bar{y}|}{\left[\frac{s_x^2}{n_x} + \frac{s_y^2}{n_y} \right]^{1/2}} \quad (3.73)$$

\bar{x}, \bar{y} – selection average

$s_{x,y}^2$ – selection variance

$n_{x,y}$ – number of measurements

Conformity of scale is performed using F-test (note: sensitive to normality condition):

$$F = \max\left(\frac{s_x^2}{s_y^2}, \frac{s_y^2}{s_x^2}\right) \quad (3.74)$$

$s_{x,y}^2$ – selection variance

The results of test statistics are compared with table values and a conclusion on conformity is made.

Multivariate random variable:

Multivariate random variable is a vector $\xi(\xi_1, \xi_2, \dots, \xi_n)$ described by united distribution function (the probability that all the components of a vector are lower than components of a selected vector). The relationship between components of a vector is revealed by covariance (the measure of the linear combination intensity):

$$\text{cov}(\xi_i, \xi_j) = E(\xi_i \xi_j) - E(\xi_i)E(\xi_j) \quad (3.75)$$

Covariance can be both positive and negative, for non correlated compounds the covariance equals zero (note: covariance for other than linear combination may also result in zero). Another measure of linear combination intensity is the correlation coefficient which reveals positively, negatively and non-correlated compounds. Multivariate data are explored graphically or by PCA (principal component analysis, when the data are strongly related).

ANOVA (analysis of variance) evaluates the significance of variability sources in data (e.g.: device, operator and sample preparation etc.). Data scattering is distributed into known sources of variability and unknown (concerned as random):

$$y_{ij} = (\mu + \alpha_i) + \varepsilon_{ij} \quad (3.76)$$

y_{ij} – result of measurement

μ – location

α_i – variability of known source

ε_{ij} – variability of unknown source (random error)

Testing requires the selection of a model. Models with fixed effects are used when information on significance of known source of variability is stressed. Models with random effects are tested when sources of variability are chosen from a group of all possible sources.

If only one variability source is inspected, one-way ANOVA is applied. The source of variability has K levels of realization, each with n_i measurements performed. Random errors ε_{ij} are assumed independent and of normal distribution, $N(0, \sigma^2)$. The average on level i is:

$$\hat{\mu}_i = \frac{1}{n_i} \sum_{j=1}^{n_i} y_{ij} \quad (3.77)$$

and whole average is:

$$\hat{\mu} = \frac{1}{K} \sum_{i=1}^K \hat{\mu}_i \quad (3.78)$$

than estimate of α effect is:

$$\hat{\alpha}_i = \hat{\mu}_i - \hat{\mu} \quad (3.79)$$

A limiting condition is applied:

$$\sum_{i=1}^K n_i \cdot \alpha_i = 0 \quad (3.80)$$

The total variance is:

$$s_c = \sum_{i=1}^K \sum_{j=1}^{n_i} (y_{ij} - \hat{\mu})^2 \quad (3.81)$$

And it can be decomposed into variance between levels (s_T) and variance within the level (s_R):

$$s_T = \sum_{i=1}^K n_i (\hat{\mu}_i - \hat{\mu})^2 \quad (3.82)$$

$$s_R = \sum_{i=1}^K \sum_{j=1}^{n_i} (y_{ij} - \hat{\mu}_i)^2 \quad (3.83)$$

Test statistic is:

$$F_e = \frac{s_T(N - K)}{s_R(K - 1)} \quad (3.84)$$

The result of test statistic is compared with the critical table values and the decision on null hypothesis $H_0: \alpha_i=0$ ($i=1, 2, \dots, K$) (the differences between levels are negligible) and alternative hypothesis $H_A: \alpha_i \neq 0$ ($i=1, 2, \dots, K$) is made. If null hypothesis is rejected, multiple comparisons can be performed and relations between levels can be revealed. Multiple comparison null hypothesis is $H_0: \mu_i = \mu_j$.¹⁶³

Multivariate ANOVA (MANOVA)

More variability sources can influence the measured variable. Moreover, the sources can be bound by interactions (e.g.: sources A,B,C and their interactions of the first order

AB, AC, AB and interaction of the second order ABC). Due to possible interactions, multivariate ANOVA requires more measurements to be performed in order to obtain a sufficient number of observations on each source combination and interaction. Null hypotheses on source insignificance are extended by hypotheses on factors interaction e.g.:

$$H_0^{AB} : \lambda_{11} = \dots = \lambda_{1k_2} = \dots = \lambda_{21} = \dots = \lambda_{2k_2} = \dots = \lambda_{k_11} = \dots = \lambda_{k_1k_2} = 0 \quad (3.85)$$

Total variance (for 3 sources of variability) is:

$$SS_T = \sum_i \sum_j \sum_r (x_{ijr} - \bar{x})^2 \quad (3.86)$$

Variance due to factor A, B, and C are:

$$SS_A = K \sum_{i=1}^K (\bar{x}_{i..} - \bar{x})^2 \quad (3.87)$$

$$SS_B = K \sum_{j=1}^K (\bar{x}_{.j.} - \bar{x})^2 \quad (3.88)$$

$$SS_C = K \sum_{r=1}^K (\bar{x}_{..r} - \bar{x})^2 \quad (3.89)$$

Residual variance is:

$$SS_R = SS_T - SS_A - SS_B - SS_C \quad (3.90)$$

The test statistic is:

$$F_A = \frac{SS_A \cdot (K-1) \cdot (K-2)}{(K-1) \cdot SS_R} = \frac{SS_A (K-2)}{SS_R} \quad (3.91)$$

Comparing the results of test statistics with the critical table values leads to a decision on the source significance.¹⁶⁴

When the distribution is not of normal distribution, then all the tests based on the assumption of normality are invalid. Non-parametric tests have to be used.

Non-parametric tests

Kruskal-Wallis rank based test

It is used for comparison of the distributions of two or more sets (continuous distribution of variable is assumed). The content of each set is marked ($o_{1...b}$ $p_{1...b}$ $q_{1...i}$ etc.). All the observations are consecutively mixed to form a single pool. The pool is ordered ascendingly and ranked from 1 to N (N is the total number of observations, the sum of the n_o , n_p , and n_q). For each selection, the sum of the ranks is calculated and the Kruskal-Wallis test determines whether the sums are different.

The test statistic is defined by:

$$H = \frac{12}{N(N+1)} \sum_{i=1}^k \frac{R_i^2}{n_i} - 3(N+1) \quad (3.92)$$

k – number of set

n_i – number of observation in the set (n_o, n_p, n_q)

N – total number of observations

R_i – sum of ranks of the set i (o, p, q)

Median test (Levene test)

The test searches for equal variances. The null hypothesis $H_0: \sigma_1 = \sigma_2 = \dots = \sigma_k$ is tested against alternative hypothesis $H_A: \sigma_i \neq \sigma_j$ (at least one pair varies). The median of each selection is determined and the observations in the set are substituted by the absolute values of differences in observations and median:

$$Z_{ij} = |Y_{ij} - \tilde{Y}_i| \quad (3.93)$$

\tilde{Y}_i - median of set i

The test statistic is:

$$W = \frac{(N-k)}{(k-1)} \cdot \frac{\sum_{i=1}^k N_i (\bar{Z}_i - \bar{Z}_{..})^2}{\sum_{i=1}^k \sum_{j=1}^{N_i} (Z_{ij} - \bar{Z}_i)^2} \quad (3.94)$$

\bar{Z}_i - the set average of Z_{ij}

$\bar{Z}_{..}$ - average of all Z_{ij}

Mann-Whitney U-Test

It uses the rank sums of two sets and similarity of the medians is tested. Again observations in each set are marked; a pool of all observations is constructed and ranked. The sums of the ranks for each set are calculated (T_a, T_b) and test statistics are calculated:

$$U_a = n_a(n_b) + 5(n_a)(n_a + 1) - T_a \quad (3.95)$$

n_a – number of observations in A selection

n_b – number of observations in B selection

T_a – sum of ranks of A selection observations

or:

$$U_b = n_b(n_a) + 5(n_b)(n_b + 1) - T_b \quad (3.96)$$

The test statistic, U , is the smaller of U_a and U_b and for sample sizes larger than 20:

$$z = \frac{[U - E(U)]}{\sigma} \quad (3.97)$$

where

$$E(U) = 5(n_a)(n_b) \quad (3.98)$$

and

$$\sigma^2 = [n_a(n_b)(n_a + n_b + 1)]/12 \quad (3.99)$$

The critical values are tabulated.¹⁶²

Wald-Wolfowitz test

Observations of each set are marked and ordered. The test observes whether the ordering is random or not. If the sets are of the same distribution, no grouping will be observed. Each group (run) of observations from one set is numbered.¹⁶⁵
The test statistic is the number of runs (groups).¹⁶⁶

4. Experimental

4.1. Samples

Analyzed clay samples are overviewed in the Table 4.1:

Table 4.1 - Clay samples analyzed in this work

Clay	Origin
STx-1, source clay	Texas, USA, delivered
SWy-2, source clay	Wyoming, USA, delivered
DR, Ca-, Mg-, Na-, Li-homoionic forms	Rokle, CZ, collected
CV1BE	Černý Vrch, level 1, CZ, collected
CV2BE	Černý Vrch, level 2, CZ, collected
CV3BE	Černý Vrch, level 3, CZ, collected
HJBE	Hájek, CZ, collected
STSTBE	Stránce, CZ, collected
Illite Füz	Füzéradvány, HU, collected
ME82	Kadaň, CZ, collected

4.1.1. Reference samples from Source Clays Repository

The Source clays standards were investigated in detail and the literature is accessible at <http://clays.org/sourceclays/SourceClaysCCM.html> . The chemical data stated below are published also at: <http://www.agry.purdue.edu/cjohnston/sourceclays/chem.htm> .

STx-1:

STx-1 was taken for analysis as delivered. The material is from Manning formation, Gonzales County, Texas, USA. White powdered material forms suspensions easily; no admixtures are evident at the first sight. The chemical composition is stated in Table 4.2. The structural formula was determined as:



with -0.68 e octahedral charge and 0.00 e tetrahedral charge.

Table 4.2 - Chemical composition of STx-1 reference sample

Oxide	%	Oxide/Element	%
SiO ₂	70.1	CaO	1.59
Al ₂ O ₃	16.0	Na ₂ O	0.27
TiO ₂	0.22	K ₂ O	0.078
Fe ₂ O ₃	0.65	F	0.084
FeO	0.15	P ₂ O ₅	0.026
MnO	0.009	S	0.04
MgO	3.69		

The XRD semi-quantitative analysis revealed the mineralogical composition as stated in¹⁶⁷ Table 4.3.

Table 4.3 - mineralogical composition of STx-1 reference sample

Mineral	Bulk material (content %)	<2 μm Fine fraction (content %)
Smectite	67	68
Opal-CT	30	30
Quartz		
Feldspar		
Kaolinite	3	2
Talc (?)		

The cation exchange capacity was determined as 84.4 meq/100g with the Ca²⁺ as the major exchange cation. The measurement of Borden and Giese by ammonia-electrode using fine fraction resulted in CEC of 89 meq/100g.¹²⁵ The infrared spectroscopy revealed the presence of quartz different from the silica phase and a trace of carbonate. The mean layer charge according to Mermut and Lagaly is 0.31 per (Si,Al)₄O₁₀ unit (0.62 per O₂₀(OH)₄ unit).¹⁵

SWy-2:

Also SWy-2 was analyzed as delivered. The material originates in Crook County, Wyoming, USA. The grey powdered material forms a sponge-like structure when soaked with water. Dark spots are visible on the bottom of the suspension. The chemical composition is in Table 4.4.

Table 4.4 - Chemical composition of SWy-2 reference sample

Oxide	%	Oxide/Element	%
SiO ₂	62.9	CaO	1.68
Al ₂ O ₃	19.6	Na ₂ O	1.53
TiO ₂	0.090	K ₂ O	0.53
Fe ₂ O ₃	3.35	F	0.111
FeO	0.32	P ₂ O ₅	0.049
MnO	0.006	S	0.05
MgO	3.05		

The structural formula is:



with -0.53 e of octahedral charge and -0.02 e tetrahedral charge. The mineral composition of the material according to Chipera and Bish¹⁶⁷ is in Table 4.5. The CEC was determined as 76.4 meq/100g with Na⁺ and Ca²⁺ as the major cations. The CEC determined by ammonia electrode in the fine fraction is 85 meq/100g.¹²⁵ The infrared spectroscopy revealed quartz and carbonate admixtures and the layer charge determined by Mermut and Lagaly is 0.32 per (Si,Al)₄O₁₀ unit (0.64 per O₂₀(OH)₄ unit).¹⁵

Table 4.5 - Mineralogical composition of SWy-2 reference sample

Mineral	Bulk material (content %)	<2 µm Fine fraction (content %)
Smectite	75	95
Quartz	8	4
Feldspar	16	
Gypsum		
Mica/illite	1	1
Kaolinite/chlorite		

4.1.2. Collected clays

Bentonites and kaolins were collected in active open-pit mines in the Czech Republic, and the illite sample comes from the Füzérradvány deposit, near the city of Miskolc, Hungary. The group includes samples with high CEC, containing predominately smectite (CV, HAJ, ST, CEC) and materials of low CEC with predominant illite or kaolinite, where expandable structures can be present only as admixtures (Füz, ME82). The localities and the samples are described below.

CV – Černý Vrch:

The bentonite deposit is located W of Braňany, Czech Republic, the upper section is mostly composed of smectite with admixtures of calcite, quartz, plagioclase and goethite. The middle section contains rock fragments (silicified marl, quartzite, gneiss) and spheroidal siderite or ankerite, and the basal bentonite contains red-coloured kaolinite, siliceous-phosphorite concretions and calcite as admixtures. The smectite is characterized as a Fe-rich montmorillonite with Ca²⁺ and Mg²⁺ as the major interlayer cations.¹⁶⁸

- CV1BE: The sample was taken at the open pit base. The originally light blue sample gradually turned grey-blue. No macroscopic impurities were observed. It contains siliceous balls of various sizes (ranging from 2 cm to 8 cm) with rusty inner parts.
- CV2BE: Sample was taken from the first terrace from the bottom. The material was green-blue and gradually turned grey-green. No macroscopic impurities could be observed.
- CV3BE: The sample was collected in the upper part of an open pit where many colour variations could be found. The sample is green-brown and contains grains of a white material – most probably calcite. Calcite admixtures were found at the same height, with tiny crystals of calcite.

Hájek – Hájek:

The Hájek deposit is located 8 km NW from Karlovy Vary. The sample taken from this deposit had brown-yellow colour with rusty spots. White impurities of calcite could also be seen. Further operations with the sample revealed the presence of magnetic particles.

STSTBE – Stránc:

The bentonite deposit is situated south of the Nový Most. A green-coloured facies of bentonite is enriched in smectite, the red-coloured in silica.¹⁶⁸ Sample was taken from the uncovered wall of an open pit. Compact material started to split into smaller particles with sharp edges covered with rust. No further impurities were visible.

Illite Füz – Füzéradvány:

Illite from Füzéradvány, Hungary, was taken from the mining gallery. The sample is pure white with very small orange rusty spots. (note: no czech sample of illite could be chosen because there is no illite deposit in the Czech Republic).

ME82 – Kadaň:

The sample was taken from the open pit kaolin mine Merkur near Kadaň. It consisted of white and grey grains, had a sandy character and was easy to manipulate.

Mineralogical characterization of collected clay is summed up in chapter 5.2.4.

4.2. XRD analysis

XRD analysis was performed on several measuring devices with various settings and sample preparations.

4.2.1. Equipment

Institute of Inorganic Chemistry, Czech Academy of Sciences – XRD devices:

- Siemens D 5005, Burker AXS, Federal Republic of Germany, operating settings – Cu X-ray tube, water cooling, 40 kV, 45 mA, stage, sample holders for front loading, θ - θ geometry, graphite monochromator, scintillation detector.

Measuring programs:

- 2 – 80 °2 θ , step scan, 0.02 °2 θ step, 1s time per step, random – front loaded – powder sample,
- 2 – 20 °2 θ , step scan, 0.02 °2 θ step, 1s time per step, oriented – glass slide – specimen, EG treated samples
- PANalytical X'PertPRO, X'Celerator detector, Almelo, The Netherlands, operating settings – Co X-ray tube, water cooling, 40 kV, 30 mA, sample holders for front loading θ - θ geometry, semiconductor detector.
Measuring program:
 - 4 – 100 °2 θ , step scan, 0.02 °2 θ step, 106s time per step, accumulation of 10 diffraction patterns, random – front loaded – powder samples

- HT-RTG (high temperature XRD diffraction) measured with: PANalytical X'PertPRO with X'Celerator detector, Almelo, The Netherlands, operating settings – Co X-ray tube, water cooling, 40 kV, 30 mA, Pt heated support as sample holder in HTK16 Anton Paar temperature chamber, Graz, Austria (Fig 4.1)

Measuring program:

- starting temperature 25 °C, final temperature 300°C, heating step 5 °C, combination with collecting XRD pattern: temperature increase Δ 5°C, heating rate 60 °C/min, 5 min delay, measurement of pattern in the range 4 – 40 °2 θ , 0.02 °2 θ step, 60 s per step (18 min per diffractogram). Sample prepared as oriented specimen from suspension applied on the heating support. The conformity of programmed and real temperature in the temperature chamber is presented in the Fig. 4.2.

Faculty of Mining, Geology and Petroleum Engineering, University of Zagreb – XRD device:

Philips PW1830 generator, Philips Analytical X-Ray BV, Almelo, The Netherlands, operating settings – Cu X-ray tube, water cooling, 40 kV, 35 mA, stage, sample holders for back loading, 0-2 θ geometry.

Measuring programs:

- 2 – 70 °2 θ , step scan, 0.02 °2 θ step, 1s time per step, random – back loaded – powder sample
- 58 – 64 °2 θ , step scan, 0.02 °2 θ step, 10 s per step, measurement of 060 diffractions, random – back loaded – powder sample
- 2 – 40 °2 θ , step scan, 0.02 °2 θ step, 1s time per step, oriented – porous ceramics – specimen, EG saturated
- 2 – 26 °2 θ , step scan, 0.02 °2 θ step, 1s time per step, oriented – porous ceramics – specimen, DMSO treated
- 2 – 40 °2 θ , step scan, 0.02 °2 θ step, 1s time per step, oriented – porous ceramics – specimen, Li⁺ treated, heated to 300 °C
- 2 – 14 °2 θ , step scan, 0.02 °2 θ step, 1s time per step, oriented – porous ceramics – specimen, heated to 300 and 550 °C

Faculty of Science, University of Zagreb – XRD device:

PANalytical X'PertPRO, X'Celerator detector, Almelo, The Netherlands, operating settings – Cu X-ray tube, water cooling, 45 kV, 40 mA, sample holders for front loading, θ - θ geometry, semiconductor detector.

Measuring program:

- 3 – 80 °2 θ , step scan, 0.02 °2 θ , 43.5 s time per step, random – RTS – powder sample.

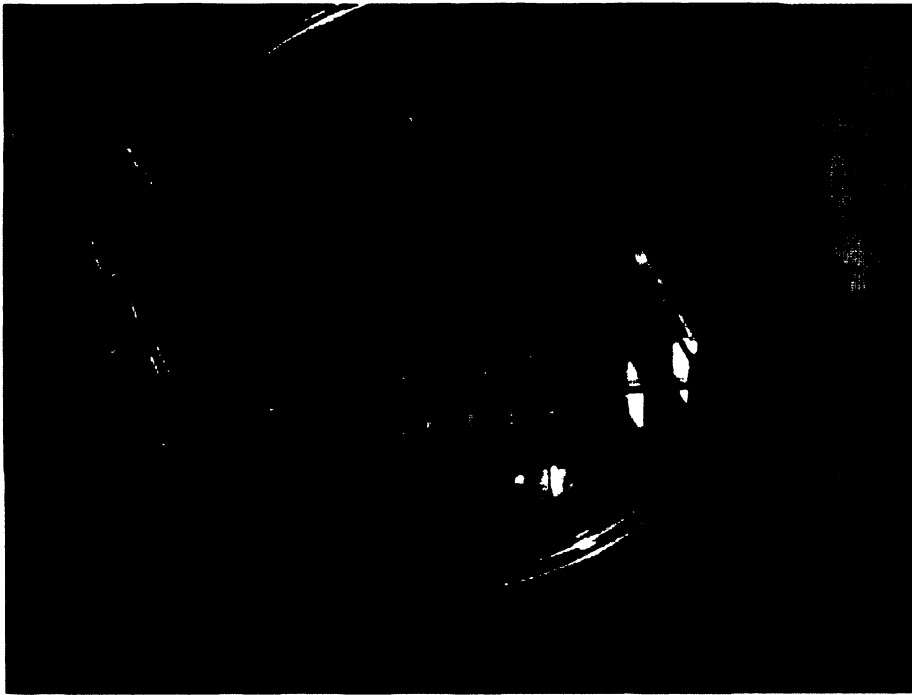


Fig. 4.1 - The construction of HTK16 Anton Paar temperature chamber, Graz, Austria with sample placed on Pt resistance-heated support and beam-knife mounted above

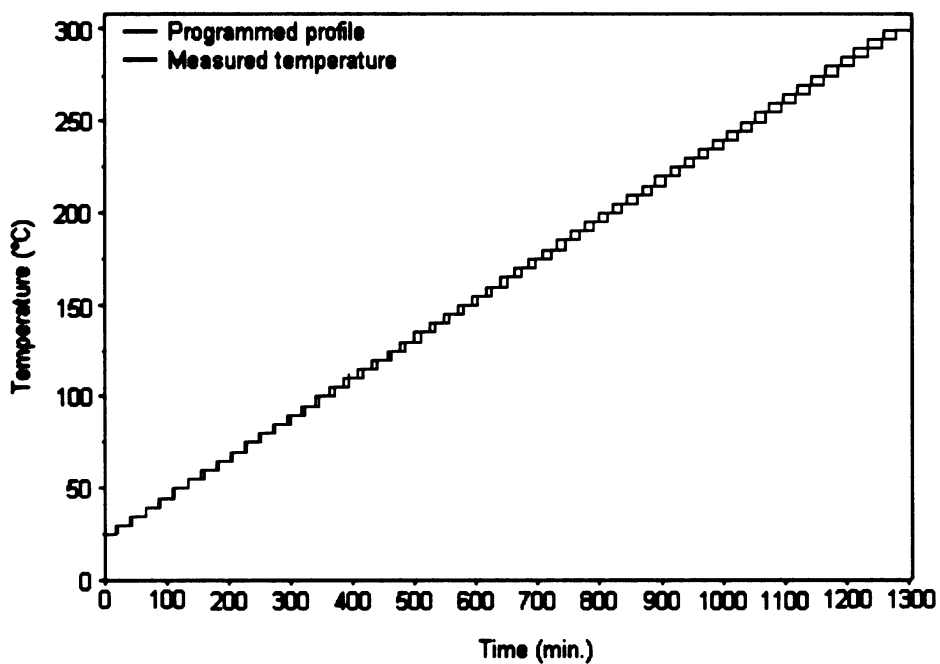


Fig. 4.2. - Correlation of programmed and real temperature in the Anton Paar HTK-16 temperature chamber

4.2.2. Specimen preparation

The random oriented specimens were prepared by

- Front loading
- Back loading
- RTS technique (Razor Tapped Surface Technique)

The oriented specimens were prepared as

- Glass slides
- Porous ceramics specimens
- Homoionic form preparation using porous ceramics specimens: The sample was dispersed using an ultrasound bath and an appropriate 4 N chloride salts solution was added. Proper dispersion was reached by overhead shaking overnight. The saturation step was followed by the washing step with distilled water. The sample was centrifuged and the supernatant was removed. Re-dispersion was performed and this procedure was applied three times. The last dispersion was used for the preparation of oriented specimen with porous ceramics support.
- Ethylene-Glycol (EG) expandability test was applied for 8 hours by saturation of oriented specimen in EG vapours (p.a. Lachema, Neratovice, Czech Republic) generated at 60 °C.
- Dimethylsulfoxide (DMSO) saturation: was performed on porous-ceramics oriented specimens. The sample was placed on a Petri dish wrapped with filter paper soaked in DMSO, covered and exposed to 70 °C temperature for 24 hours. Next 24 hours the sample was stored under ambient temperature.
- Heating procedures: the samples were heated to 300 or 550 °C for 2 hours in a furnace.

4.3. FTIR spectroscopy

FTIR spectra were obtained using a Nicolet Magna 760 spectrophotometer equipped with a DTGS detector. Accumulation of 32 scans in 4000 – 400 cm^{-1} region with 4 cm^{-1} resolution was used for qualitative evaluation of the octahedral and tetrahedral site occupancy of smectites. The samples were measured using potassium bromide (KBr) pellets in the transmission mode. The pellets were prepared by mixing 0.001 g of a sample with 0.3 g of optical grade KBr (Aldrich, Milwaukee, WI, USA) and pressed under a low pressure.

4.4. CEC determination

Source Clays Repository samples, STx-1 and Swy-2, were tested as supplied. The weight loss was determined by heating at 105°C for 24 hours and found to be 8.4% for STx-1 and 3.0% for SWy-2 sample.

Rokle bentonite, North-west Bohemia Czech Republic, was size separated by sedimentation in distilled water and a fine fraction (< 2 μm) was collected. Homoionic forms were prepared using appropriate salts ($\text{CaCl}_2 \cdot 2\text{H}_2\text{O}$, $\text{MgCl}_2 \cdot 6\text{H}_2\text{O}$, NaCl, LiCl) and the mass loss was determined by heating to 105°C for 24 hours (see Table 4.6).

Table 4.6 - Weight loss of homoionic DR sample by heating (105 °C/24h)

Sample	CaDR	MgDR	NaDR	LiDR
Weight loss (%)	14.0	11.2	8.0	7.5

The CEC values for collected clays were determined on the bulk sample, the sample after chemical removal of carbonates and the fine fraction after carbonates removal. The weight loss was determined for each type of sample by heating at 105 °C for 24 hours (see Table 4.7).

Table 4.7 - Weight losses of various types of collected clays

Weight loss (%)	Sample						
Sample	CV1BE	CV2BE	CV3BE	HAIJE	STSTBE	Illite Füz	ME82
Raw material	8.94	10.7	11.23	11.02	9.37	2.12	0.27
Raw material CO ₃ ²⁻ removed	6.57	8.34	9.2	8.66	7.96	1.92	0.28
<2 µm fraction CO ₃ ²⁻ removed	6.92	7.81	8.65	8.16	11.82	2.98	1.64

4.4.1. Copper trien method

Chemicals:

Anhydrous copper sulphate (CuSO₄·0 H₂O, p.a., Lachema Neratovice, Czech Republic) and triethylenetetramine (C₆H₁₈N₄, purum ≥ 97% (GC), Fluka Chemie, Buchs, Switzerland) were used for the preparation of stock solutions without further purification. The CuSO₄ content of anhydrous powder was determined chelometrically and the 5 % humidity content was found. Approximately 1.6 g of copper sulphate was dissolved in a volumetric flask and made to 1 litre with distilled water. The appropriate amount of trien was weighed using a syringe. All trien was quantitatively transferred to the volumetric flask and made to 100 ml with distilled water. The stock solution was finally prepared under continuous stirring in a 3 l beaker by mixing the two solutions of trien and copper sulphate. The coloured complex was formed immediately. The mixing of stock solution is shown in Table 4.8.

Table 4.8 - The stock solution mixing

Solution	A	B	C	D	E	F	G
CuSO ₄ (g), corrected for 5 % humidity content	1.5132	1.5135	1.5133	1.5135	1.5638	1.5650	1.5651
Trien (g), corrected for 3 % for of admixtures	1.4632	1.6097	1.8291	2.1950	1.4185	1.7023	2.1278
Resulting concentration (Cu, mol/dm ³)	0.009	0.009	0.009	0.009	0.009	0.009	0.009
Resulting concentration trien, mol/dm ³)	0.009	0.010	0.011	0.014	0.009	0.011	0.013
Molar ratio	1:1.05	1:1.15	1:1.3	1:1.6	1:1.0	1:1.2	1:1.5

Procedure:

Reference samples:

- **Centrifuged samples:** Approximately 0.110 ± 5 g of powdered dry sample was weighed out, transferred into a 50 ml volumetric flask. The sample was dispersed in 10 ml of distilled water. Ultrasonic bath and wortex were used if needed. Stock solution A, B, C or D was added in 6, 8 or 10 ml amounts (see Fig. 4.3). The sample was re-dispersed and the volume was fixed to 50 ml. The prepared suspension was left to react for approximately 15 minutes (strong aggregation occurred). The supernatant was carefully removed after centrifugation at 9800 rpm for 15 minutes. Supernatants were stored in PE flasks before analysis.
- **Filtered samples:** Approximately 0.110 ± 5 g of powdered dry sample was weighed out into a 25 ml beaker. The sample was placed in distilled water and left to soak overnight. The dispersion was swirled using a magnetic stirrer and 6, 8 or 10 ml of stock solution A, B, C or D were added. After 15 minutes of stirring, the suspension was allowed to settle and filtered through quantitative cellulose filters (Filtrak, grade 389, white stripe). The solid phase remaining on the filter was rinsed with distilled water. The supernatant volume was made to 50 ml in a volumetric flask. The samples were stored in glass flasks before analysis.

Reference samples (STx-1 and SWy-2) CEC experimental settings

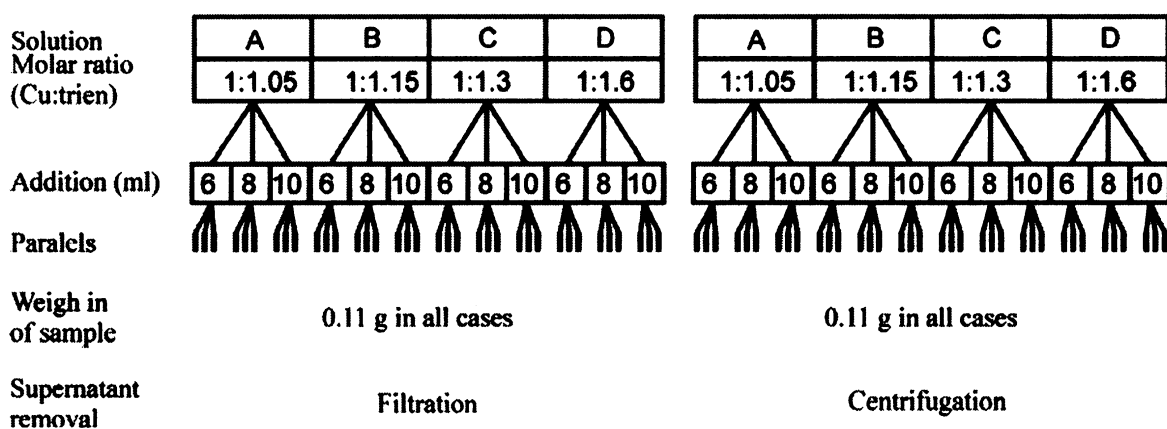


Fig. 4.3 - Experimental setting of reference samples

Rokle homoionic samples:

Approximately 0.110 ± 5 g of powdered dry sample was weighed out and transferred into a 50 ml volumetric flask and dispersed in 10 ml of distilled water. Ultrasonic bath and wortex were used if needed. Stock solution E, F, G was added in 6, 8, 10, 12 or 14 ml volume and the content was swirled again (see Fig. 4.4). The total volume was made to 50 ml with distilled water and left to stand for 15 minutes. The suspension was filtered using Filtrak white stripe paper and stored in glass bottles.

The experiments were carried out for each setting in three parallels except for the sodium form and solution G, where only two parallels were prepared, and the lithium form, where sample depletion allowed only one measurement.

Rokle homoionic(Ca^{2+} , Mg^{2+} , Na^+ and Li^+) samples CEC experimental settings

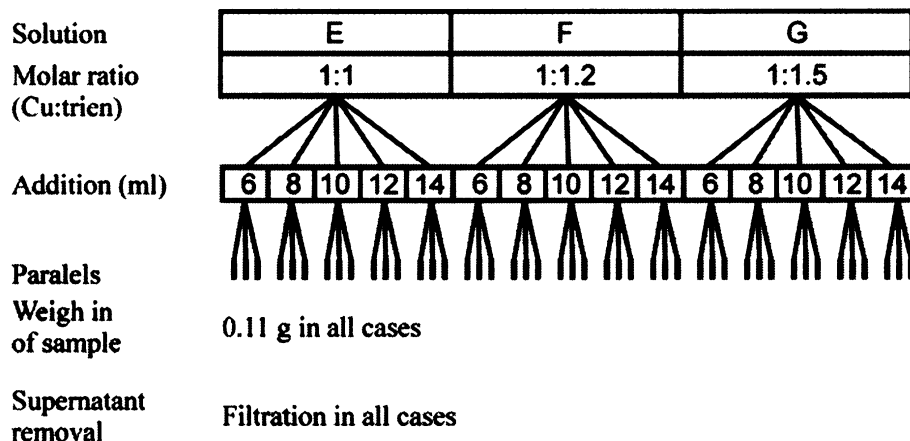


Fig. 4.4 - Experimental settings of Rokle samples

Collected samples:

A 0.009 M stock solution with 1:1 molar ratio was prepared by mixing 2.4990 g of copper sulphate pentahydrate ($\text{CuSO}_4 \cdot 5\text{H}_2\text{O}$, Lachema, Neratovice, Czech Republic) dissolved in 1 litre of distilled water with 1.5063 g of triethylenetetramine dissolved in 100 ml of distilled water ($\text{C}_6\text{H}_{18}\text{N}_4$, purum $\geq 97\%$ (GC), Fluka Chemie, Buchs, Switzerland). The bentonite samples (CVBE, STSTBE and HAJBE) were equilibrated with 8 ml of the stock solution. For Illite Füz and ME82 sample, 5 ml of the stock solution added were found satisfactory. The volume was made 50 ml with distilled water and the supernatant was separated by centrifugation. The samples were stored in PE bottles prior to the analysis.

Detection:

Atomic spectroscopy

AAS was performed using a flame AAS spectrometer Zeiss3 (Carl-Zeiss, Federal Republic of Germany) or an SP9 Atomic absorption spectrometer (Pye-Unicam Ltd., Cambridge, United Kingdom). The copper cations remained in the supernatant and the released magnesium ions were determined by atomic absorption and Ca^{2+} , Na^+ , Li^+ and K^+ by atomic emission spectroscopy. The atomization fuel was a mixture of acetylene and air. Concentrations in ppm were obtained using the calibration curve technique. The CEC_{Cu} was calculated from Cu^{2+} consumption and CEC_{sum} from the native cations released to the supernatant.

UV-Vis spectroscopy

UV-Vis was performed using a Perkin Elmer lambda 35 spectrophotometer (Perkin Elmer Inc., Waltham, MA, United States). The absorption maximum was determined at 576 nm (see Fig. 4.5). The samples were measured against distilled water and evaluated

using a calibration curve. The calibration curve was linear over a wide range of concentrations. The results were calculated as CEC_{UV-Vis} from the absorbance of the free Cu-trien complex.

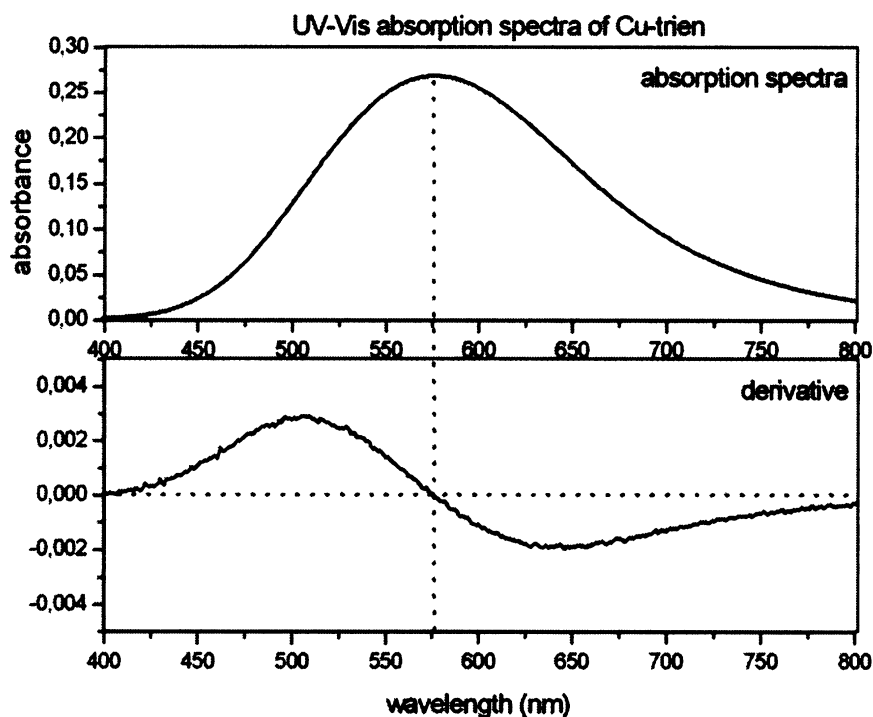


Fig. 4.5 - Determination of Cu-trien complex absorption maximum

4.4.2. Ammonium acetate method

Chemicals:

The ammonium acetate stock solution was prepared by dissolution of 154.2 g of ammonium acetate salt (CH_3COONH_4 , p.a., Kemika, Zagreb, HR) to obtain the 2 M concentration. A solution of ammonium chloride was used as the tracking agent (diluted solution, NH_4Cl , p.a., Kemika, Zagreb, HR). The washing steps were performed with a 30 % vol. mixture of ethanol (C_2H_5OH , 96%, p.a., Alkaloid ad., Skoplje, Macedonia) and distilled water. The chloride anions were detected using silver nitrate ($AgNO_3$, p.a., Kemika, Zagreb, HR). Ammonium was consecutively released from the sample by 15 % wt. sodium hydroxide solution ($NaOH$, p.a., Gram -mol d.o.o. Zagreb, 176.47g dissolved in 1 litre of distilled water, strong exothermic reaction). The 4 % wt. solution of boric acid (H_3BO_3 , p.a., Kemika, Zagreb, HR) was used as NH_4^+ trapping agent. Trapped NH_4^+ was titrated by 0.005 M solution of sulphuric acid (H_2SO_4 , Merck-Alkaloid, Skoplje, Macedonia) with methyl red (Merck, Darmstadt, Germany) and methyl blue (Acros Organics, Geel, Belgium), as the indicators.

The titration factor of sulphuric acid was determined using sodium carbonate (Na_2CO_3 , anhydrous, p.a., Kemika, Zagreb) and the methyl orange (Merck, Darmstadt, Germany), indicator. The sodium carbonate was weighed after water desorption (250 °C heating for 2 hours).

Procedure:

The measurement was performed in two parallels. Precisely 0.1 g of sample was taken for the analysis. Saturation by NH_4^+ cation was performed by 24 hr wetting in 10 ml of 2 M ammonium acetate solution with occasional steering. Saturation followed with three washings by 10 mL of ammonium acetate. The supernatant was always removed by centrifugation (3000 rpm for 5 minutes) and careful effusion. The third washing solution was enriched by few drops of ammonium chloride to track the access salt removal. The NH_4^+ access is washed with ethanol/water mixture. Triple washing should be sufficient. Silver nitrate check was used to detect the presence of chlorides.

Ammonium ions present in the interlayer of the sample were consecutively detected by the Kjeldahl method. The sample was transferred quantitatively using distilled water into a round bottle and 150 ml of 15% NaOH were added. The bottle was sealed and connected to a water-cooler. On the other side of the cooler, the condenser tip was placed in an Erlenmeyer flask just above the surface of a H_3BO_3 solution (2 ml, 4 % concentration). The round flask was placed on the heating element, water supply to cooler was opened and the heating element was switched on. Distillation was run until 100 ml of the distillation product were obtained. The condenser tip was rinsed with distilled water and four drops of methyl red and 1 drop of methyl blue were added to the distillation product in the Erlenmeyer flask, changing the colour to green. The solution was titrated with 0.005 M H_2SO_4 solution through the colourless to light pink colour. CEC was recalculated from H_2SO_4 consumption and corrected for water loss.

4.4.3. Silver thiourea method

Chemicals:

A solution of silver cations with 0.04 M concentration was prepared from silver nitrate (AgNO_3 , p.a., Kemika, Zagreb) by dissolution of 3.4016 g and making the total volume to 500 ml. The thiourea ($(\text{NH}_4)_2\text{CS}$, p.a., Kemika, Zagreb) solution was prepared by dissolving 15.2227 g of thiourea and fixing the final volume to 1000 ml. The stock solution of silver thiourea complex ($\text{Ag}(\text{TU})_2$) was prepared by slowly adding AgNO_3 solution to thiourea under constant stirring. The stock solution was stored no longer than two days.

Procedure:

Orientative experiments were carried out in order to determine the most suitable experimental settings (Table 4.9). The sample was weighed in an appropriate amount and the stock solution of $\text{Ag}(\text{TU})_2$ was added. The samples were shaken overnight, centrifuged and the supernatant was carefully removed for analysis. Supernatants were stored in PE bottles prior to the measurement which was performed within shortest time possible.

Table 4.9 - Experimental settings for collected sample using silver thiourea method

Sample	Weight (g)	Addition (ml)
CV1BE	0.6	50
CV2BE	0.4	50
CV3BE	0.3	50
H AJBE	0.4	50
STSTBE	0.4	50
Illite Füz	0.5	25
ME82	0.6	25
CV1BE < 2 µm	0.3	50
CV2BE < 2 µm	0.4	50
CV3BE < 2 µm	0.3	50
H AJBE < 2 µm	0.4	50
STSTBE < 2 µm	0.3	50
Illite Füz < 2 µm	0.5	25
ME82 < 2 µm	0.5	25

Detection:

The Ag⁺ ions were determined by atomic absorption spectroscopy using an SP9 Atomic absorption spectrometer (Pye-Unicam Ltd., Cambridge, United Kingdom). The atomization fuel was a mixture of acetylene and air. Concentrations in ppm were obtained using the calibration curve technique. The CEC values were calculated from differences in the Ag⁺ contents in the sample and the stock solution.

4.5. Statistical methods, evaluation of results

For each group of measurements the location and scale were determined.

Location:

- selection average
- median

Scale:

- minimum and maximum
- lower and upper quartile
- variance
- standard deviation

Data distribution was inspected using a box-plot, histogram and normality testing with Kolmogorov-Smirnov and Shapiro-Wilks test. The influence of the experimental conditions was tested with MANOVA, Kruskal-Wallis rank based test, median test, one-way ANOVA and Wald-Wolfowitz test. All the statistical procedures were performed using StatSoft.Inc (2005), STATISTICA, (software system for data analysis), version 7.1.

5. Results and Discussion

5.1. Sample treatment

Physical treatment:

- Disaggregating sample: the samples were dried on a heated support and gently crushed in an agate mortar to obtain a powder sample. The samples were stored in plastic containers or further processed.
- Size separation was performed by sedimentation in distilled water according to the Stokes law. The settling time for 2 μm fraction is 15.5 hours when taken in a 15 cm depth. The suspension was dried at 60 °C and crushed in an agate mortar or processed to obtain a homoionic form.

Chemical treatment:

- Carbonate removal: was performed on samples containing calcite and siderite. Chemicals: Acetic acid (CH_3COOH acid 99.5%, density 1050 g/1000 ml p.a. grade, TTT, HR), the stock solution was prepared from 57 ml of acetic acid diluted by distilled water to 1000 ml volume resulting in 1 M concentration. The buffer was prepared by mixing of 22.8 ml CH_3COOH (99.5%) diluted in 500 ml with 61 g of sodium acetate NaOOCCH_3 (anhydrous, p.a. grade, Kemika Zagreb) diluted in 500 ml of distilled water. The final volume was 1000 ml and pH 5. Procedure: Samples were dispersed in 200 ml of the acetate buffer and left to stand overnight. Approximately 200 ml of acetic acid were consecutively added dropwise with simultaneous steering and heating. The mixture was left to stand over weekend and then centrifuged (3500 rpm for 15 minutes). Excess salt was washed out with distilled water. Washing was performed three times. The samples were dried on a water bath.
- Homoionic form preparation was performed with a suspension of clay fraction. The 1 M solution of appropriate chloride was added (CaCl_2 , MgCl_2 , NaCl and LiCl , grade p.a., Lachema Neratovice, Czech Republic). The suspension was stirred using a magnetic stirrer for several hours and left to soak overnight. An addition of a salt solution caused flocculation. Clear supernatant was removed and a new portion of 1 M solution was added. The saturation steps were performed three times. The salt was washed with distilled water. The suspension was stirred, allowed to settle and the supernatant was carefully removed. This step was performed until the sample was no longer capable of settling. A few drops of 1 M salt solution were added (only the necessary amount to cause flocculation) and the supernatant was removed. The suspension was transferred to a dialysis membrane and dialysed to negative reaction with silver nitrate solution (AgNO_3 , chloride test). Homoionic samples were dried at 60 °C and powdered using an agate mortar. Note: the lithium homoionic form was prepared from sodium homoionic form (prepared as described above up to the dialysis step which was substituted by lithium saturation).

5.2. Mineralogy of collected clays

The mineralogical characterization was performed using XRD diffraction. The samples were dried on a heated support and gently crushed in an agate mortar. The diffraction patterns were evaluated according to Moore and Reynolds (1997). The mineral composition of the samples can be seen in Table 5.1. The diffraction patterns are given in Figs. 5.1 – 5.7.

Table 5.1 - Mineral composition of collected clays

Admixture	Sample						
	CV1BE	CV2BE	CV3BE	HAJBE	STSTBE	IlliteFüz	ME82
Clay	Smectite	+	+	+	+	+	
	Illite	+			+	+	+
	Kaolinite	+	+		+	+	
	Mix. m.						+
Non-clay	Quartz	+	+		+	+	+
	Anatase	+	+	+	+	+	
	Siderite		+		+		
	Calcite	+		+			
	Feldspar						+
	Hematite				+		

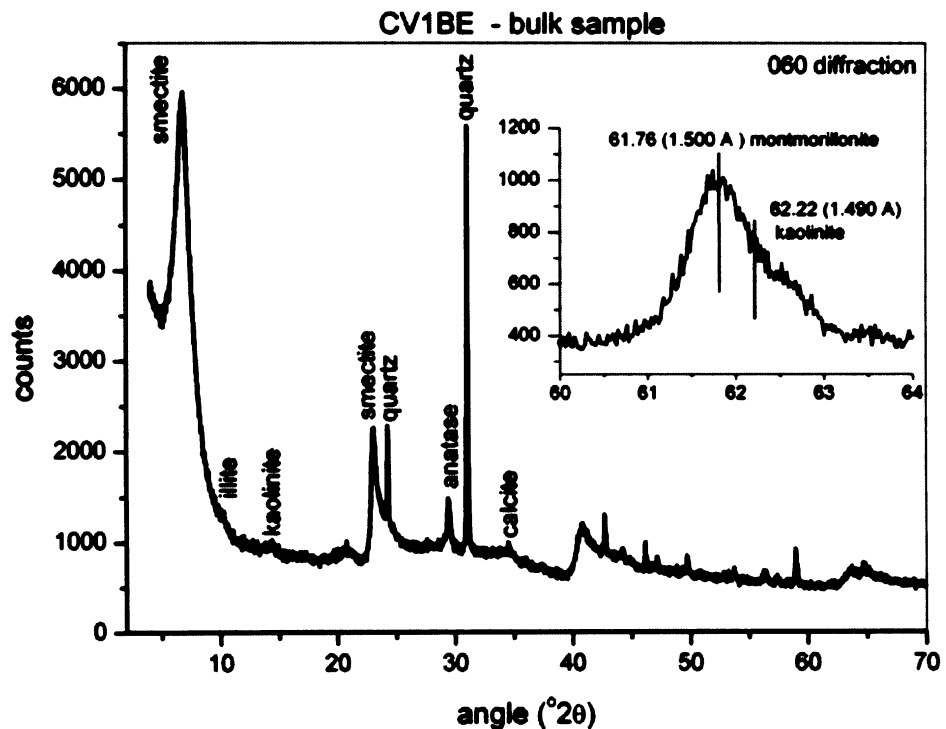


Fig. 5.1 - Mineralogical characterization of CV1BE (XRD pattern is based on 10 diffraction records using CoK α radiation). The insert shows the 060 diffractions of clay minerals (after carbonates removal in NaOAc, using CuK α radiation)

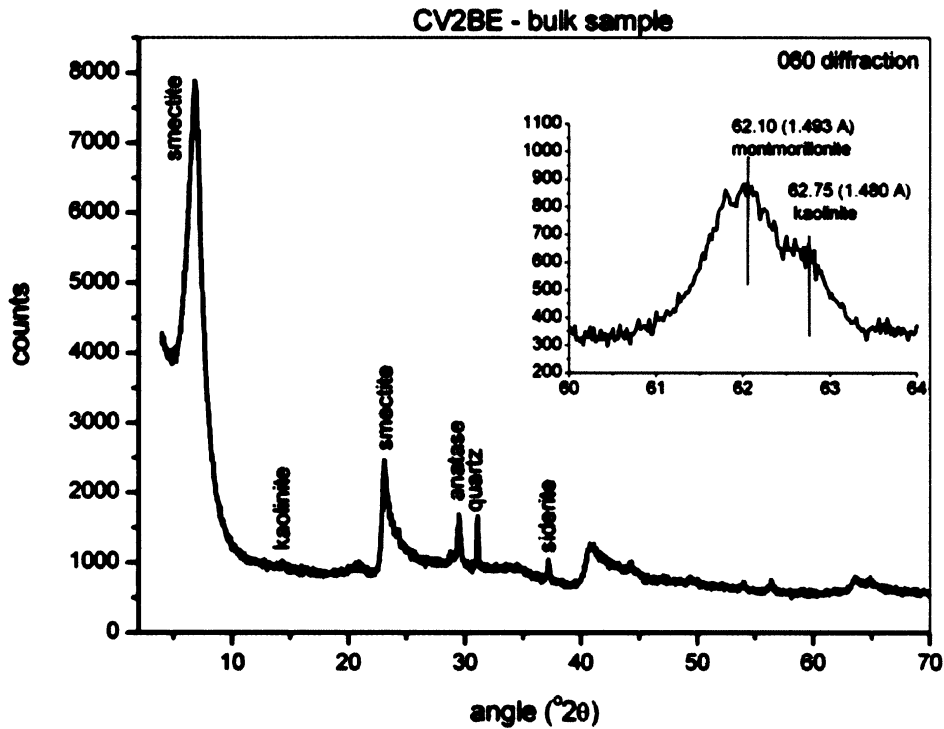


Fig. 5.2 - Mineralogical characterization of CV2BE (XRD pattern is based on 10 diffraction records using $\text{CoK}\alpha$ radiation). The insert shows the 060 diffractions of clay minerals (after carbonates removal in NaOAc, using $\text{CuK}\alpha$ radiation)

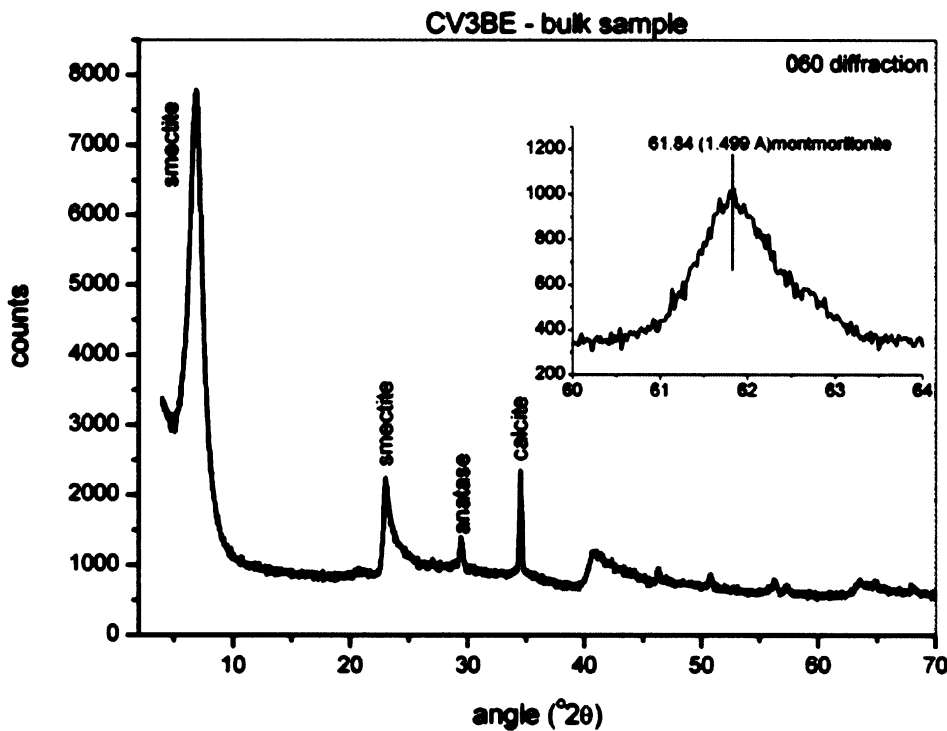


Fig. 5.3 - Mineralogical characterization of CV3BE (XRD pattern is based on 10 diffraction records using $\text{CoK}\alpha$ radiation). The insert shows 060 diffractions of the clay minerals (after carbonates removal in NaOAc, using $\text{CuK}\alpha$ radiation)

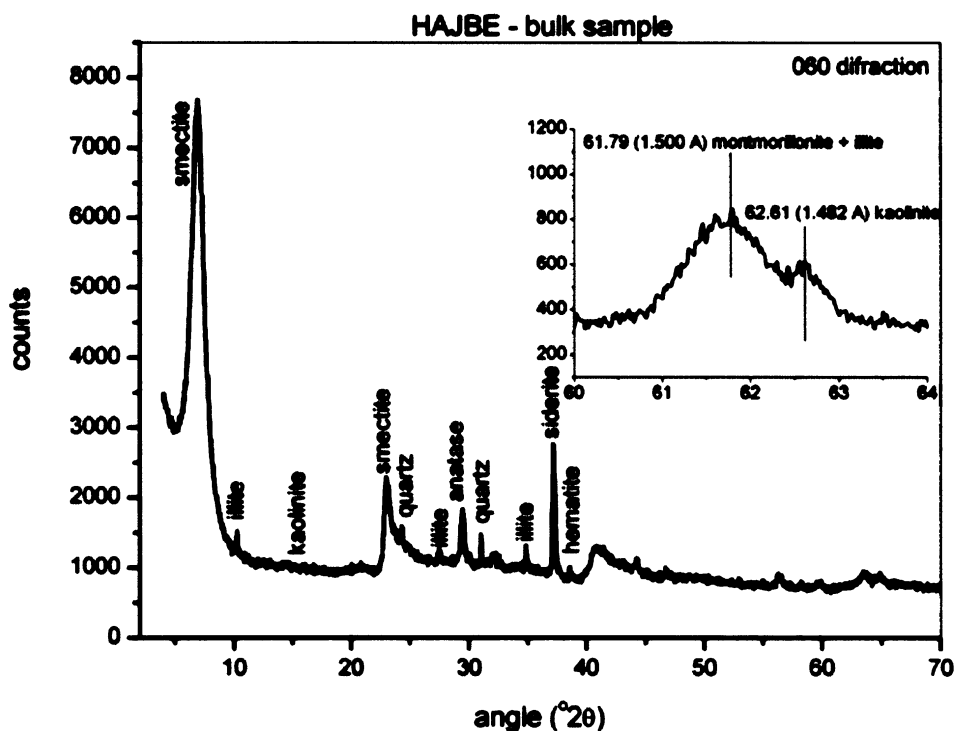


Fig. 5.4 - Mineralogical characterization of HAJBE (XRD pattern is based on 10 diffraction records using CoK α radiation). The insert shows 060 diffractions of clay minerals (after carbonates removal in NaOAc, using CuK α radiation)

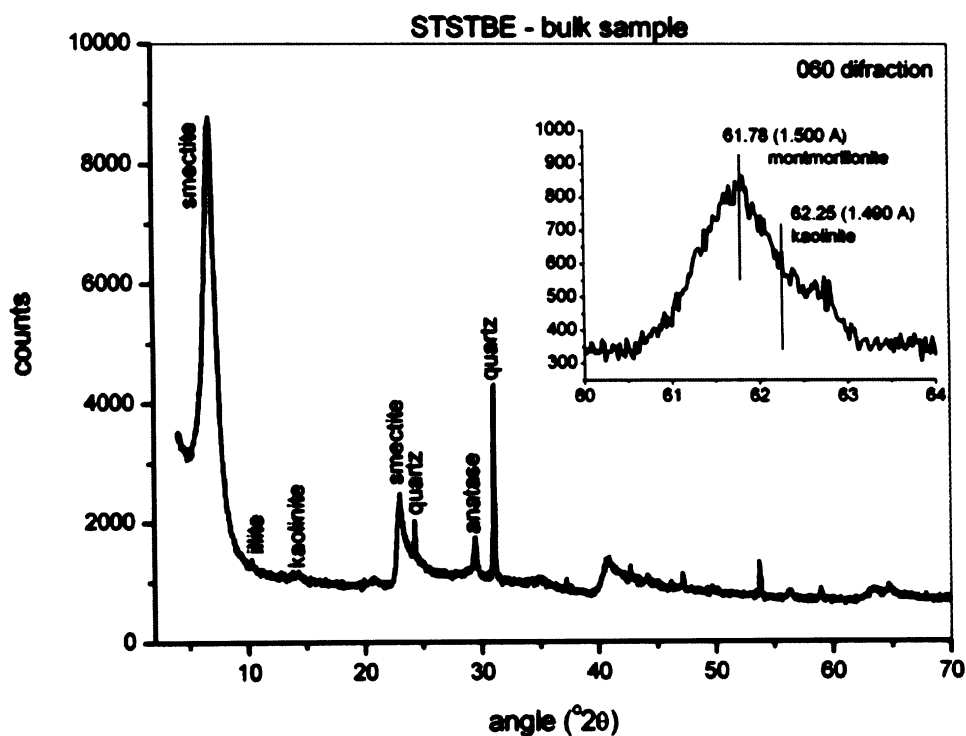


Fig. 5.5 - Mineralogical characterization of STSTBE (XRD pattern is based on 10 diffraction records using CoK α radiation). The insert shows 060 diffractions of clay minerals (after size separation, using CuK α radiation)

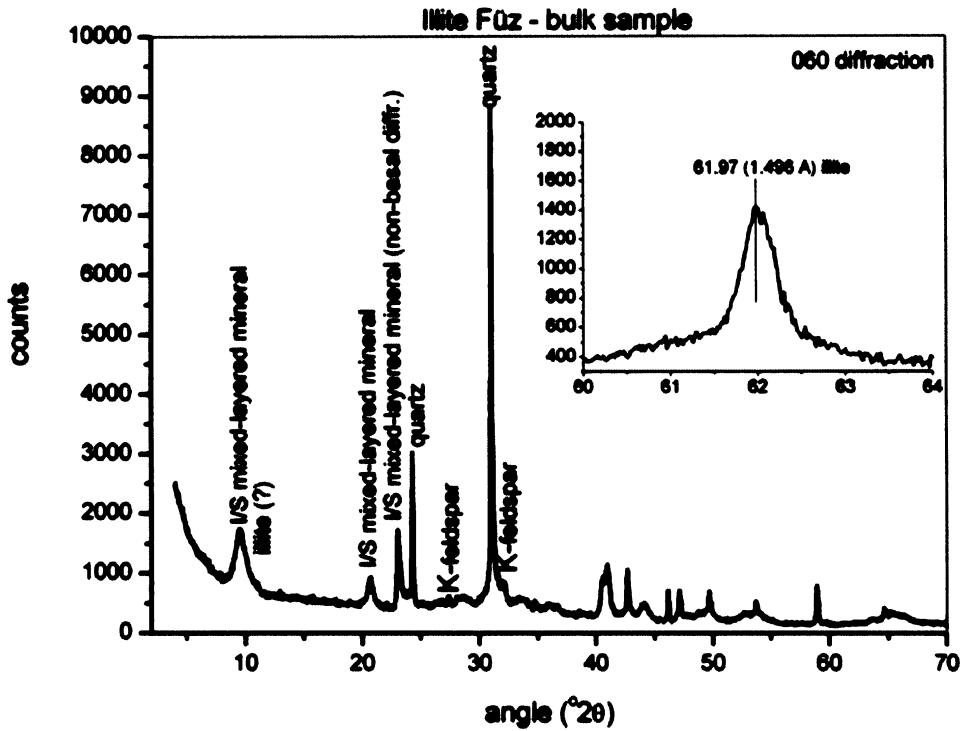


Fig. 5.6 - Mineralogical characterization of Illite Füz (XRD pattern is based on 10 diffraction records using $\text{CoK}\alpha$ radiation). The insert shows 060 diffractions of clay minerals (after size separation, using $\text{CuK}\alpha$ radiation)

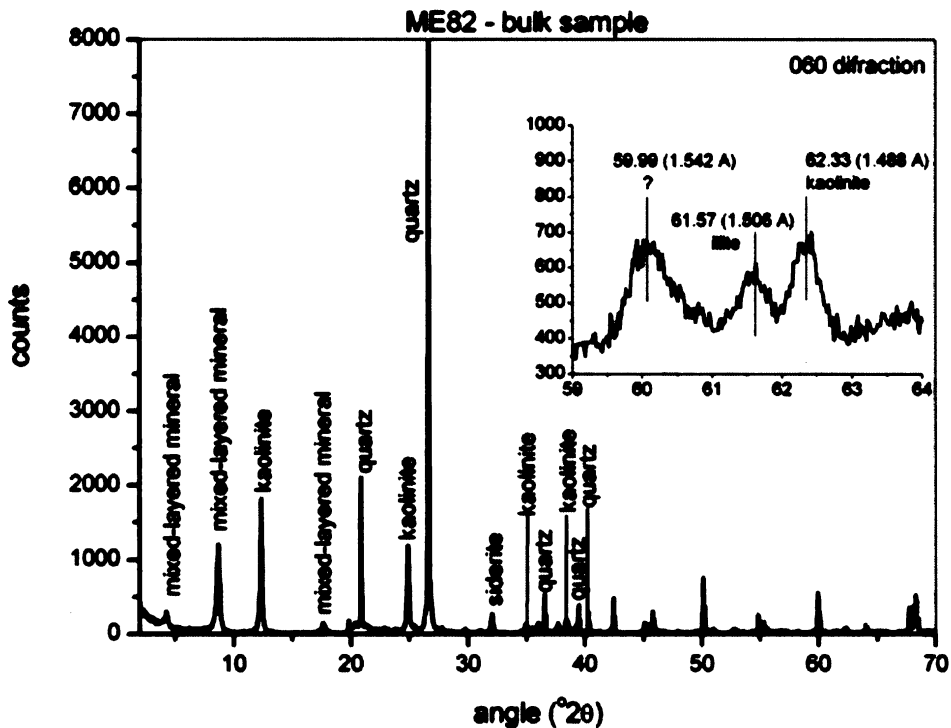


Fig 5.7 - Mineralogical characterization of ME82 (XRD pattern is recorded using $\text{CuK}\alpha$ radiation). The insert shows 060 diffractions of clay minerals (after carbonates removal in NaOAc , using $\text{CuK}\alpha$ radiation)

Clay fractions were collected by sedimentation in distilled water following the Stokes law. The particles with sizes under 2 μm were obtained. Samples containing carbonates (siderite and calcite) were treated with acetic acid (CH_3COOH) in sodium acetate buffer ($\text{NaOAc} - \text{CH}_3\text{COONa}/\text{CH}_3\text{COOH}$ mixture) prior to the collection of the clay fraction. Results of the carbonate removal and size separation are given in Table 5.2. Corresponding diffraction patterns are depicted in Figs. 5.8 – 5.14.

Table 5.2 - The results of the removal strategy and size separation applied to the clay samples

Admixture	Sample						
	CV1BE	CV2BE	CV3BE	HAJBE	STSTBE	IlliteFüz	ME82
Clay							
Smectite	+	+	+	+	+		
Illite	+			?	?	?	
Kaolinite	+	+		+	+		+
Mix. m.						+	+
Non-clay							
Quartz	lowered	lowered		removed	lowered	lowered	removed
Anatase	+	+	+	+	+		
Siderite		removed		removed			removed
Calcite	removed		removed				
Feldspar						?(removed)	
Hematite				removed			

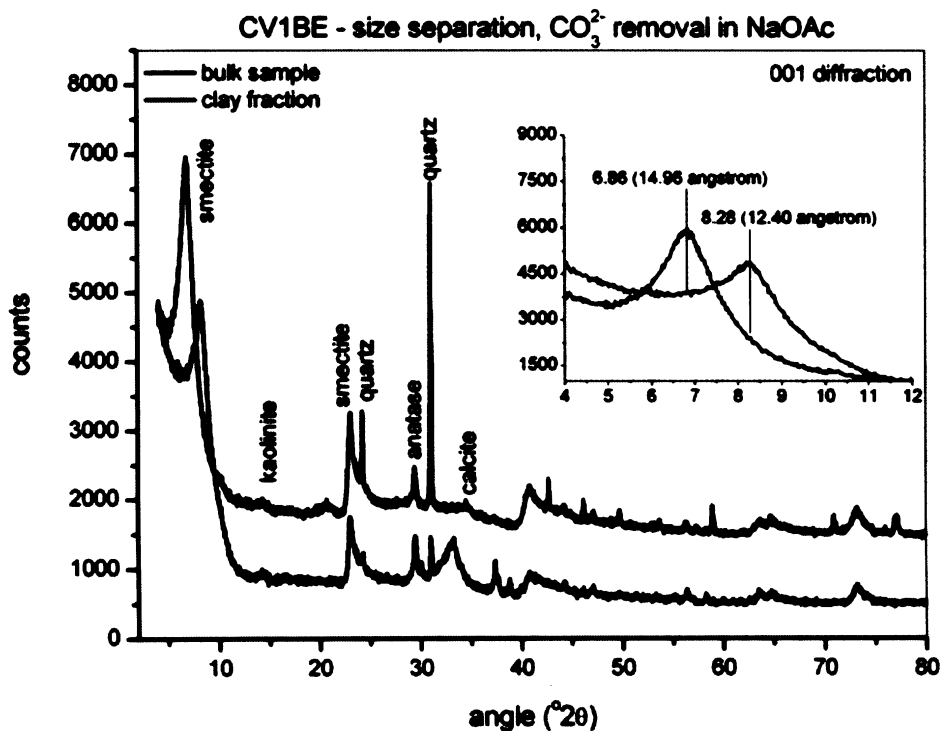


Fig. 5.8 - Result of CV1BE size separation and chemical treatment (diffractograms are accumulations of 10 diffraction patterns, $\text{CoK}\alpha$ radiation). The zoom shows an influence of the treatment on 001 diffraction (replacement of the original M^{2+} by Na^+)

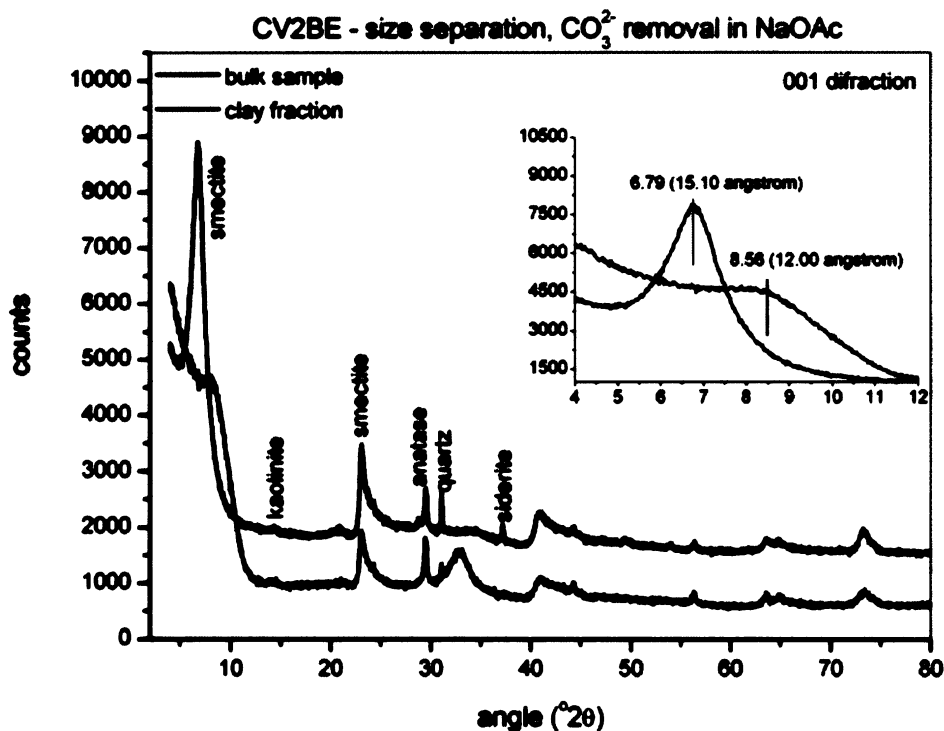


Fig. 5.9 - Result CV2BE size separation and chemical treatment (diffractograms are accumulations of 10 diffraction patterns, CoK α radiation). The zoom shows an influence of the treatment on 001 diffraction (replacement of the original M²⁺ by Na⁺)

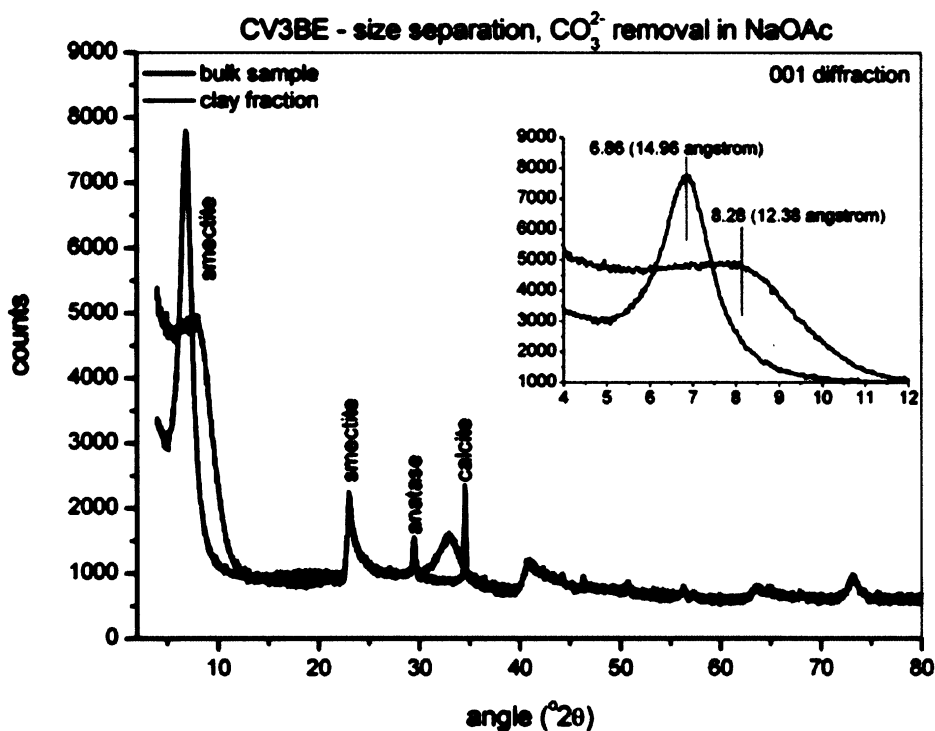


Fig. 5.10 - Result of CV3BE size separation and chemical treatment (diffractograms are accumulations of 10 diffraction patterns, CoK α radiation). The zoom shows an influence of the treatment on 001 diffraction (replacement of the original M²⁺ by Na⁺)

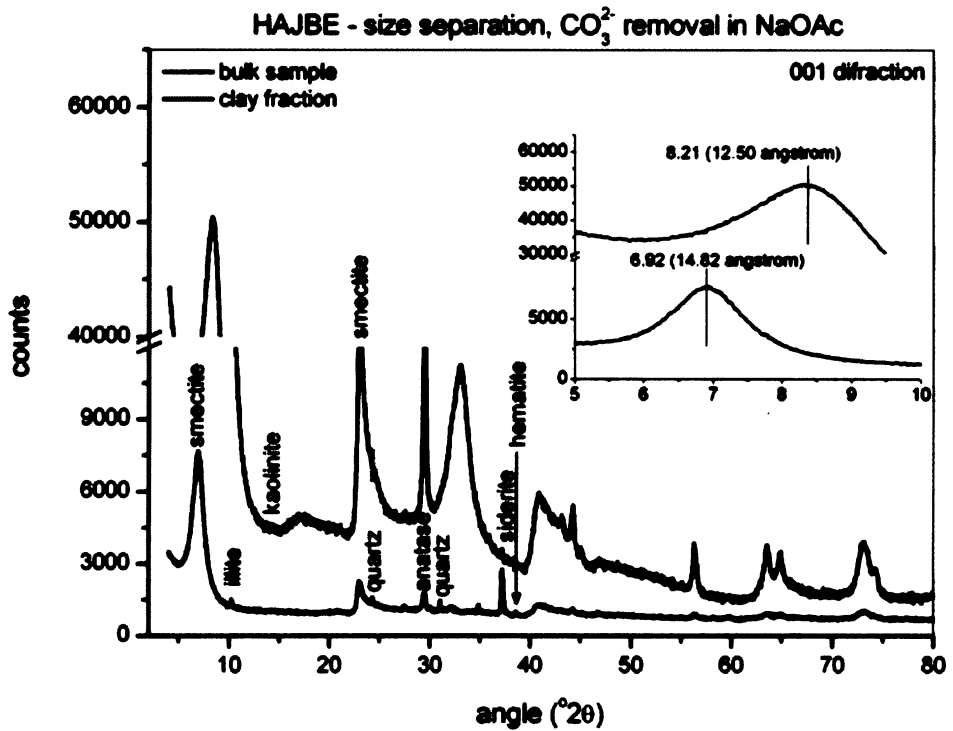


Fig. 5.11 - Results of HJBE size separation and chemical treatment (diffractograms are accumulations of 10 diffraction patterns, CoK α radiation). The zoom shows an influence of the treatment on 001 diffraction (replacement of the original M²⁺ by Na⁺)

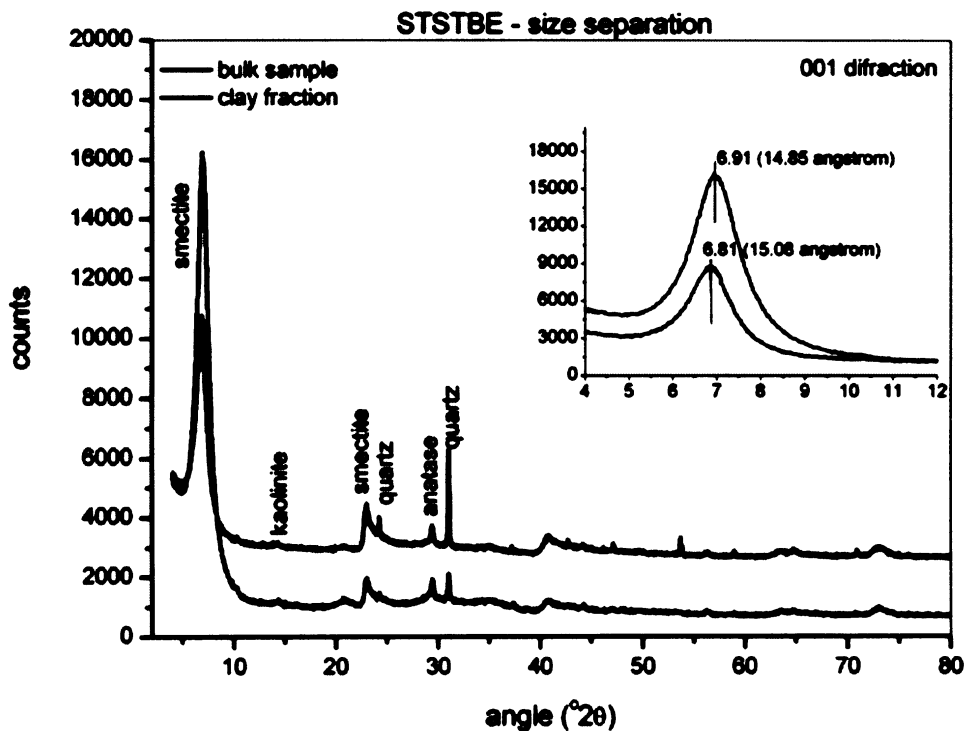


Fig. 5.12 - Result STSTBE size separation (diffractograms are accumulations of 10 diffraction patterns, CoK α radiation). The zoom shows the 001 diffractions

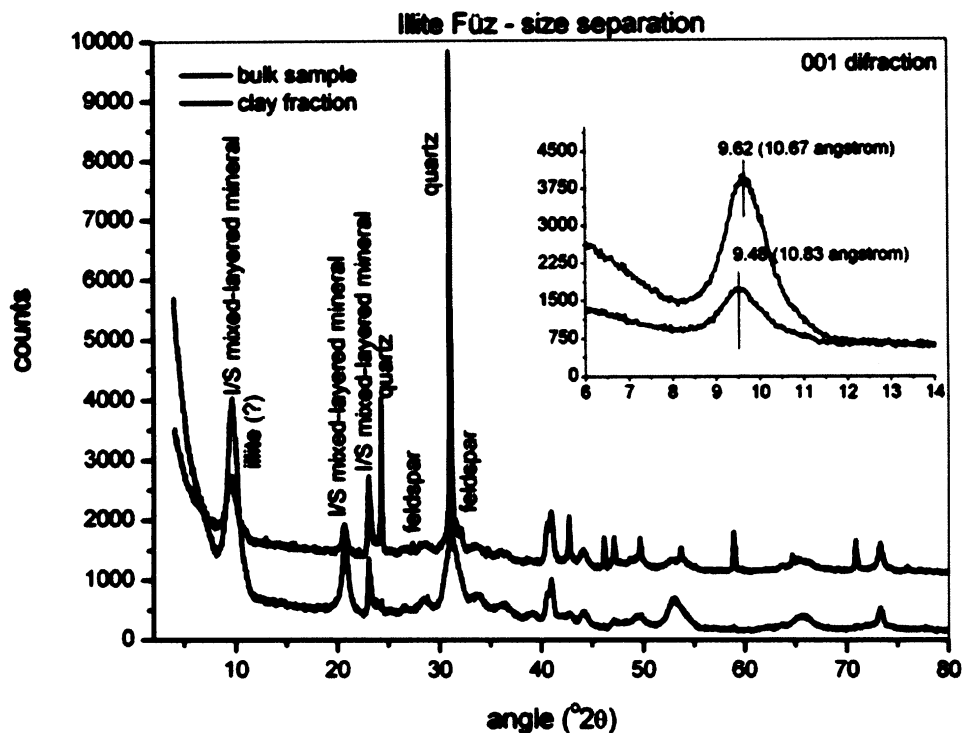


Fig. 5.13 - Result of Illite Füz size separation (diffractograms are accumulations of 10 diffraction patterns, CoK α radiation). The zoom shows the 001 diffractions

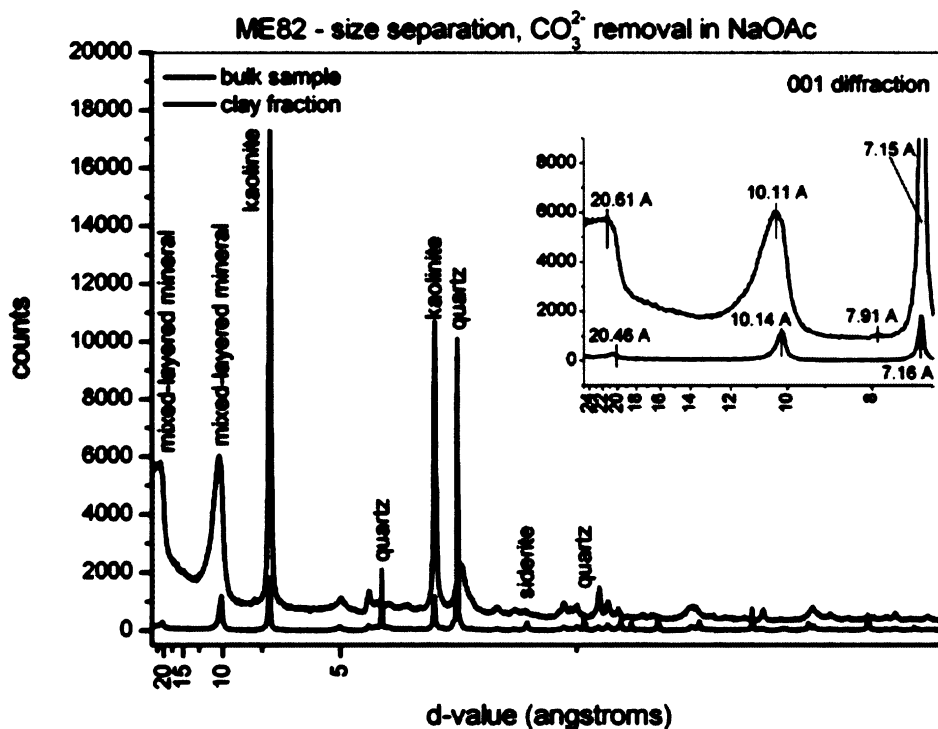


Fig.5.14 - Result of ME82 size separation and chemical treatment (clay fraction pattern is accumulation of 10 diffraction patterns, CoK α radiation, single diffraction pattern presents bulk sample diffractogram, CuK α radiation)

5.2.1. Characterization of bentonites

According to the 060 diffractions (inserts in the bulk sample diffractograms of appropriate samples) smectites can be classified as montmorillonites. The position of montmorillonite 060 diffraction varies from 1.492 to 1.504 Å because of variable Al^{3+} , Fe^{2+} , Fe^{3+} , Mg^{2+} content in octahedral sheet. Further characterization, using the ethylene-glycol expandability, Green-Kelly tests and FTIR spectroscopy is necessary.

5.2.1.1. X-ray diffraction

Diffractograms of expandability tests are shown in Fig. 5.15 – 5.19. The results of Green-Kelly tests are given in Figs. 5.20, 5.21, 5.24 and 5.25.

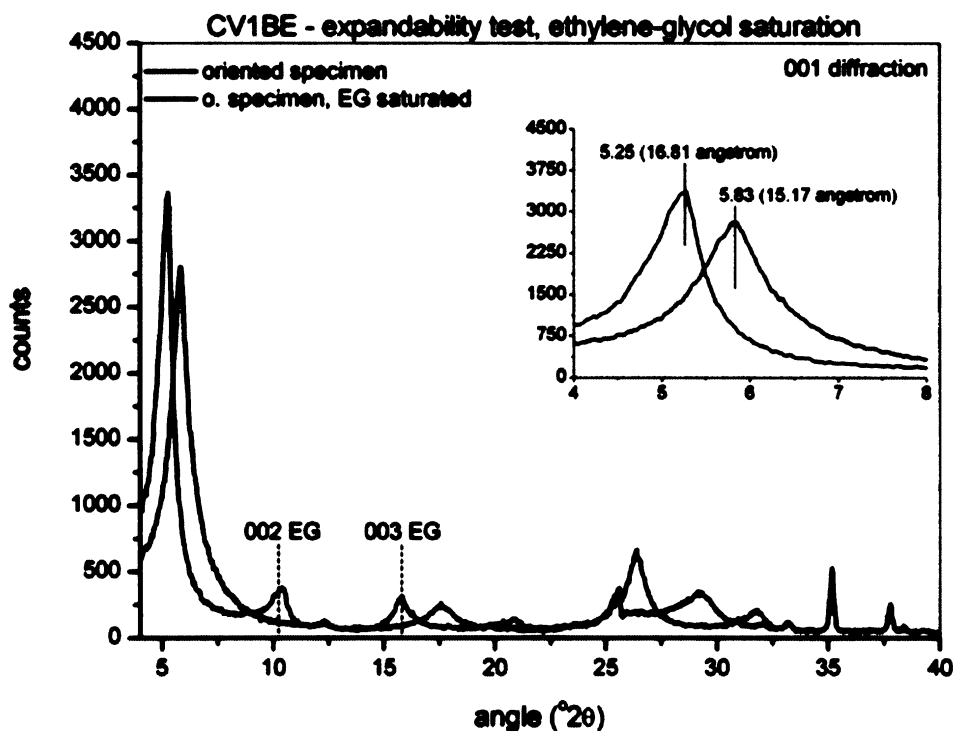


Fig. 5.15 - The ethylene-glycol expandability test of CV1BE (the XRD patterns of oriented porous ceramics specimen prepared under low pressure, $\text{CuK}\alpha$ radiation), the insert describes the 001 diffraction positions

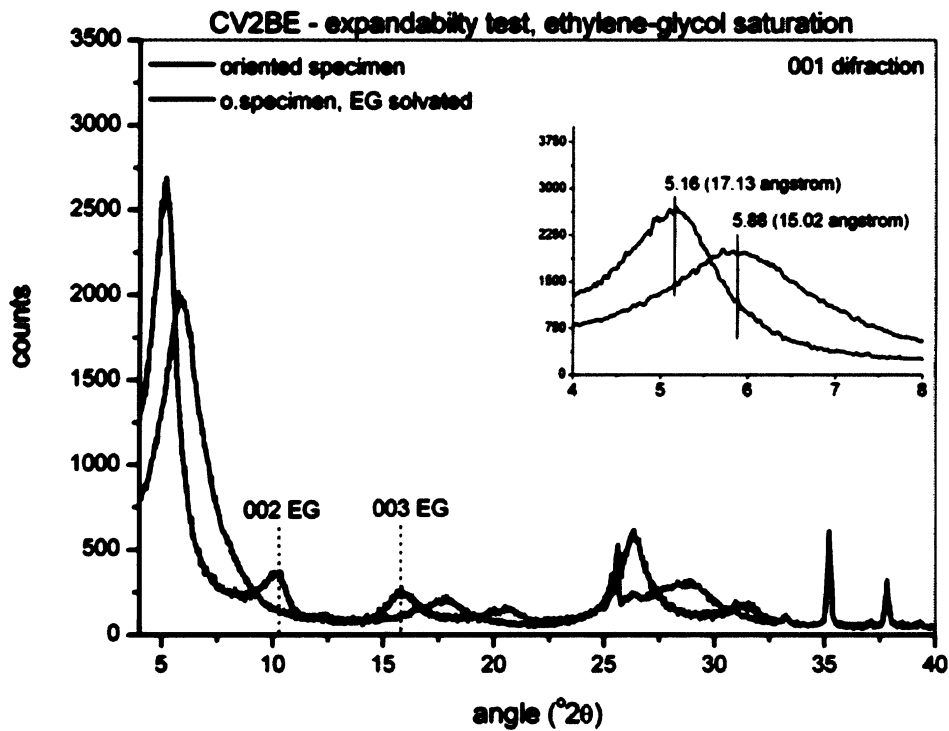


Fig. 5.16 - The ethylene-glycol expandability test of CV2BE (the XRD patterns of oriented on porous ceramics specimen prepared under low pressure, CuK α radiation), the insert describes the 001 diffraction positions

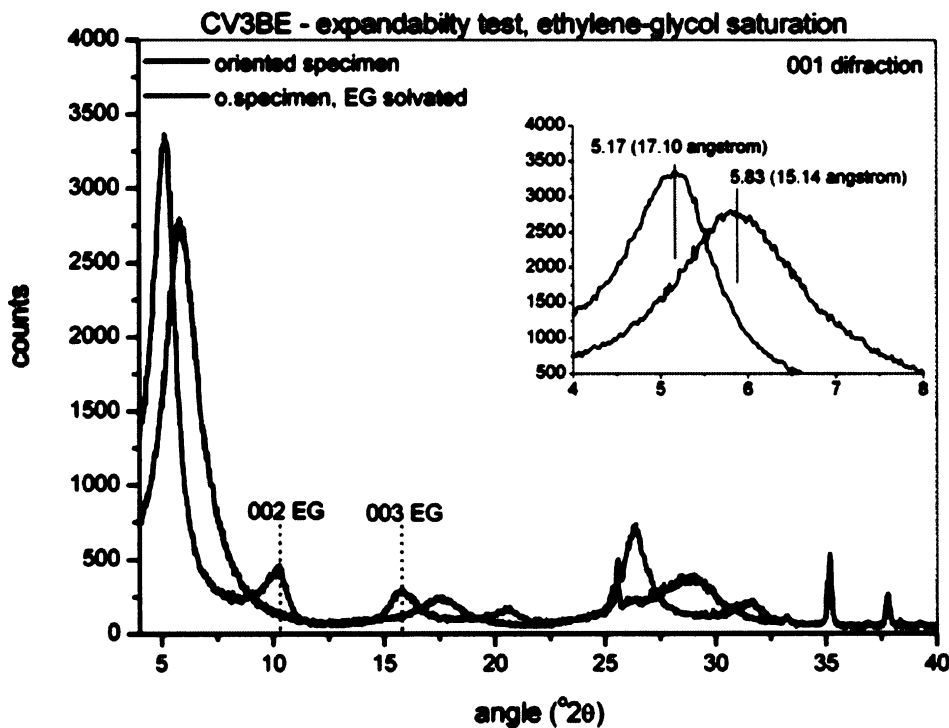


Fig. 5.17 - The ethylene-glycol expandability test of CV3BE (the XRD patterns of oriented porous ceramics specimen prepared under low pressure, CuK α radiation), the insert describes the 001 diffraction positions

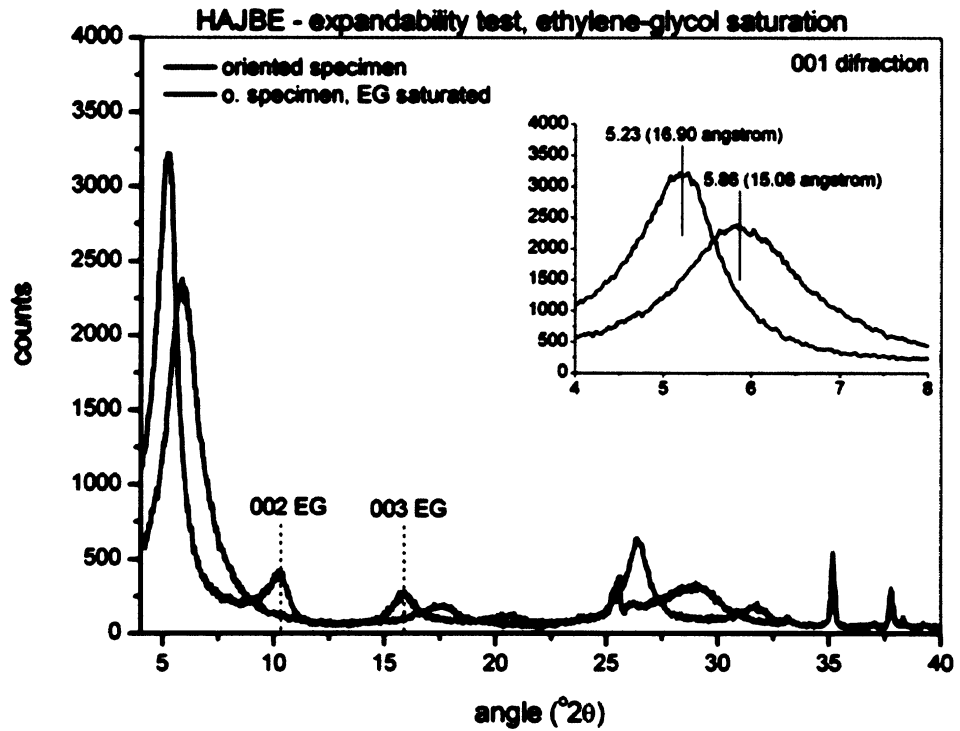


Fig. 5.18 - The ethylene-glycol expandability test of HAJBE (the XRD patterns of oriented porous ceramics specimen prepared under low pressure, CuK α radiation), the insert describes the 001 diffraction positions

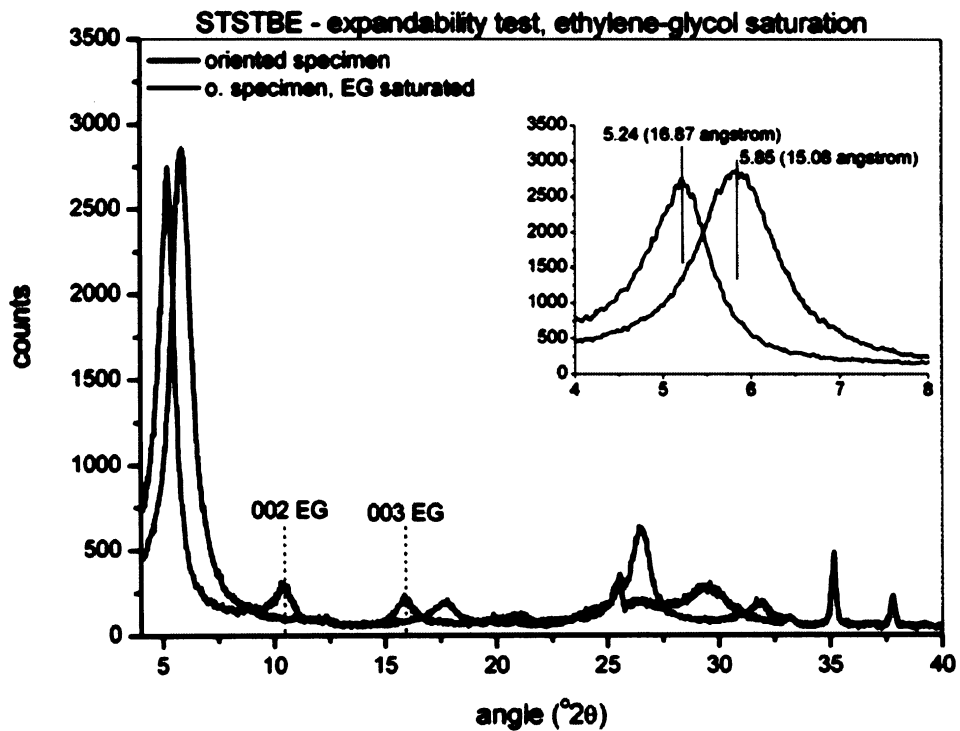


Fig. 5.19 - The ethylene-glycol expandability test of STSTBE (the XRD patterns of oriented porous ceramics specimen prepared under low pressure, CuK α radiation), the insert describes the 001 diffraction positions

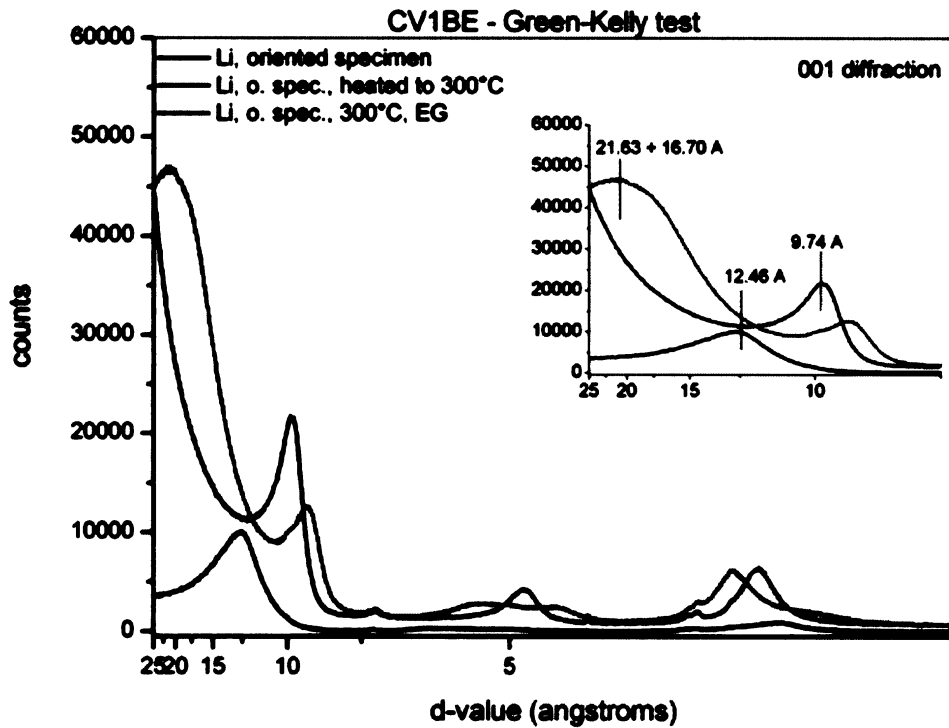


Fig.5.20 - The Green-Kelly test of CV1BE (the XRD patterns of oriented glass slide specimen, clay-fraction, CuK α and CoK α radiation), the insert describes the 001 diffraction positions

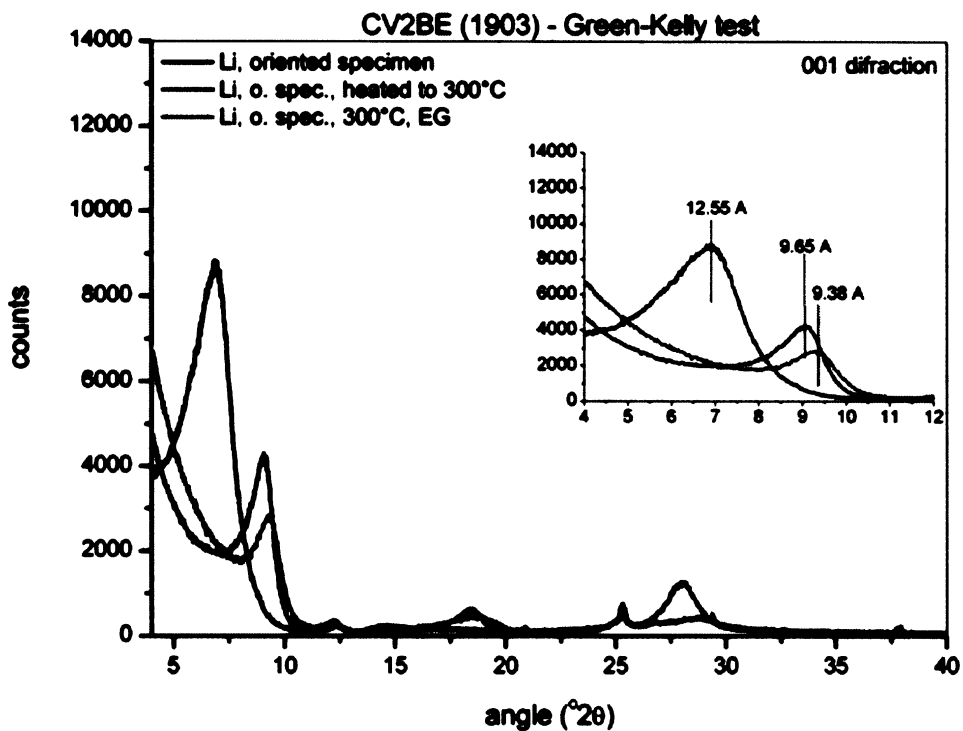


Fig. 5.21 - The Green-Kelly test of CV2BE (the XRD patterns oriented glass slide specimen, clay-fraction, CuK α radiation), the insert describes the 001 diffraction positions

With the CV1BE sample only a partial re-expansion is attained. This conclusion is supported by the presence of diffraction in the region $9 - 10^\circ 2\theta$, which is also observable in the diffraction patterns of Li^+ saturated STx-1 montmorillonite heated to a lower temperature (200, 250 °C) and then saturated with ethylene-glycol (Fig. 5.22). Therefore, the CV1BE shows at 300 °C only a non-complete loose of expandability similar to STx-1 reference montmorillonite at 200 °C (see Fig. 5.23). The extent of lithium migration is higher with the CV2BE sample. Green-Kelly test of CV3BE is not shown because homoionic form preparation failed but the same genetic origin suggests the same result as in CV1BE and CV2BE case.

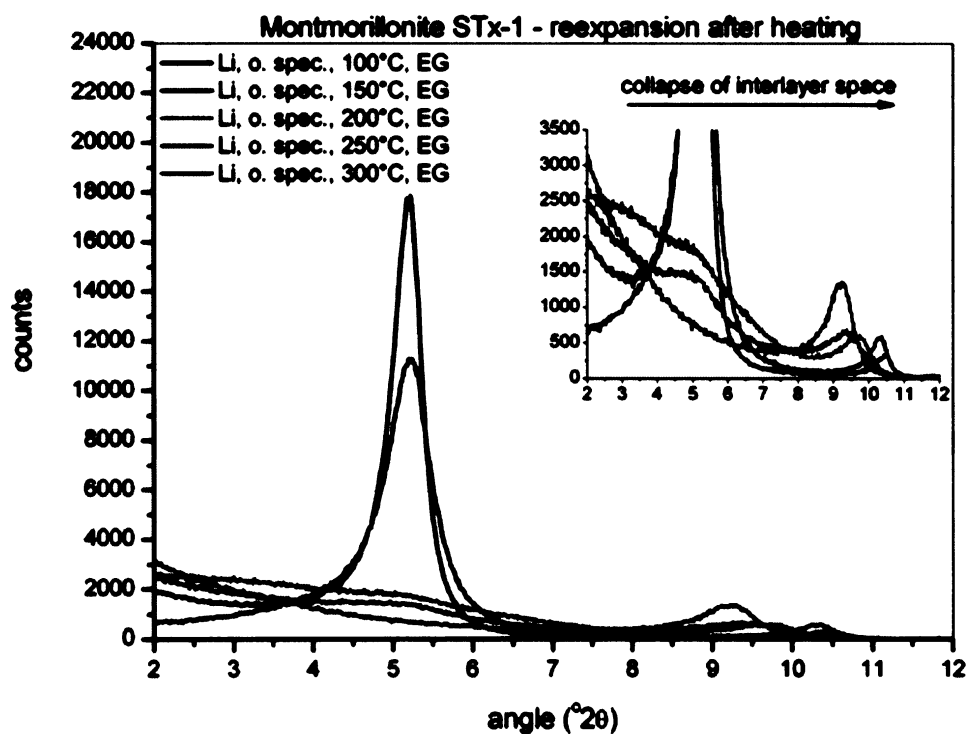


Fig.5.22 - The Green-Kelly test of STx-1 sample performed after different heating temperatures (the XRD patterns of glass slide oriented specimens, $\text{CuK}\alpha$ radiation), the insert describes the 001 diffraction positions

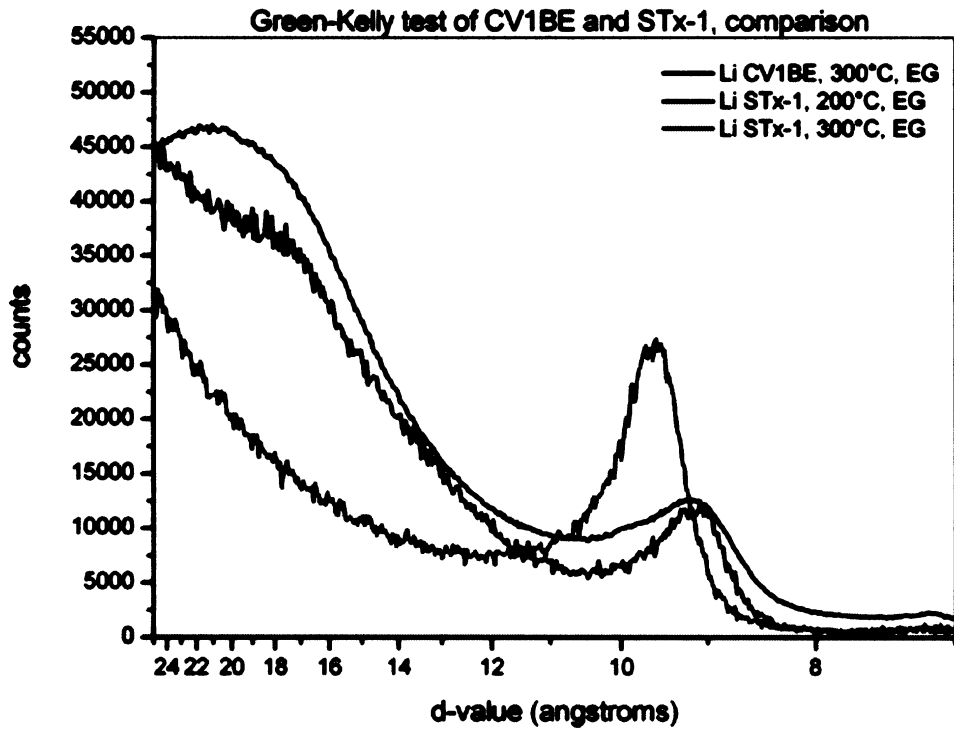


Fig. 5.23 - Comparison of Green-Kelly test results of CV1Be and STx-1 (the XRD patterns of glass slide and porous ceramics oriented specimens, CuK α and CoK α radiation), the insert describes the 001 diffraction positions

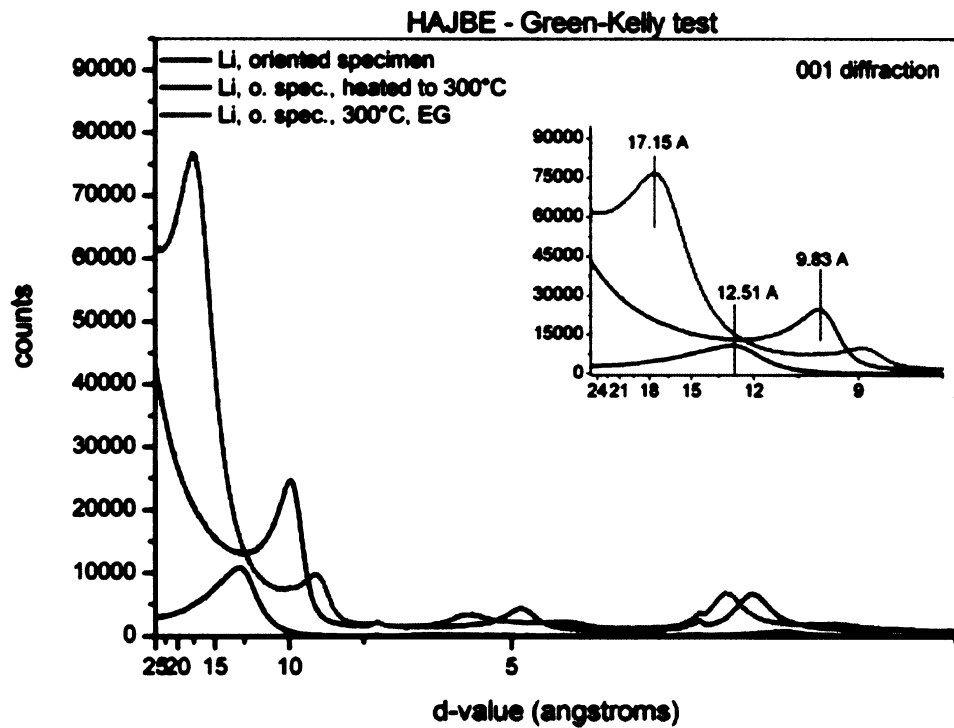


Fig. 5.24 - The Green-Kelly test of HAJBE sample (the XRD patterns of glass slide oriented specimen, clay-fraction, CuK α and CoK α radiation), the insert describes the 001 diffraction positions

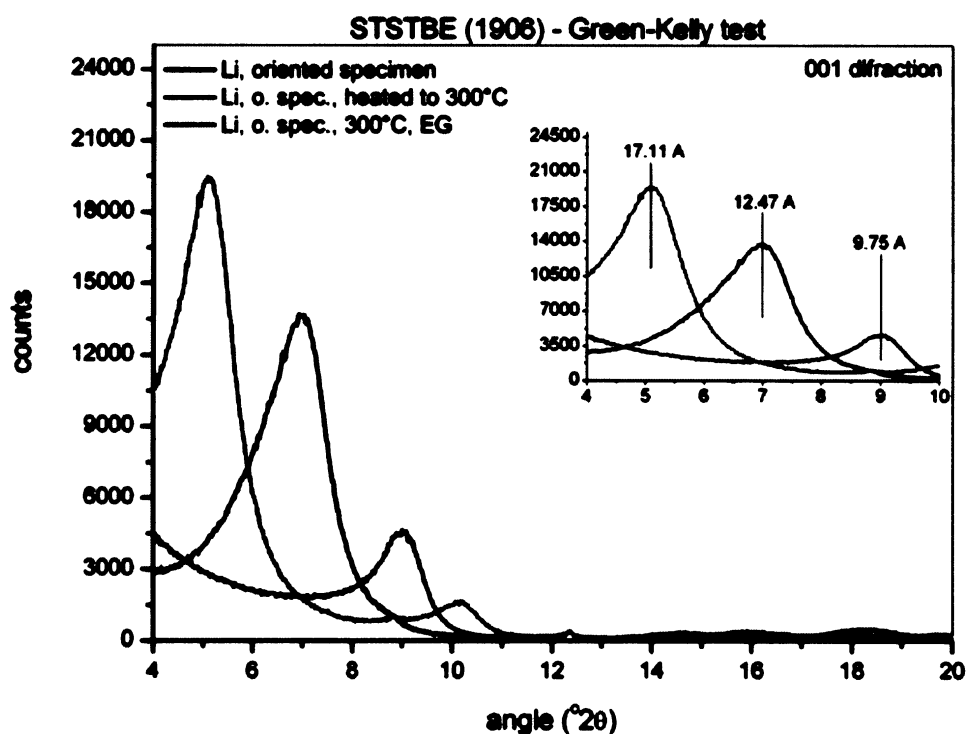


Fig 5.25 - The Green-Kelly test of STSTBE sample (the XRD patterns were collected using oriented specimen of clay-fraction sample prepared on a glass slide and $\text{CuK}\alpha$ radiation), the insert describes the 001 diffraction positions

The results of smectite characterization of bentonite collected samples are summed up in Table 5.3. All the smectites are expandable and no vermiculites or chlorites are present in the samples. The ratio of 002 and 003 diffractions of EG saturated specimens equal approximately unity which indicates a smectite with Al occupation with partial substitution by Fe in the octahedral sheet.

Table 5.3 - Characterization of smectite in collected bentonites

Test	Sample (<i>d</i> -values)				
	CV1BE	CV2BE	CV3BE	HAIJE	STSTBE
EG-expandability test	15.17 → 16.81 Å	15.02 → 17.13 Å	15.15 → 17.10 Å	15.06 → 16.90 Å	15.08 → 16.87 Å
EG-expandability test	expandable	expandable	expandable	expandable	expandable
EG-expandability test	≈ 1	≈ 1	≈ 1	≈ 1	≈ 1
002/003 EG ratio	moderate Fe content	moderate Fe content	moderate Fe content	moderate Fe content	moderate Fe content
Green-Kelly test (300°C heated samples, EG reexpansion)	to 16.70 Å partial charge red.	to 9.38 Å reduced		to 17.15 Å no charge reduction	to 17.11 Å no charge reduction

The result of the Green-Kelly test for CV is disputable. The re-expansion compared to re-expansion of STx-1 (reference montmorillonite, Fig 5.22) at different temperatures is similar. It seems that heating to 300 °C is insufficient for CV. The CV structures can be

characterized as montmorillonites with a moderate content of Fe. The reason for retardation of Li^+ migration is unclear. The Green-Kelly test of HAJBE and STSTBE is negative, no charge reduction was attained and re-expansion is full. The 060 diffraction, the 002/0003 EG ratio and the Green-Kelly test characterize the samples as ferruginous smectites.

5.2.1.2. FTIR spectroscopy

The FTIR spectroscopy was applied in order to investigate crystallo-chemical composition of the octahedral sheet. The spectroscopy was performed in the transmission mode in the MID region ($4000 - 400 \text{ cm}^{-1}$), using KBr pellets. The whole spectra with the region of interest marked are reported in Fig. 5.26.

Admixtures indicated in the spectra:

- Kaolinite: is clearly observable in CV1BE, CV2BE and STSTBE samples due to its characteristic vibration at 3697 cm^{-1} (Fig. 5.27)
- Quartz: provides a double peak in the spectra of CV1BE and STSTBE, at 800 and 780 cm^{-1} . (Fig. 5.28)

The chemical composition of the octahedral sheet is similar for all samples. The structure is rich in Al^{3+} substituted by Fe^{3+} (see Fig. 5.28 and Table 5.4 pp.94). None of the spectra displays FeFeOH vibration at 815 cm^{-1} which is characteristic for nontronites. According to the position of OH bending vibrations, all the samples can be characterized as Fe-montmorillonites.¹⁶⁹

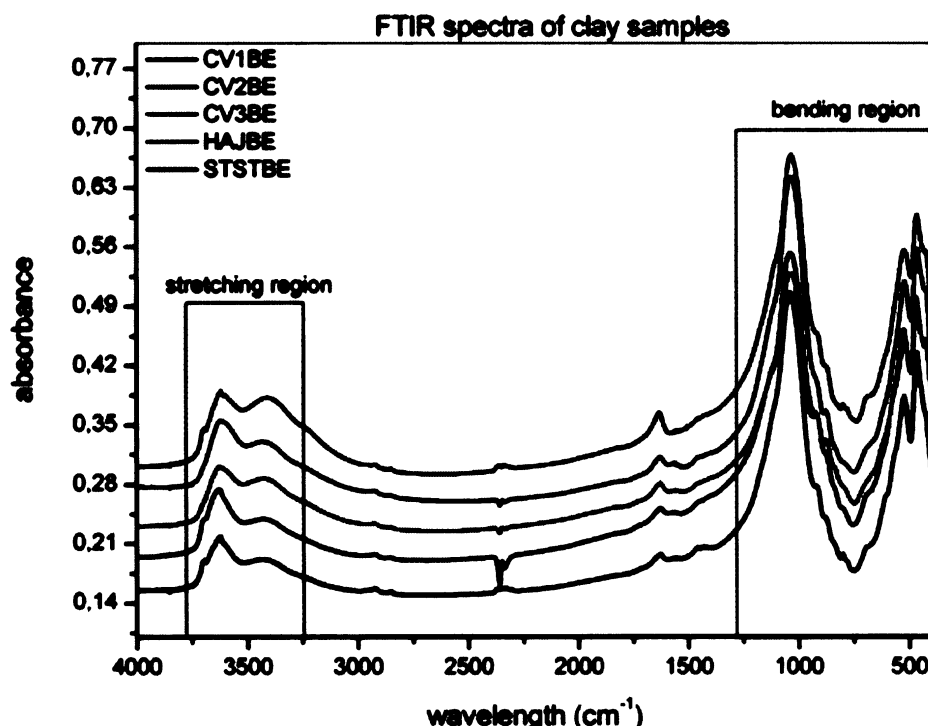


Fig. 5.26 - The FTIR spectra of clay samples, MID region, $4000 - 400 \text{ cm}^{-1}$, transmission mode using KBr pellets

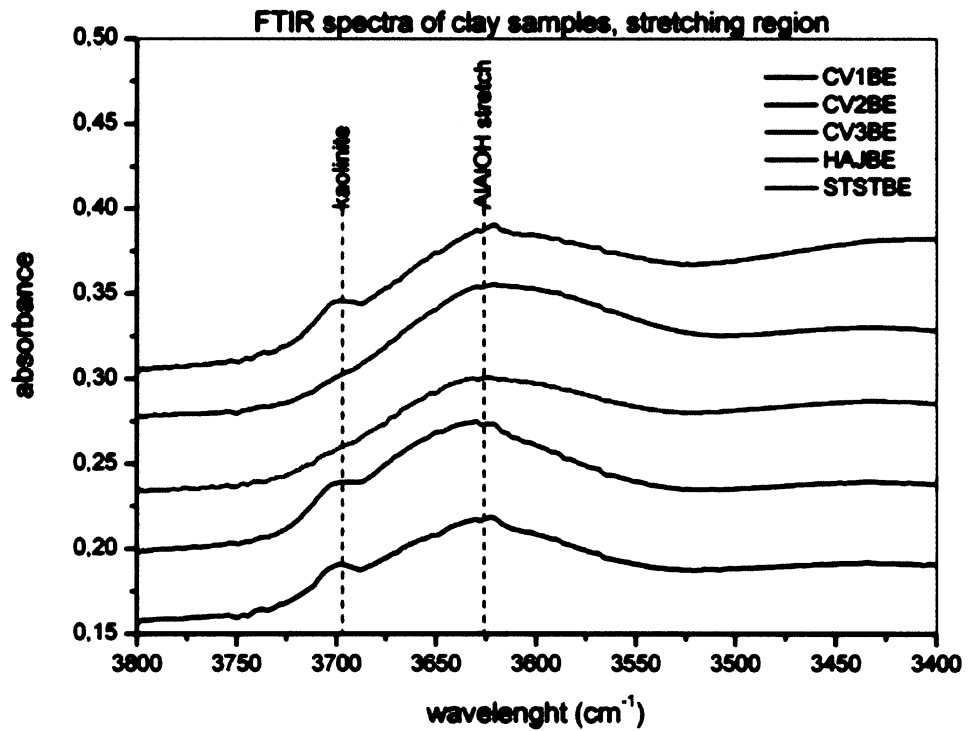


Fig. 5.27 - The zoom of FTIR spectra, stretching region of clay samples

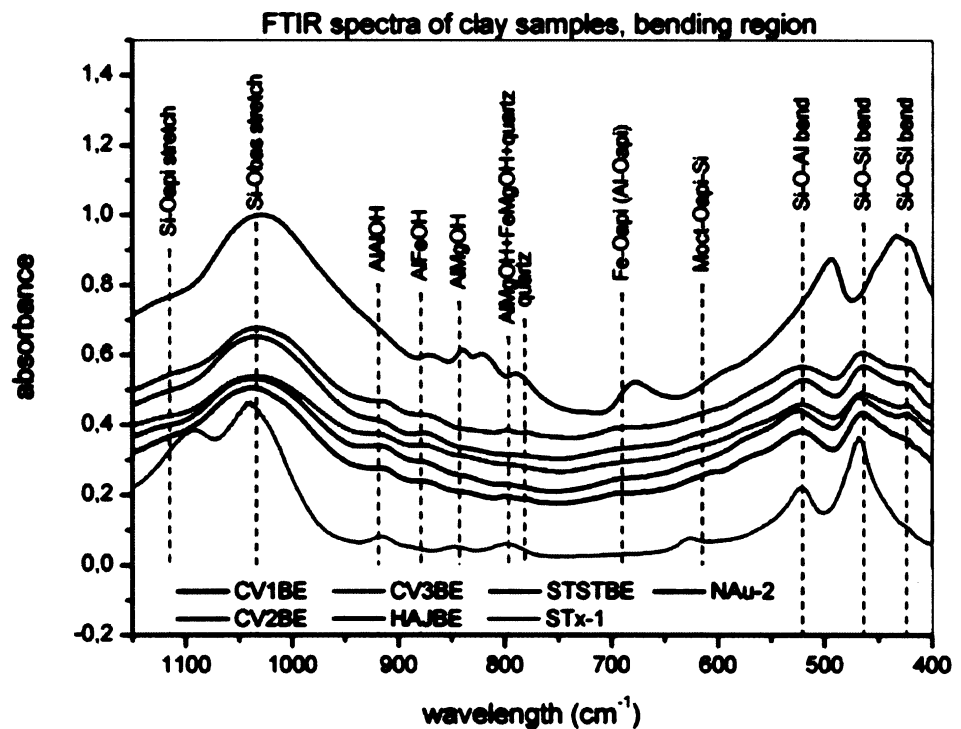


Fig. 5.28 - The zoom of FTIR spectra, bending region of clay samples, comparison with montmorillonite STx-1 and nontronite NAu-2 reference samples

Table 5.4 - Vibrational bands observed in the MID region for the clay samples

CV1BE		CV2BE		CV3BE		HAJBE		STSTBE	
(cm ⁻¹)	Attributed to	(cm ⁻¹)	Attributed to	(cm ⁻¹)	Attributed to	(cm ⁻¹)	Attributed to	(cm ⁻¹)	Attributed to
3697	Kaolinite	3697	Kaolinite			3697	Kaolinite		
3622	AlAlOH _{stretch}	3629	AlAlOH _{stretch}	3623	AlAlOH _{stretch}	3621	AlAlOH _{stretch}	3620	AlAlOH _{stretch}
1116	Si-O _{apical stretch}	1115	Si-O _{apical stretch}	1112	Si-O _{apical stretch}	1115	Si-O _{apical stretch}	1106	Si-O _{apical stretch}
1035	Si-O _{basal stretch}	1036	Si-O _{basal stretch}	1036	Si-O _{basal stretch}	1032	Si-O _{basal stretch}	1032	Si-O _{basal stretch}
915	AlAlOH _{bend}	919	AlAlOH _{bend}	922	AlAlOH _{bend}	921	AlAlOH _{bend}	914	AlAlOH _{bend}
880	AlFeOH _{bend}	881	AlFeOH _{bend}	878	AlFeOH _{bend}	874	AlFeOH _{bend}	874	AlFeOH _{bend}
842	AlMgOH _{bend}	840	AlMgOH _{bend}	843	AlMgOH _{bend}	831	AlMgOH _{bend}	836	AlMgOH _{bend}
799	AlMgOH	798	FeMgOH _{bend}	798	FeMgOH _{bend}	795	FeMgOH _{bend}	797	AlMgOH
	+FeMgOH _{bend}								+FeMgOH _{bend}
	+quartz								+quartz
784	Quartz							778	Quartz
	(double peak)								(double peak)
693	Fe-O _{apical, out of plane}	691	Fe-O _{apical, out of plane}	681	Fe-O _{apical, out of plane}	688	Fe-O _{apical, out of plane}	691	Fe-O _{apical, out of plane}
606	M-O _{apical-Si}	618	M-O _{apical-Si}	615	M-O _{apical-Si}	613	M-O _{apical-Si}	601	M-O _{apical-Si}
524	Si-O-Al _{bend}	523	Si-O-Al _{bend}	520	Si-O-Al _{bend}	520	Si-O-Al _{bend}	520	Si-O-Al _{bend}
463	Si-O-Si _{bend}	466	Si-O-Si _{bend}	463	Si-O-Si _{bend}	464	Si-O-Si _{bend}	464	Si-O-Si _{bend}
424	Si-O-Si _{bend}	425	Si-O-Si _{bend}	422	Si-O-Si _{bend}	426	Si-O-Si _{bend}	425	Si-O-Si _{bend}

5.2.2. Illite Füz sample characterization

The expandability test was performed using ethylene-glycol saturation. The patterns are shown in Fig. 5.29. The 001 diffraction at 10.73 Å splits to “double-peak” diffraction with maxima at higher and lower d values than the original diffraction indicating a mixed-layered structure. The expandable part of the structure creates 001/004*-EG diffraction at 11.1 Å, thus proving expandability and indicating that the expandable part is smectite. A comparison with the R3 I(0.9)/S XRD diffraction pattern (in Moore and Reynolds 1997⁶) leads to the conclusion that the structure has the R3 ordering.

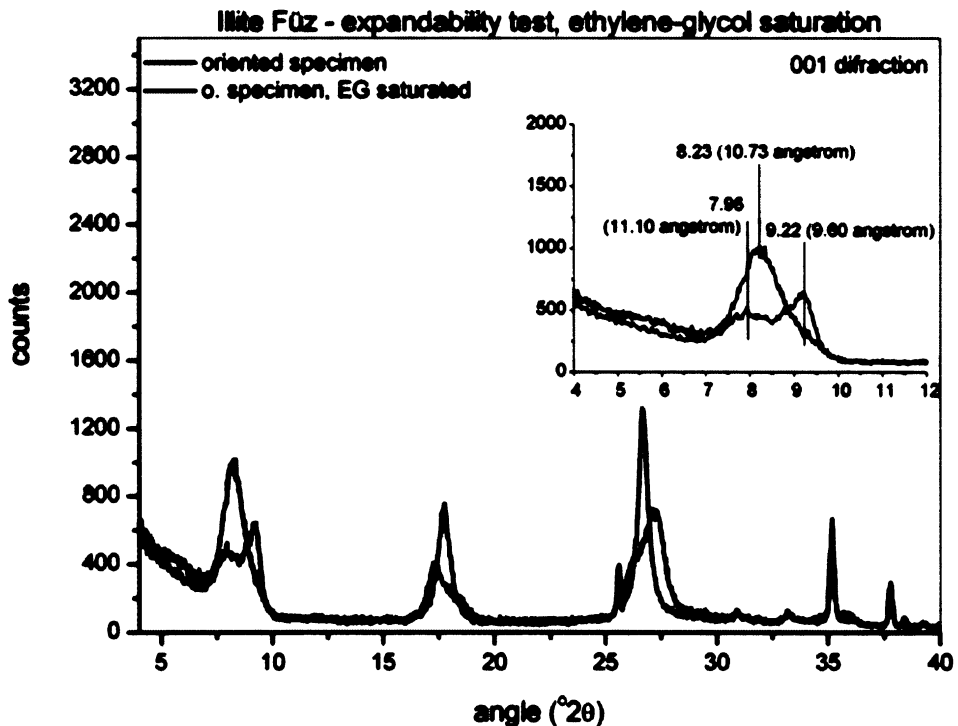


Fig. 5.29 - The ethylene-glycol expandability test of Illite Füz (the XRD patterns of oriented porous ceramics specimen prepared under low pressure, CuK α radiation)

5.2.3. ME82 sample characterization

The expandability test applied to the chemically untreated sample (Fig. 5.30) shows expansion of phases at 20.6 Å and 10 Å respectively. It indicates the presence of two different mixed-layered structures both with expandable component. One has R3 ordering (similar to Illite Füz) and one R1 ordering showing 001* superstructural diffraction at 20.6 Å.

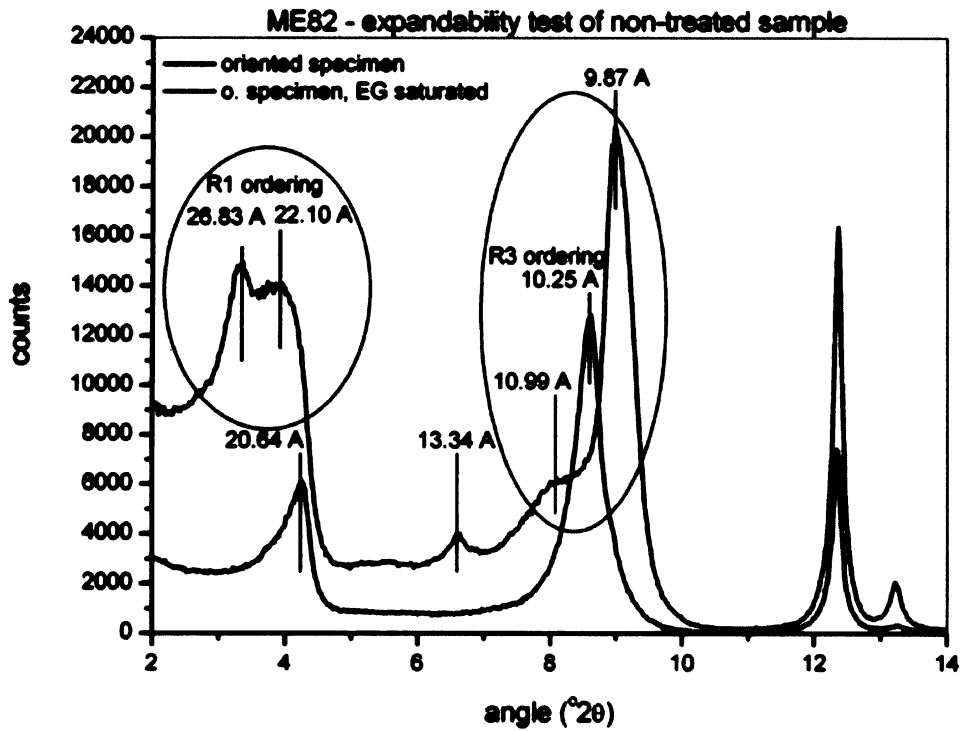


Fig. 5.30 - The ethylene-glycol expandability test of ME82, chemically untreated sample (the XRD patterns of glass slide oriented specimen, CuK α radiation)

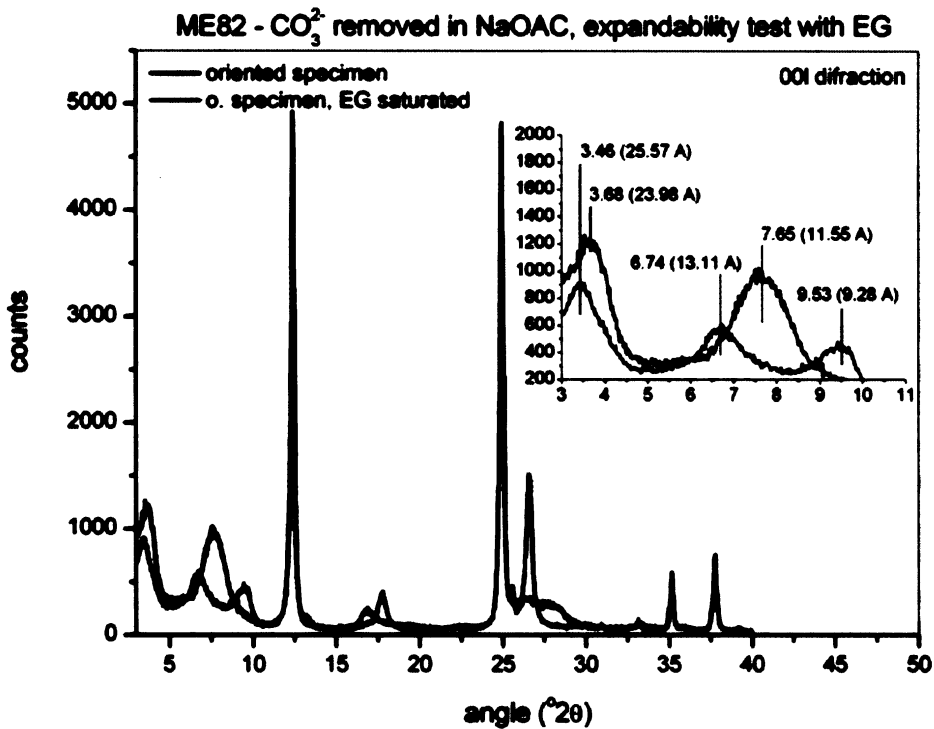


Fig. 5.31 - The ethylene-glycol expandability test of ME82, chemically treated sample (the XRD patterns of oriented porous ceramics specimen prepared under low pressure, CuK α radiation)

The same test applied to the chemically treated sample (Fig. 5.31) shows a complete shift of the 001* diffraction towards higher d values, from 24 to 25.6 Å. This expansion excludes chlorite as a component of the mixed-layered structure. Vermiculite is more probable expandable component instead of smectite. The presence of regular R1 illite/vermiculite structure should be proved by further tests.

The sample was treated with a magnesium chloride solution in order to obtain Mg^{2+} homoionic form and EG saturated. The result is shown in Fig. 5.32.

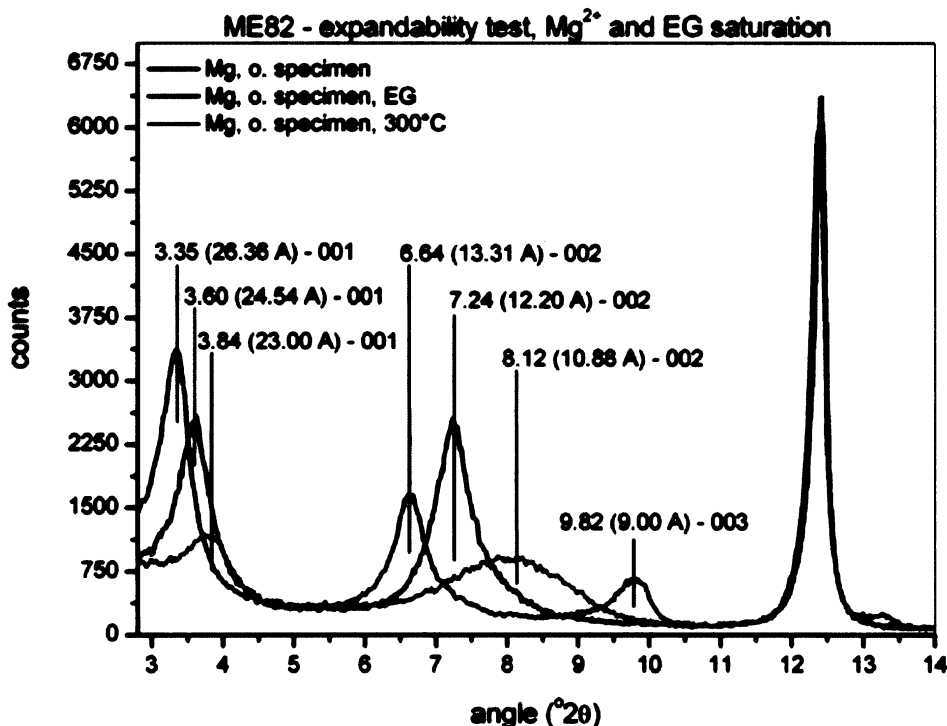


Fig.5.32 - The ethylene-glycol expandability test of ME82, chemically treated, Mg^{2+} saturated sample (the XRD patterns of porous ceramics oriented specimen prepared under low pressure, $CuK\alpha$ radiation)

The XRD pattern of the EG saturated Mg^{2+} -ME82 sample confirms the presence of vermiculite layers. The other component is a mica layer (illite). After Mg^{2+} saturation, the 001* diffraction lies at 24.54 Å which is the sum of the 10 Å layer and the 14.4 Å Mg^{2+} -vermiculite layer. The EG saturation shifts 001* diffraction to 26.36 Å. The resistance of vermiculite interlayer after heating to 300 °C, position at 13 Å (23 Å 001* diffraction is summ of 10 Å illite layer and 13 Å vermiculite layer), is in a good agreement with the fact that Mg-vermiculites dehydrates at higher temperatures than smectites.¹¹

The clay fraction was further saturated with potassium chloride solution. The 001 diffraction collapsed to 22.6 Å and an expansion to 26 Å (26.1 Å) was observed after EG saturation. The saturation with dimethylsulfoxide (DMSO) was more important. The 001 diffraction of kaolinite shifted to 11.2 Å and revealed remaining diffraction at of 7.14 Å which might point to chlorite (Fig. 5.33).

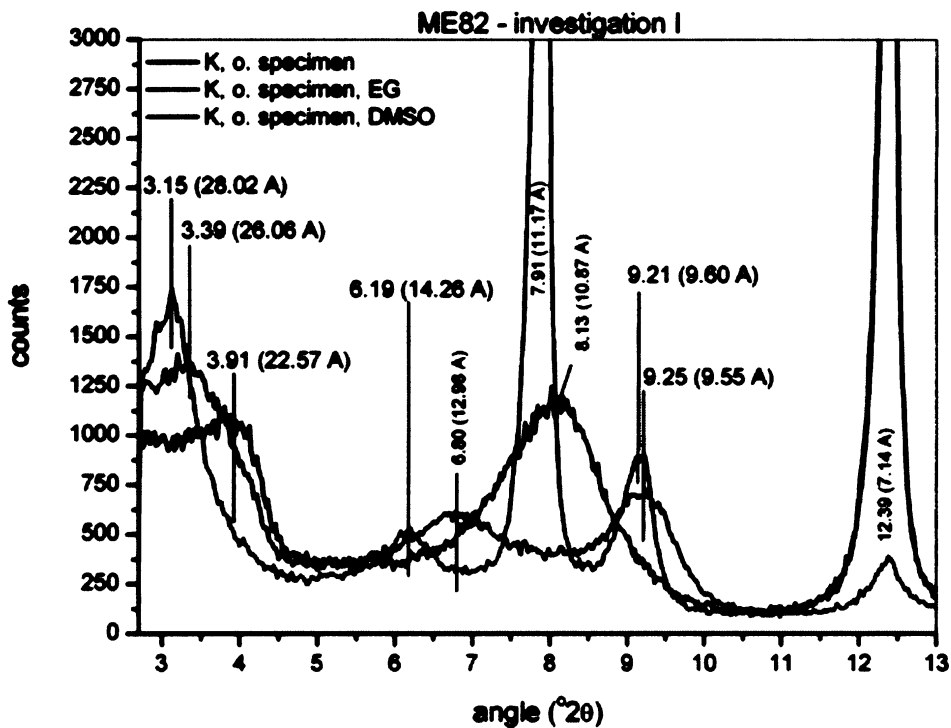


Fig. 5.33 - Investigation of ME82, K⁺ saturated sample (the XRD patterns of porous ceramics oriented specimen prepared under low pressure, CuK α radiation)

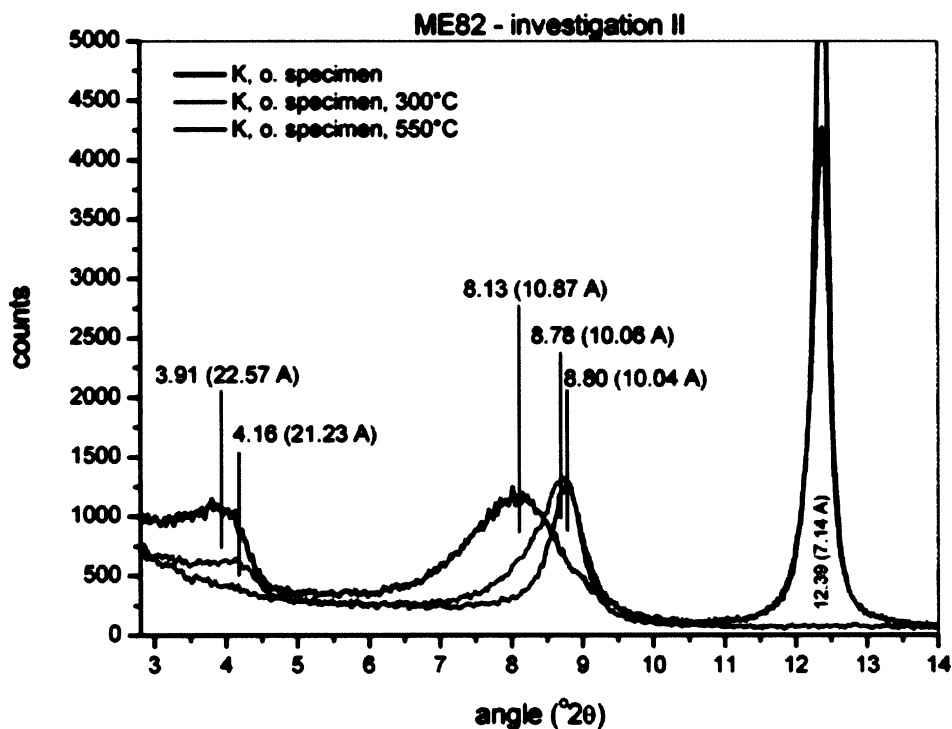


Fig. 5.34 - Investigation of ME82, K⁺ saturated sample (the XRD patterns of porous ceramics oriented specimen prepared under low pressure, CuK α radiation)

The results of heating procedures are depicted in Fig.5.34. Heating of K⁺ saturated sample to 300 °C should cause a collapse of the vermiculite interlayer space to 10 Å while heating to 550 °C preserves the chlorite structure and transforms kaolinite into an amorphous phase.⁶ Heating to 300 °C collapsed 001* diffraction of the mixed-layered structure to 21.23 Å (10 + 11.23 Å) which might be caused by incomplete exchange of the interlayer space. Heating to 550 °C caused disappearance of the 7.14 Å diffraction; therefore no chlorite is present.

5.2.4. Conclusion of collected clays characterization

All CVBE smectites can be characterized as montmorillonites with a moderate iron content in the octahedral sheet (according to 060 diffraction, 002/0003 EG ratio and loose of expansion during the Green-Kelly test). The mixed-layered structures were characterized. The Illite Füz was described as I(0.9)/S with R3. This structure is probably resulting from weathering of illite where K⁺ ions have been replaced by a divalent cation. The same mixed-layered structure is present also in ME82 kaoline. Besides this, a mica/vermiculite mixed-layered mineral is present. The positions of superstructural diffractions reveal a R1 mica(0.5)/vermiculite structure. Comparison with the diffraction pattern of hydrobiotite (Moore and Reynolds, 1997) and performed tests confirm the R1 mica(0.5)/vermiculite structure. Summation is given in the Table 5.5.

Table 5.5 - Characterization of collected clays

	CV1BE	CV2BE	CV3BE	Sample HAJBE	STSTBE	IlliteFüz	ME82
Removable admixtures	calcite	siderite	calcite	quartz siderite hematite	none	feldspar (?)	quartz siderite
Quartz in clay fraction	+	+	-	-	+	+	-
Smectite	Fe- montmo- rillonite	Fe- montmo- rillonite	Fe- montmo- rillonite	Fe- montmo- rillonite	Fe- montmo- rillonite		
Green-Kelly test	partial	+	(?)	-	-		
Mixed-layered structure						R3 I(0.9)/S	R1 mica/V + R3 mica/S

5.3. Homoionic Rokle samples characterization

Mineralogical characterization of clay-fraction homoionic samples is depicted in the Fig 5.35. All of the samples contain kaolinite and anatase admixtures.

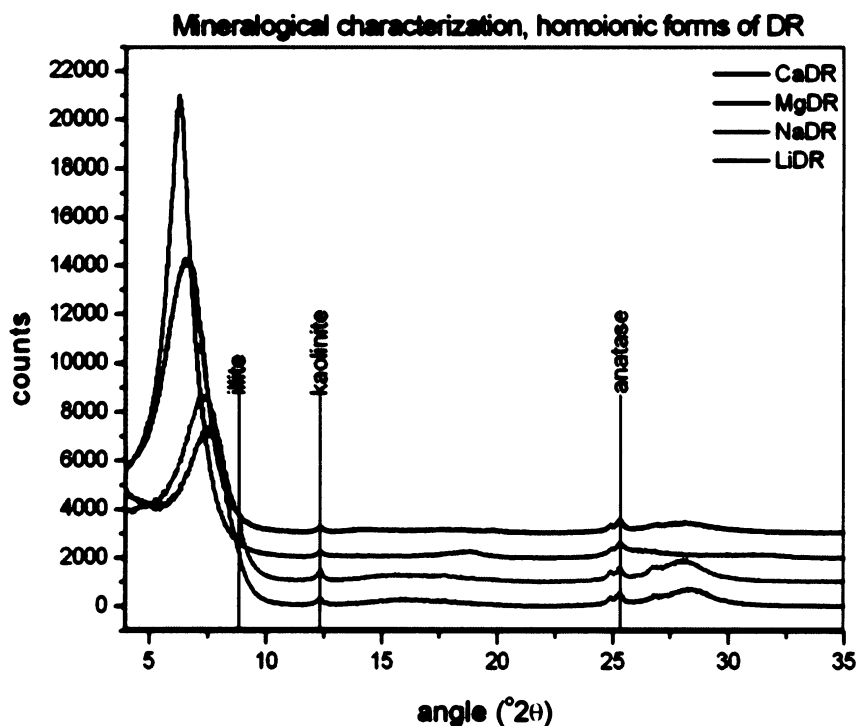


Fig. 5.35 - XRD diffraction patterns, oriented specimens of homoionic forms, prepared by suspension drying under laboratory conditions

The samples were further investigated using HTXRD (high temperature XRD, measured during in-situ heating). The 001 region of the data collected is shown in Figs. 5.36 – 5.39. The process of dehydration was evaluated by diffraction deconvolution using the Origin Pro PFM module. The position, height and full width in half maximum (FWHM) was examined. A ratio of diffraction height and FWHM was taken as a descriptor of the diffraction shape. A maximum value is reached when the diffraction is high and narrow – the structure is well defined. A minimum value is reached when the diffraction is low and wide and structural changes occur.

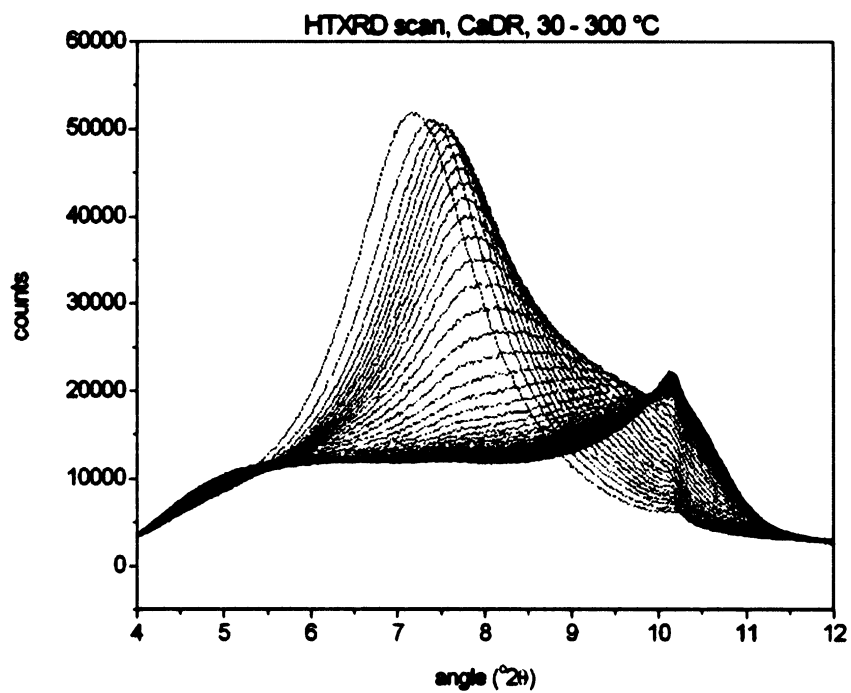


Fig. 5.36 - HTXRD scan of Ca-homoionic form of DR

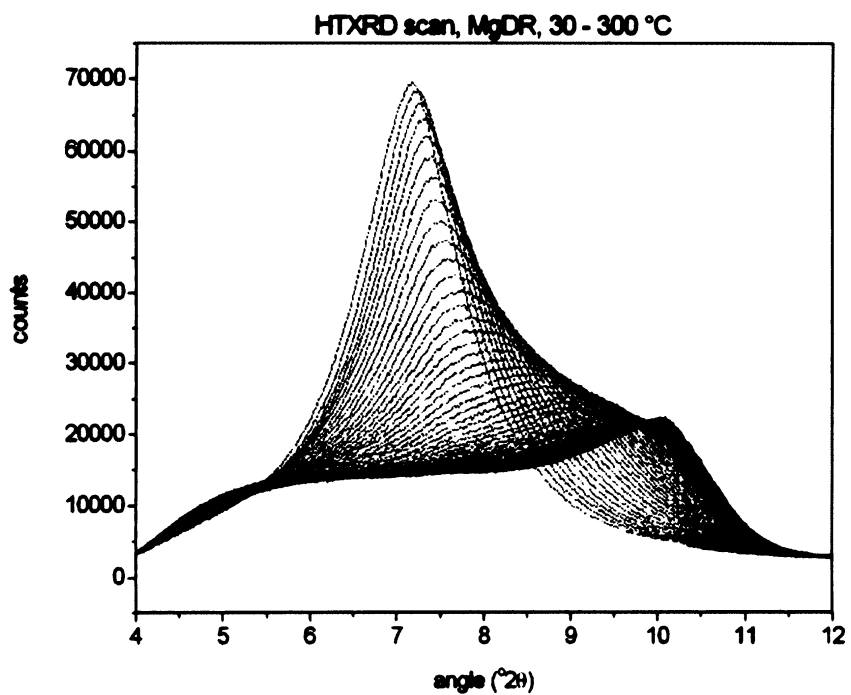


Fig. 5.37 - HTXRD scan of Mg-homoionic form of DR

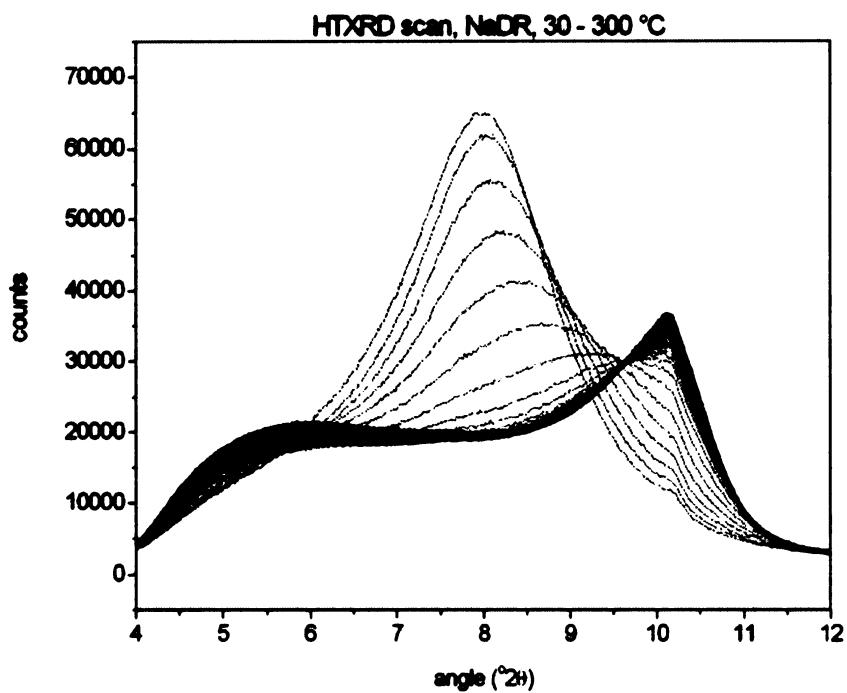


Fig. 5.38 - HTXRD scan of Na-homoionic form of DR

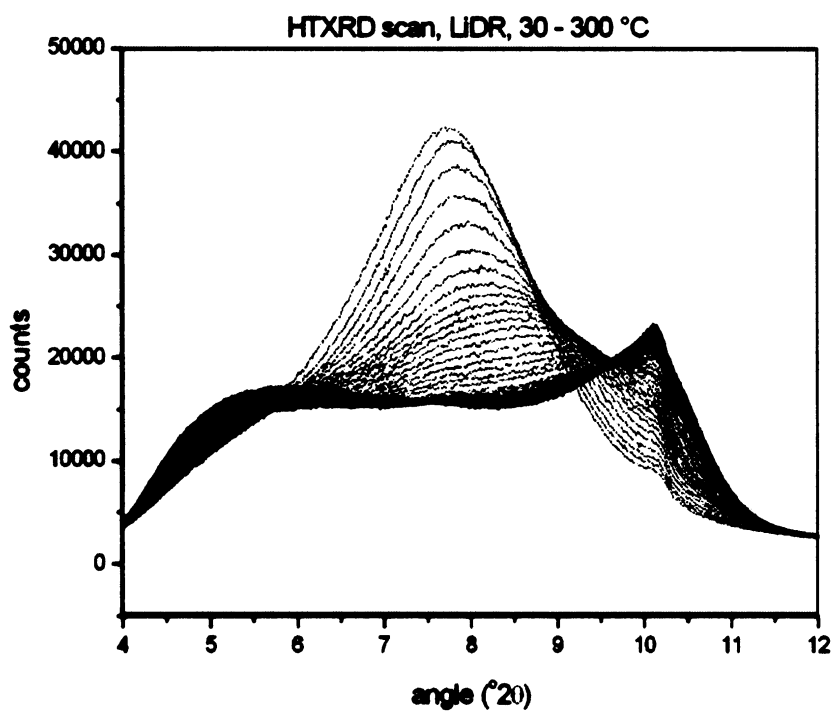


Fig. 5.39 - HTXRD scan of Li-homoionic form of DR

The results of 001 diffraction analysis are summed up in Figs. 5.40 and 5.41. The samples are separated into two groups. Monovalent-interlayer-cation samples dehydrate in one step within a 50 – 60 °C temperature interval. No further structural changes are observable after dehydration; the properties of 001 diffraction remain unchanged. The sodium sample dehydrates rapidly; the lithium sample dehydrates over a wider temperature interval (due to an inhomogeneous interlayer space occupation). Divalent-interlayer-cation samples show two dehydration steps. The first hydration shell is released over a 70 – 90 °C temperature interval, the remaining second hydration shell is released over a 110 – 135 °C interval. Reconstitution of the structure after dehydration is slow. The Mg²⁺ form exhibits higher thermo-resistance in comparison with the Ca²⁺ form (dehydration is shifted about 20 °C to higher temperatures).

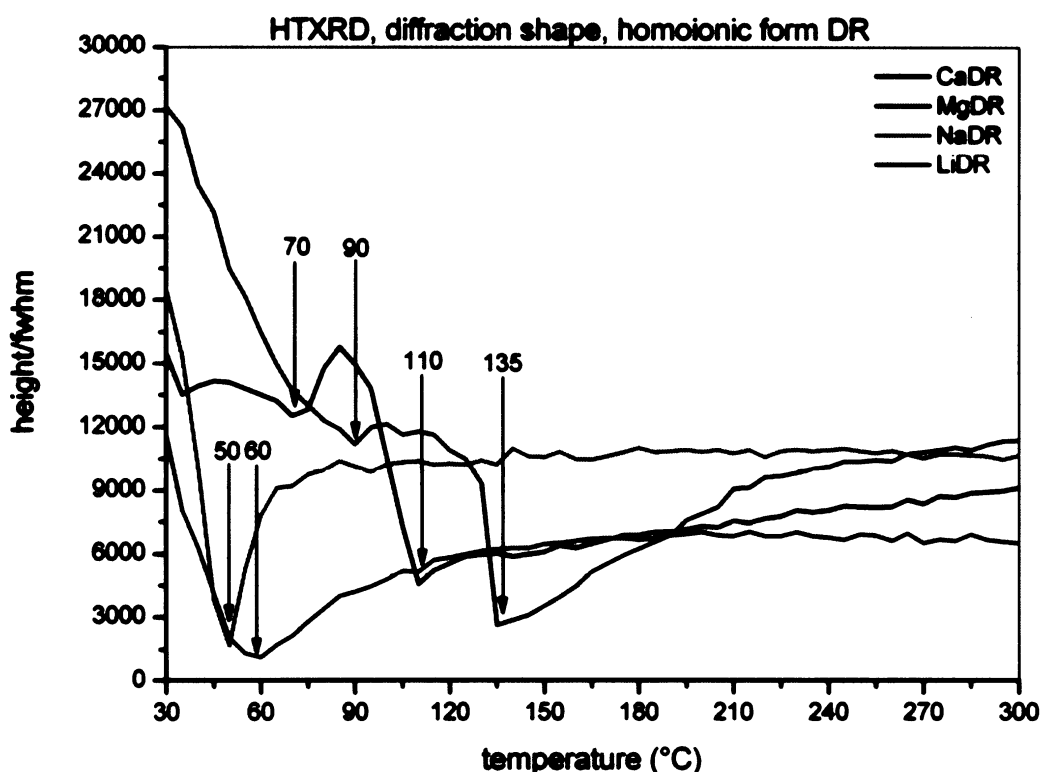


Fig. 5.40 - The results of deconvolution, evaluation of 001 diffraction shape

The analysis of 001 diffraction d-value is less informative, the first dehydration step is not observable, only the final collapse of the structure can be seen (Fig. 5.41). The structures with divalent cations collapse to approximately 10 Å, those with monovalent cations collapse to 10.4 Å. The results of dehydration are summarized in Table 5.6.

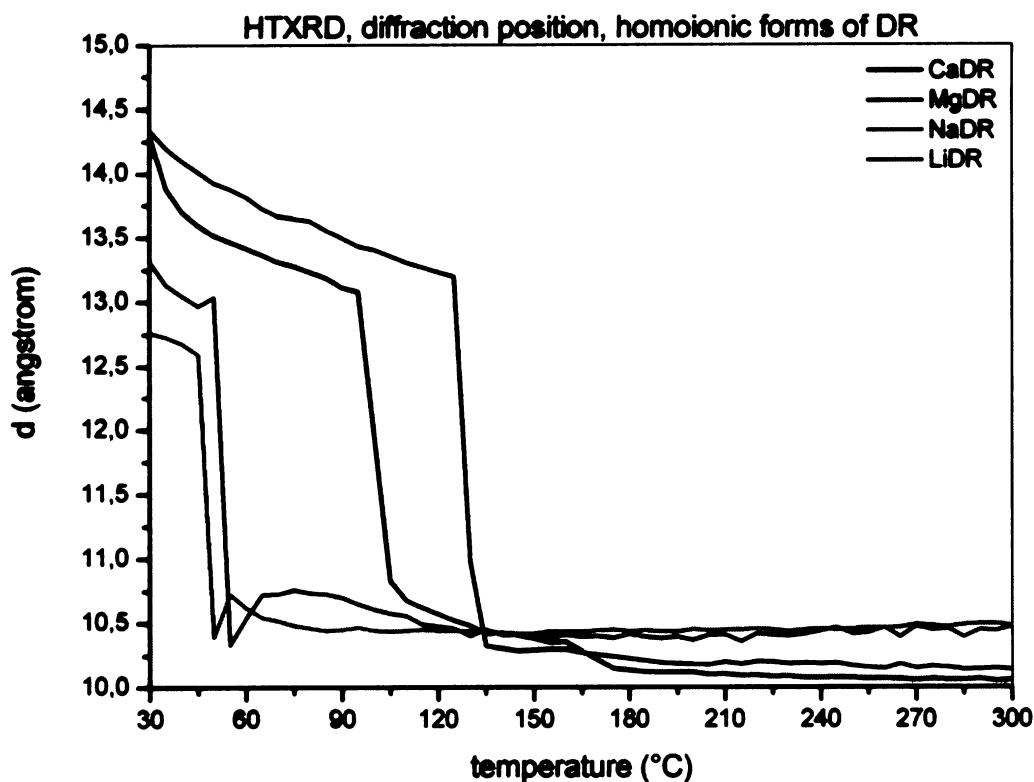


Fig. 5.41 - Result of deconvolution, evaluation of the 001 diffraction position

Table 5.6 - A comparison of dehydration temperatures according to the diffraction evaluation

Sample	Temperature (°C)	
	Diffraction shape (interval of 001 shift)	Diffraction position (ill-defined structure)
CaDR	95-100	110
MgDR	125-130	135
NaDR	45-50	50
LiDR	50-55	60

Conclusion on DR samples:

The fine-fractions of DR samples contain traces of illite, kaolinite and anatase. Transformation to the homoionic form was not completed concerning sodium and lithium form because of initial 001 diffracton position. The non-homogeneous interlayer space occupation can be seen from LiDR dehydration process which is very broad.

5.4. Cu-trien method

5.4.1. Reference samples

STx-1

For general overview of the results, *location and scale* estimates have been determined and are shown in Table 5.7. Graphical evaluation of *data dispersion* was performed using a box-plot (Fig. 5.42).

Table 5.7 - Estimates of the location and scale for the observation groups (sorted according to supernatant acquisition and CEC calculation)

Supernatant	CEC	Selection average	Median	Minimum	Maximum	Lower quartile	Upper quartile	Variance	Standard deviation
Centrifuged	Cu	75.00	75.36	65.94	81.32	73.13	76.53	11.90	3.45
	sum	79.88	79.07	73.08	87.80	76.95	82.90	18.59	4.31
	uv-vis	80.29	79.93	74.69	89.67	77.01	82.30	14.58	3.82
Filtered	Cu	76.05	76.12	66.70	83.23	75.01	76.93	12.94	3.60
	sum	76.52	76.57	69.61	82.79	74.13	78.44	12.35	3.51
	uv-vis	81.20	81.22	72.04	89.34	79.11	83.93	17.11	4.14

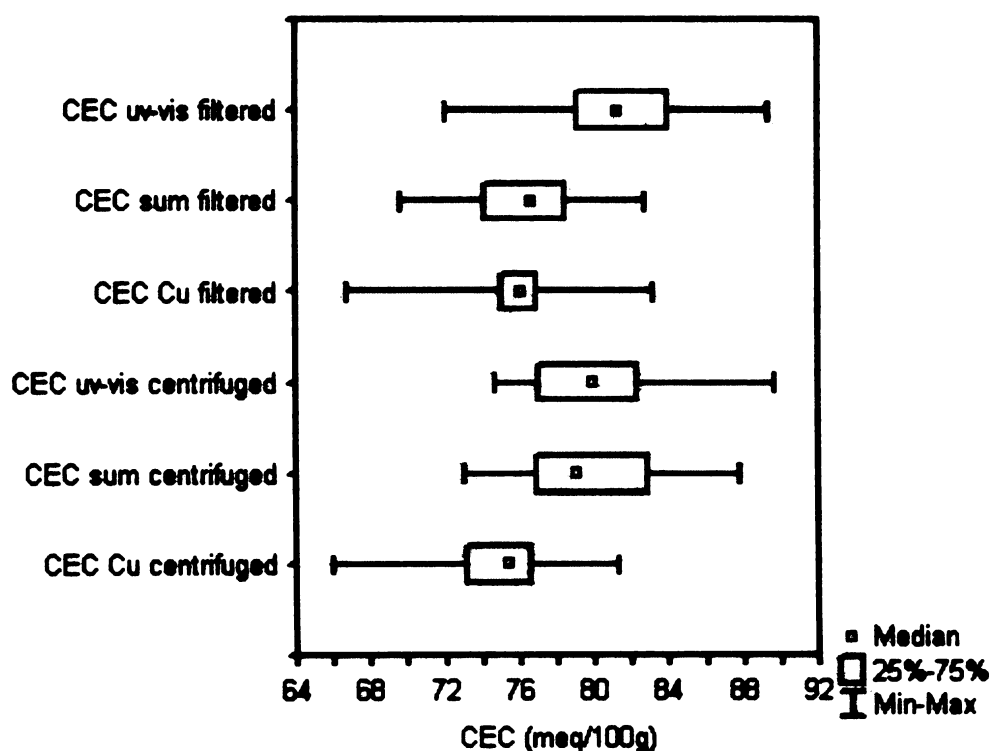


Fig. 5.42 - Box plot of CEC groups (according to supernatant acquisition and CEC calculation)

The smallest dispersion between the lower and upper quartile was found for CEC_{Cu} (AAS measurement, consumption of Cu²⁺), where supernatant was obtained by filtration. Centrifuged samples tend to exhibit asymmetric dispersion. Medians vary within a narrow interval of CEC values.

Normality of data distribution:

The data were tested for normal distribution using a histogram (Fig. 5.43) and tested with Kolmogorov-Smirnov and Shapiro-Wilks tests. The results are summarized in Table 5.8. (Note: the result of testing is the p-value, the lowest probability level when null hypothesis on normality of distribution is rejected. Common 5% lowest probability level (p = 0.05) is accepted, therefore, p values higher than 0.05 point to normal distribution). None of the observation groups was found to be of other than normal distribution using the two tests.

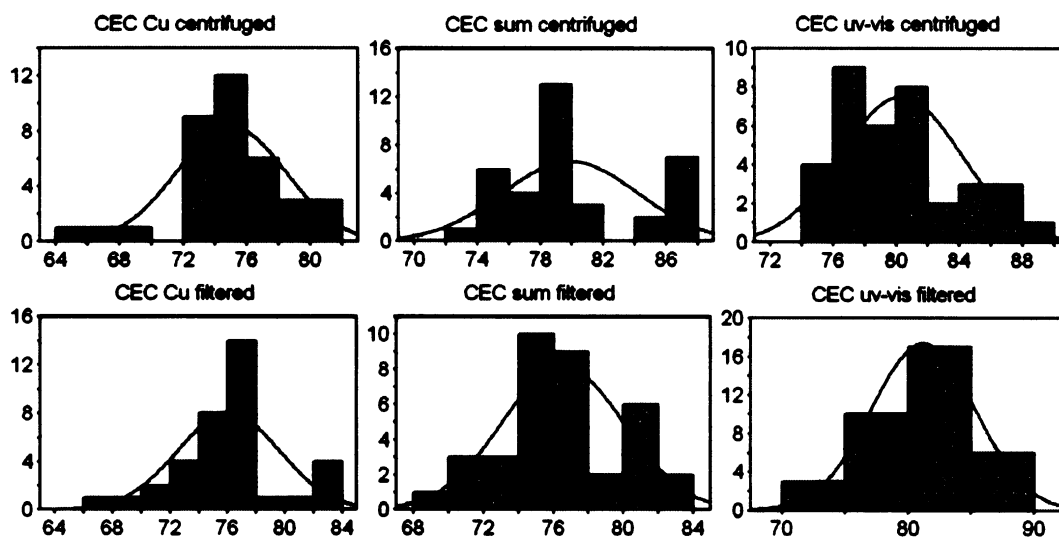


Fig. 5.43 - Histograms of observation groups (according to supernatant removal and CEC calculation), the red line represents normal distribution

Table 5.8 - Results of normality testing, groups with rejected normality are marked by grey colour

CEC	Test	P-value	
		Centrifuged	Filtered
CEC Cu	Kolmogorov-Smirnov	> 0.20	< 0.15
	Shapiro-Wilks	< 0.06	
CEC sum	Kolmogorov-Smirnov	< 0.15	> 0.20
	Shapiro-Wilks		< 0.31
CEC uv-vis	Kolmogorov-Smirnov	> 0.20	> 0.20
	Shapiro-Wilks	< 0.08	< 0.81

The influence of the addition and solution factors was inspected using multidimensional ANOVA. The test results are shown in Table 5.9. The influence of addition, solution and its interaction were found to be significant (except solution*addition interaction on CEC_{uv-vis}, filtered samples) concerning the resultant CEC.

Table 5.9 - Multidimensional ANOVA (MANOVA) table, results of addition and solution factors testing, p-values

MANOVA table (P-values)	Centrifuged samples			Filtered samples		
	CEC	CEC	CEC	CEC	CEC	CEC
	Cu	sum	uv-vis	Cu	sum	uv-vis
Solution	0.00	0.00	0.00	0.00	0.00	0.01
Addition	0.00	0.00	0.00	0.00	0.00	0.00
Interaction solution*addition	0.00	0.03	0.00	0.00	0.00	0.73

Influence of the analytical method used (calculation of CEC) was inspected using parametric and non-parametric tests. The results in the form of p-values are summarized in Table 5.10. The analytical method was found to be significant concerning both the ways of supernatant removal (Fig.5. 44).

Table 5.10 - Results of analytical method (calculation of CEC) influence

Test	Type	P-values	
		Centrifuged samples	Filtered samples
Kruskal-Wallis rank based	non-parametric	0.00	0.00
Median	non-parametric	0.00	0.00
One way ANOVA	parametric	0.00	0.00

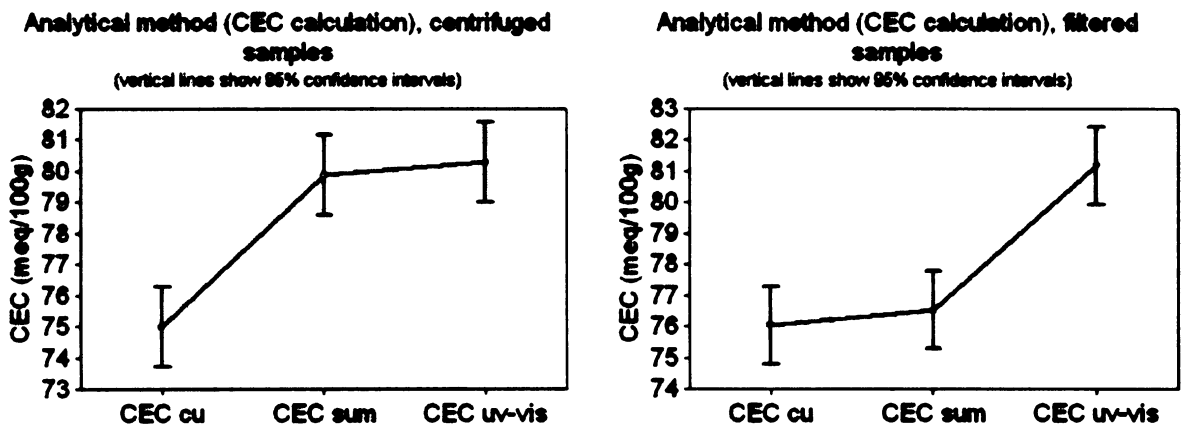


Fig. 5.44 - Investigation of analytical method (CEC calculation) influence on the results

For better resolution of differences in the results according to the analytical method used, a multiple mutual comparison of p-values was performed using the Kruskal-Wallis test. The results are shown in Table 5.11. In the case of centrifuged samples, there were no differences found in the location and distribution function in CEC_{sum} (AAS, sum of released ions) and CEC_{uv-vis} (determined colorimetrically). In the case of filtered samples, the CEC_{Cu} (AAS, Cu consumption) and CEC_{sum} were found to be of the same location and distribution.

Table 5.11 - Results of Kruskal-Wallis test, multiple mutual comparison of p-values, detailed investigation of analytical method (CEC calculation) influence

	Centrifuged			Filtered		
	CEC Cu	CEC sum	CEC uv-vis	CEC Cu	CEC sum	CEC uv-vis
CEC Cu		0.00	0.00		1.00	0.00
CEC sum	0.00		1.00	1.00		0.00
CEC uv-vis	0.00	1.00		0.00	0.00	

The influence of supernatant acquisition was investigated using parametric and non-parametric tests. The results of testing are shown in Table 5.12. According to the test results, there is no influence of supernatant acquisition concerning CEC_{Cu} and CEC_{uv-vis} . The sum of cations was found to be dependent by all the tests applied (see also Fig.5.45).

Table 5.12 - Testing the supernatant acquisition influence

Test	Type	P-value		
		CEC Cu	CEC sum	CEC uv-vis
Mann-Whitney U test	non-parametric	0.13	0.001	0.23
Kolmogorov-Smirnov	non-parametric	>0.10	<0.005	>0.10
Wald-Wolfowitz	non-parametric	0.48	1.002	0.81
One way ANOVA	parametric	0.21	0.002	0.34

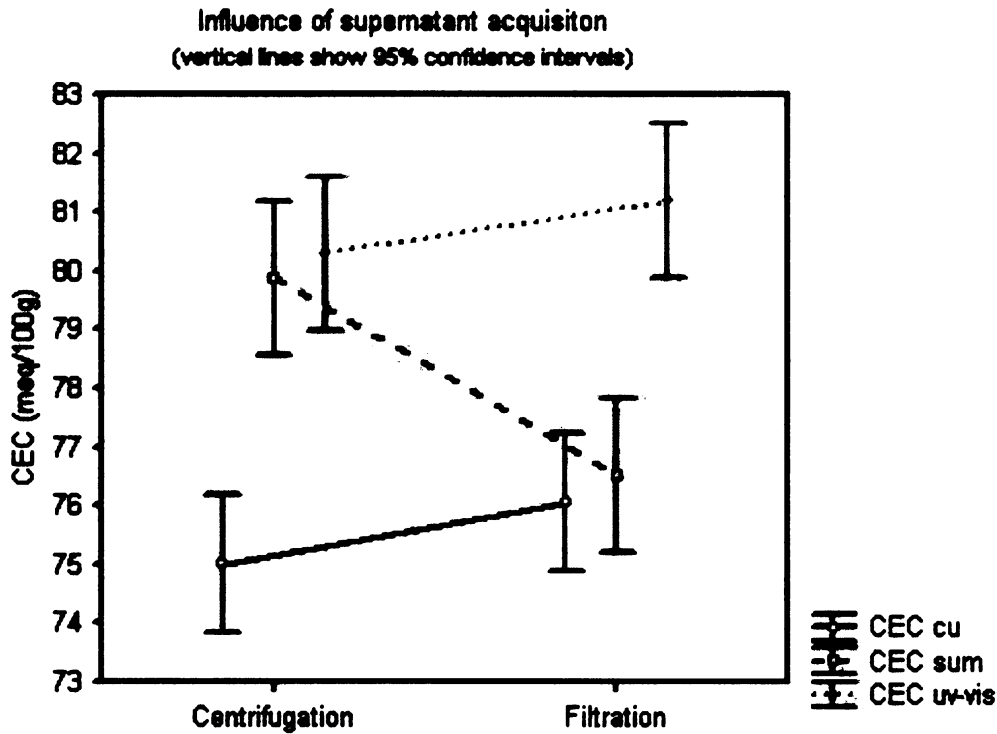


Fig. 5.45 - Influence of supernatant acquisition on the CEC results

SWy-2

Location and scale estimates for groups of observations (sorted according to the supernatant acquisition and CEC calculation) were calculated and are shown in the Table 5.13. The data *dispersion* was expressed graphically, using the box-plot shown in Fig. 5.46.

Table 5.13 - Location and scale estimates for groups of observations (sorted according to the supernatant acquisition and CEC calculation)

Supernatant	CEC	Selection average	Median	Minimum	Maximum	Lower quartile	Upper quartile	Variance	Standard deviation
Centrifuged	Cu	73.15	73.97	67.00	78.19	71.57	75.07	7.42	2.72
	sum	96.89	97.87	88.77	103.94	92.94	100.75	21.59	4.65
	uv-vis	76.64	76.76	71.57	80.74	75.07	78.92	7.01	2.65
Filtered	Cu	74.53	75.14	67.99	80.99	72.07	76.52	11.64	3.41
	sum	86.24	86.14	80.37	93.05	84.95	87.60	7.46	2.73
	uv-vis	78.74	78.43	73.66	86.89	75.02	81.75	14.14	3.76

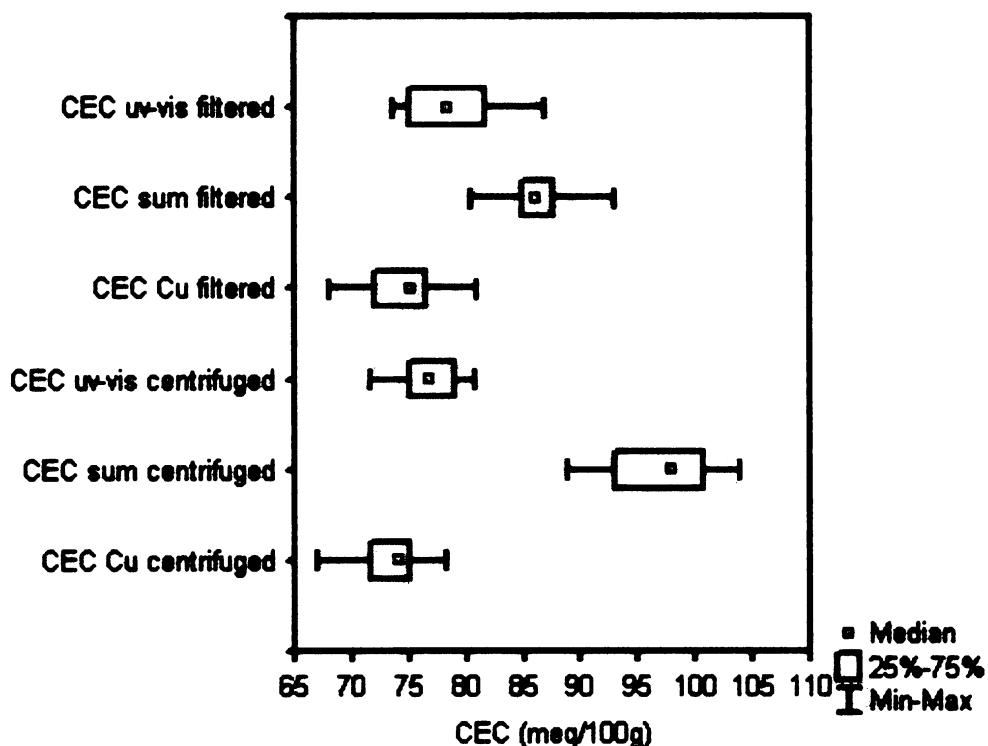


Fig. 5.46 - Box plot of groups of observations (sorted according to the supernatant acquisition and CEC calculation)

All CEC's determined as the sum of the released cations are significantly different concerning the location (median). The most symmetrical distribution (omitting CEC_{sum}) seems to be exhibited by the CEC_{Cu}, filtered samples.

Normality of the data distribution was investigated using histogram and statistical testing (Kolmogorov-Smirnov and Shapiro-Wilks tests). The histograms are shown in Fig. 5.47 and the results of statistical testing in the form of p-values can be seen in Table 5.14. None of the observations was found by using the two tests to be of another distribution.

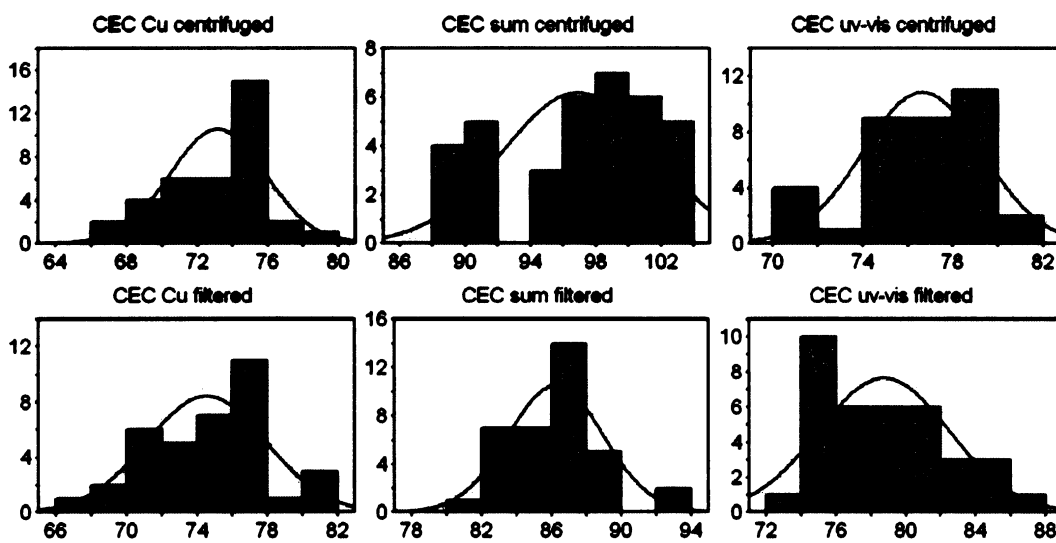


Fig. 5.47 - Histograms of groups of observations (sorted according to supernatant acquisition and CEC calculation), red line represents normal distribution

Table 5.14 - Results of normality testing (cases with rejected normal distribution are highlighted grey)

CEC	Test	P- value	
		Centrifuged	Filtered
CEC Cu	Kolmogorov-Smirnov	> 0.20	> 0.20
	Shapiro-Wilks	< 0.37	< 0.25
CEC sum	Kolmogorov-Smirnov	> 0.20	> 0.20
	Shapiro-Wilks	< 0.01	< 0.16
CEC uv-vis	Kolmogorov-Smirnov	> 0.20	> 0.20
	Shapiro-Wilks	< 0.01	< 0.01

Influence of solution and addition factors and their interaction was performed using multidimensional ANOVA (MANOVA). The results are summarized in Table 5.15. Both the factors were found to be significant (except for the addition in the case of filtered samples calculating CEC_{sum}) as well as their interactions.

Table 5.15 - Results of MANOVA, influence of solution and addition factors

MANOVA table (p-values)	Centrifuged samples			Filtered samples		
	CEC	CEC	CEC	CEC	CEC	CEC
	Cu	sum	uv-vis	Cu	sum	uv-vis
Solution	0.00	0.00	0.00	0.00	0.00	0.00
Addition	0.00	0.00	0.00	0.00	0.75	0.00
Interaction solution*addition	0.00	0.00	0.00	0.00	0.02	0.00

Influence of analytical method (calculation of CEC) was investigated by parametric and non-parametric tests. The results of testing are shown in Table 5.16. Analytical method (CEC calculation) has an influence on the results in both centrifuged and filtered groups of samples (Fig. 5.48).

Table 5.16 - Results of analytical method (calculation of CEC) influence testing

Test	Type	P-values	
		Centrifuged	Filtered
Kruskal-Wallis, rank based	non-parametric	0.00	0.00
Median	non-parametric	0.00	0.00
One way ANOVA	parametric	0.00	0.00

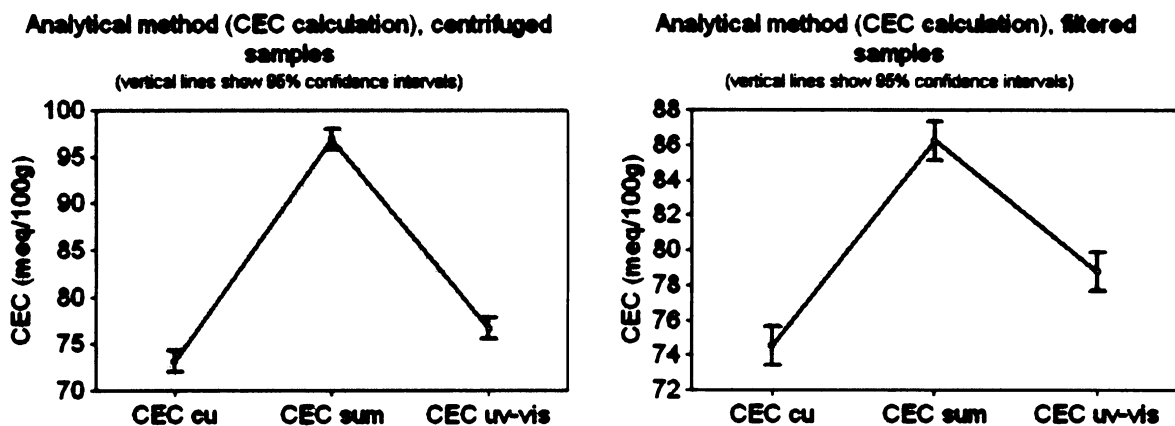


Fig. 5.48 - Influence of analytical method (CEC calculation), sorted by supernatant acquisition

For detailed inspection of analytical method influence, a multiple mutual comparison of p-values using the Kruskal-Wallis test was employed. The results are shown in Table 5.17. Testing revealed no similarity among groups of results. Each method (CEC calculation) leads to a different result.

Table 5.17 - Multiple mutual comparisons of p-values of Kruskal-Wallis test, detailed inspection of analytical method (CEC calculation) influence

(p-values)	Centrifuged			Filtered		
	CEC Cu	CEC sum	CEC uv-vis	CEC Cu	CEC sum	CEC uv-vis
CEC Cu		0.00	0.00		0.00	0.01
CEC sum	0.00		0.00	0.00		0.00
CEC uv-vis	0.00	0.00		0.01	0.00	

Testing of *supernatant acquisition* influence was performed using parametric and non-parametric tests. The results are shown in Table 5.18. Considering the non-parametric tests in all the CEC calculated, the influence of supernatant acquisition is significant (see Fig. 5.49).

Table 5.18 - Testing the supernatant acquisition influence

Test	Type	P-value		
		CEC Cu	CEC sum	CEC uv-vis
Mann-Whitney U test	non-parametric	0.04	0.00	0.06
Kolmogorov-Smirnov	non-parametric	0.05	0.00	0.05
Wald-Wolfowitz	non-parametric	0.10	0.00	0.05
One way ANOVA	parametric	0.06	0.00	0.05

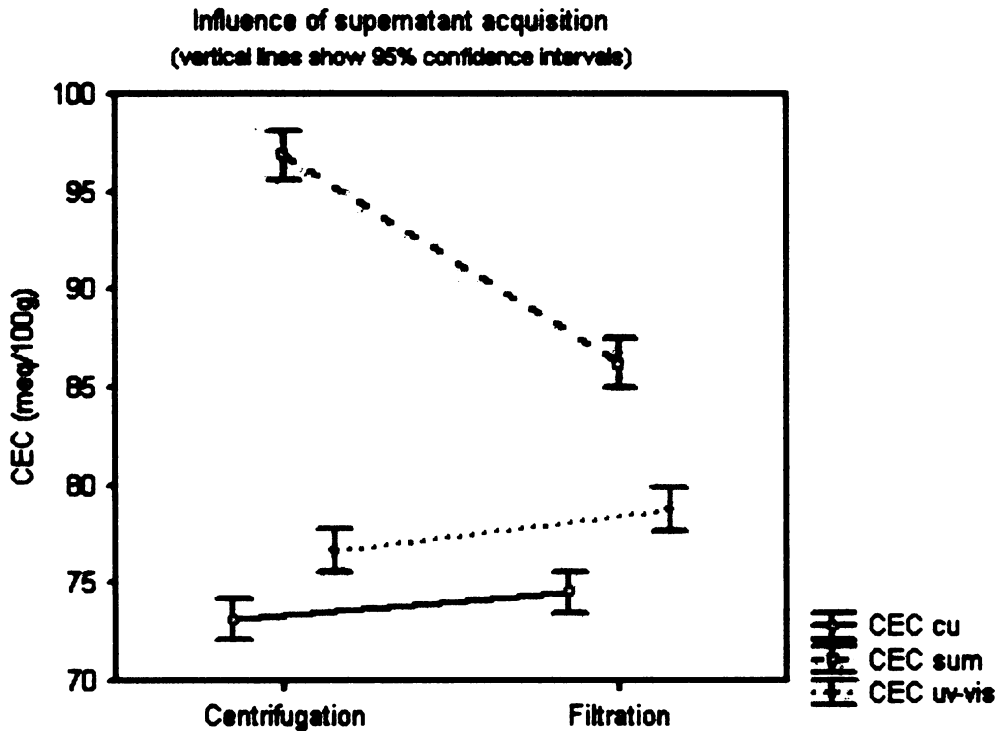


Fig. 5.49 - Influence of supernatant acquisition on CEC results

Summary:

All the standards and the groups of observations were found by both the normality tests to be normal (nevertheless non-parametric testing is stressed). Measurement of standards showed:

- Addition and solution factors and their interaction have influence on the CEC result
- Chosen analytical method (CEC calculation) has an influence on the CEC results, STx-1 showed similarity of CEC_{sum} and CEC_{uv-vis} concerning centrifuged samples and CEC_{Cu} and CEC_{sum} concerning filtered samples, SWy-2 did not show any similarities
- Supernatant acquisition was found to be significant in the case of CEC_{sum} of STx-1 sample and in all the cases concerning SWy-2 sample

Filtration generally causes lowering of CEC_{sum} and a slight increase in CEC_{Cu} and CEC_{uv-vis} . A significant difference in the CEC values was found for the SWy-2 sample where CEC_{sum} is significantly higher amongst other CEC values. Dissolution of calcite admixture is supposed. Higher scattering of SWy-2 sample compared with STx-1 is probably caused by the monovalent Na^+ cation being exchanged for divalent Cu^{2+} . (Note: the small number of results lowers the reliability of statistical testing. Faster filtration procedure and a lower significance of released cations (risk of contamination by admixture dissolution, difficulties in homoionic form preparation) led to the application of filtration in investigation of CEC for homoionic DR samples.

5.4.2. Homoionic DR samples

Location and scale descriptions were calculated and are shown in Table 5.19.

Table 5.19 - Location and scale estimates of homoionic DR observations

Form	CEC	Selection average	Median	Minimum	Maximum	Lower quartile	Upper quartile	Variance	Standard deviation
CaDR	Cu	71.82	71.46	62.56	91.88	66.63	74.15	45.81	6.77
	Ca	62.88	64.15	56.16	72.04	58.55	65.34	17.80	4.22
	uv-vis	71.77	72.13	65.78	77.22	69.54	73.71	9.15	3.03
MgDR	Cu	71.82	72.73	61.45	83.78	67.56	75.38	34.15	5.84
	Mg	61.07	59.76	54.65	72.05	56.56	64.35	27.29	5.22
	uv-vis	72.89	71.09	65.26	89.78	69.30	77.02	27.17	5.21
NaDR	Cu	72.88	70.67	63.65	89.61	67.62	76.59	52.61	7.25
	Na	46.98	46.48	44.13	50.83	45.73	48.61	3.58	1.89
	uv-vis	75.86	74.56	64.73	100.26	68.81	78.88	83.66	9.15
LiDR	Cu	77.07	77.10	68.76	91.70	73.62	79.49	24.30	4.93
	Li	51.05	51.01	49.76	53.35	50.44	51.38	0.56	0.75
	uv-vis	78.46	75.43	71.81	98.87	73.31	82.65	43.41	6.59

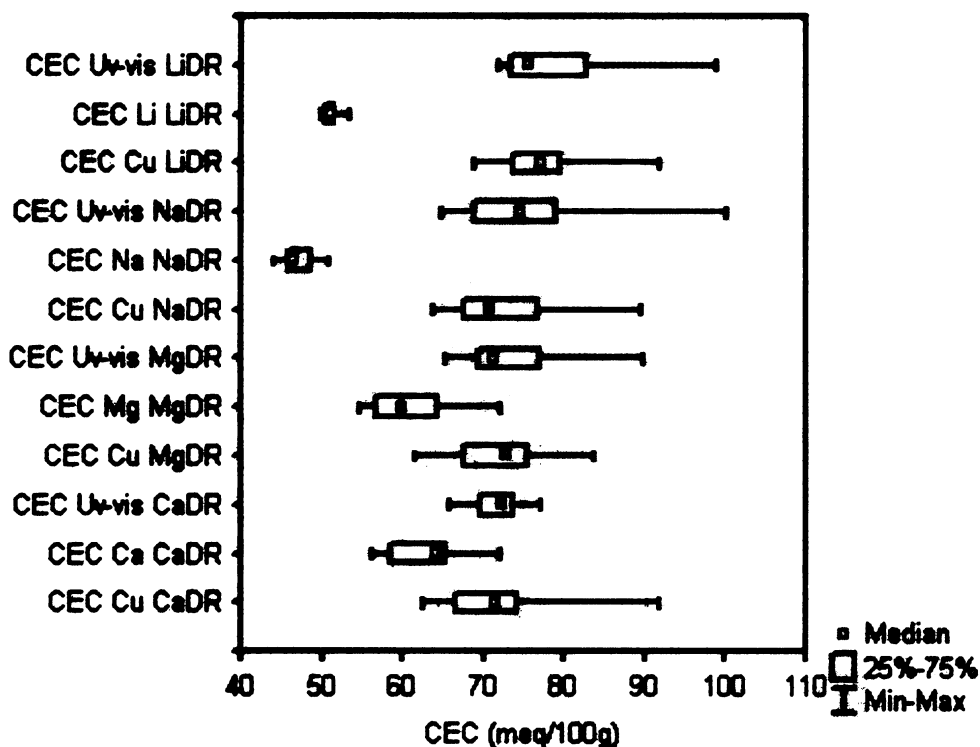


Fig. 5.50 - Box plot of homoionic DR samples observation

Data *dispersion* was observed using box plot (Fig. 5.50). Medians of CEC calculated from released interlayer cation deviates towards lower CEC value in the order, $\text{Ca}^{2+} > \text{Mg}^{2+} > \text{Li}^+ > \text{Na}^+$. Dispersion of CEC_{Na} and CEC_{Li} is influenced by the lower number of measurements.

Normality of data distributions was inspected using histogram (Fig 5.51) and statistical tests. Table 5.20 summarizes the results of testing. None of the groups of homoionic samples observed (sorted according to homoionic form and the analytical method (CEC calculation)) was confirmed by both the tests to be of different than normal distribution. Non-parametric testing should be stressed.

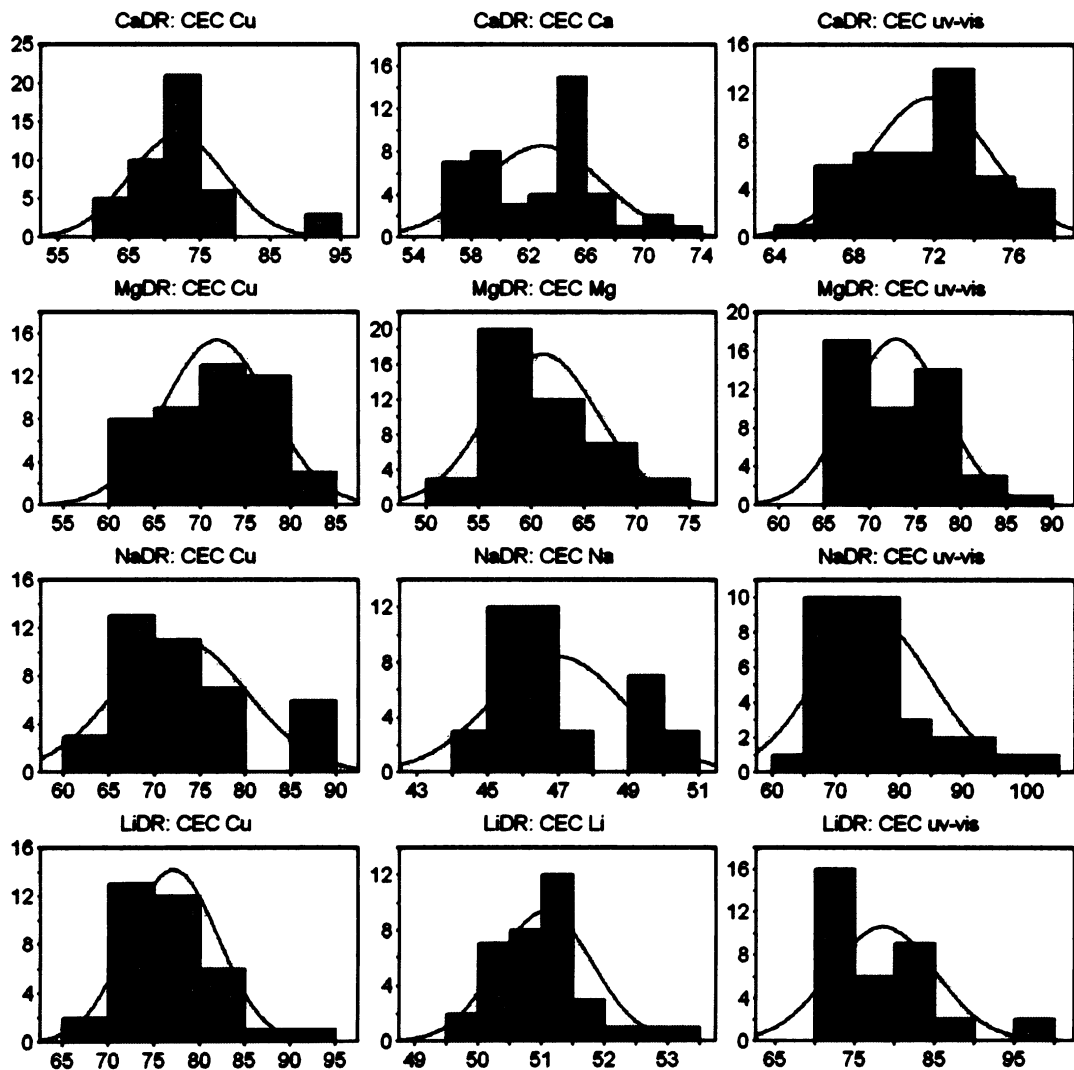


Fig. 5.51 - Histograms of homoionic DR samples (sorted according to homoionic form and calculated CEC)

Table 5.20 - Testing the normality of distribution, homoionic DR samples, sorted according to the analytical method (CEC calculation), table contains p-values

Homoionic form	Test	CEC		
		Cu	M	uv-vis
CaDR	Kolmogorov-Smirnov	> 0.20	> 0.20	> 0.20
	Shapiro-Wilks	< 0.00	< 0.00	< 0.35
MgDR	Kolmogorov-Smirnov	> 0.20	< 0.10	< 0.15
	Shapiro-Wilks	< 0.36	< 0.00	< 0.00
NaDR	Kolmogorov-Smirnov	< 0.10	< 0.10	> 0.20
	Shapiro-Wilks	< 0.00	< 0.00	< 0.00
LiDR	Kolmogorov-Smirnov	> 0.20	> 0.20	< 0.15
	Shapiro-Wilks	< 0.08	< 0.11	< 0.00

The influence of *addition and solution factors* and their interaction was observed applying multidimensional ANOVA (MANOVA). The results of MANOVA testing are

shown in Table 5.21. The influence of both the factors and their interaction were found to be significant (except for addition in the case of CEC_{Na}). The influence of the addition factor on CEC is shown in Fig. 5.52 and points to interesting relations in CEC_{Mg} and CEC_{uv-vis} of NaDR and LiDR samples (Fig.5.53, 5.54 and 5.55). Increasing concentration of free trien and addition of the stock solution increases the results for CEC_{uv-vis} of monovalent cations. Magnesium is released in proportion to the addition of the stock solution. The release of Mg²⁺ is inversely proportional to the increasing concentration of free trien in the stock solution.

Table 5.21 - MANOVA table, statistical testing of solution and addition factors (sorted according to the homoionic form and analytical method -CEC calculation)

Homoionic form	CEC	P-values		
		Solution	Addition	Interaction solution*addition
CaDR	CEC Cu	0.00	0.00	0.00
	CEC Ca	0.00	0.00	0.00
	CEC uv-vis	0.00	0.00	0.00
MgDR	CEC Cu	0.00	0.00	0.00
	CEC Mg	0.00	0.00	0.00
	CEC uv-vis	0.00	0.00	0.00
NaDR	CEC Cu	0.00	0.00	0.00
	CEC Na	0.00	0.23	0.03
	CEC uv-vis	0.00	0.00	0.00
LiDR	CEC Cu	0.00	0.00	0.00
	CEC Li	0.00	0.02	0.00
	CEC uv-vis	0.00	0.00	0.00

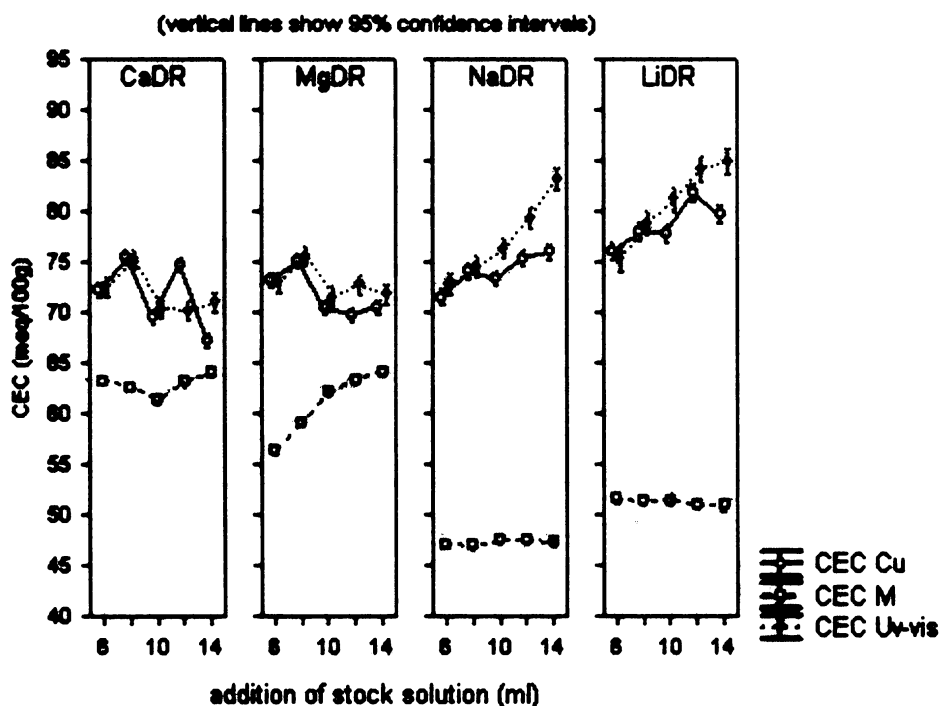


Fig. 5.52 - Influence of addition factor on CEC values

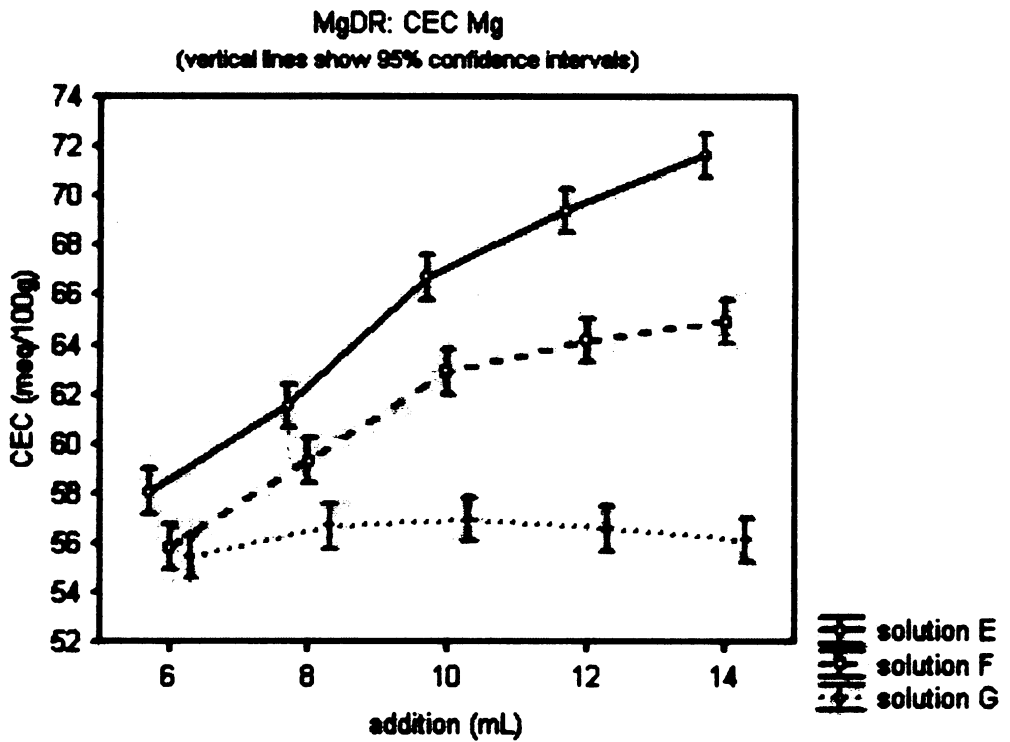


Fig. 5.53 - Interaction of solution and addition factors in MgDR sample, group of CEC_{Mg} observations

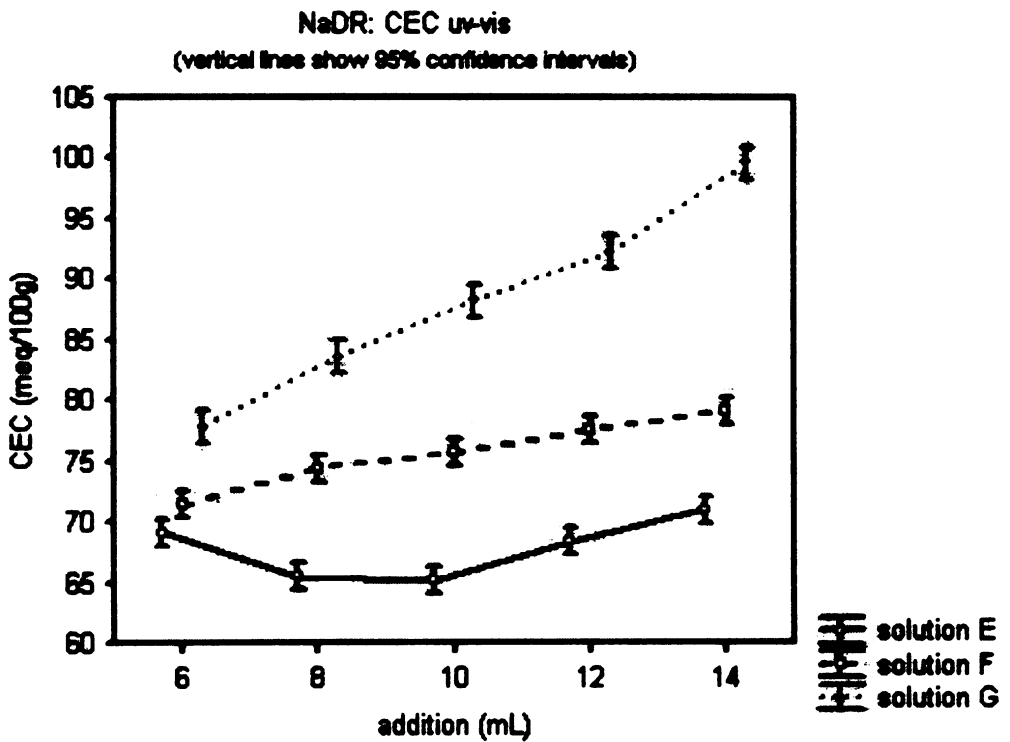


Fig. 5.54 - Interaction of solution and addition factors in NaDR sample, group of CEC_{uv-vis} observations

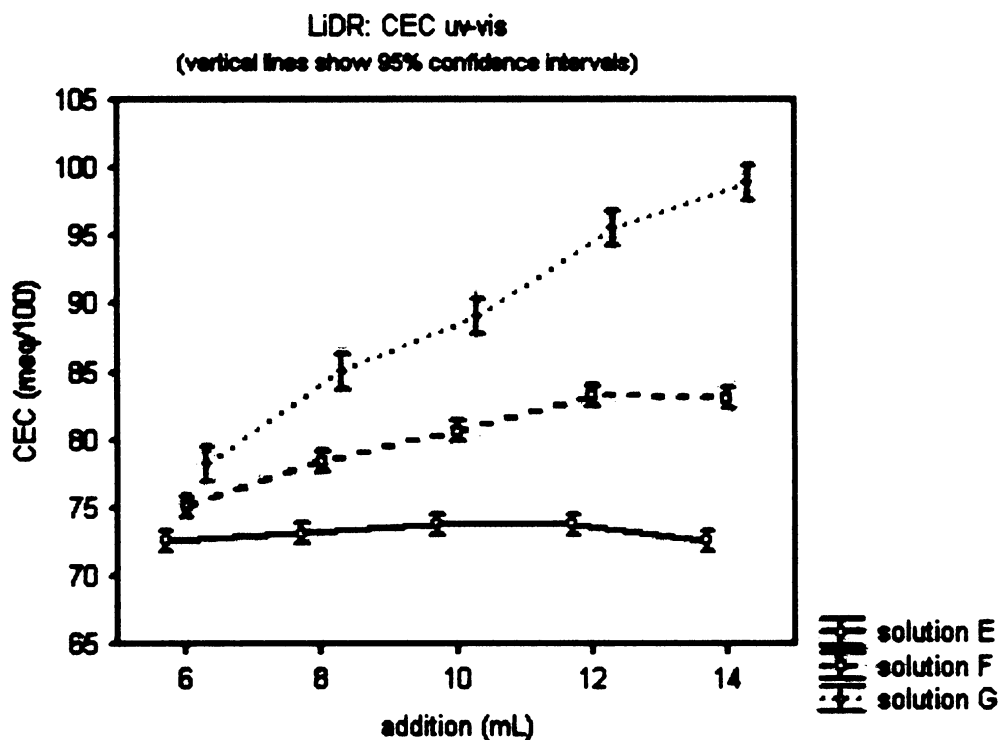


Fig. 5.55 - Interaction of solution and addition factors in LiDR sample, group of CEC_{uv-vis} observations

The influence of the *analytical method* (CEC calculation) on the results was tested with parametric and non-parametric tests and in all cases was found to be significant (Table 5.22). For better resolution of relations within the homoionic form groups a multiple mutual comparisons of p-values was performed using the Kruskal-Wallis test (Tables 5.23, 5.24, 5.25, and 5.26). In all the cases, CEC_{Cu} and CEC_{uv-vis} were found to yield similar results. The CEC determined from the released interlayer cations (Ca²⁺, Mg²⁺, Na⁺, and Li⁺) differed in all the cases.

Table 5.22 - Influence of analytical method (CEC calculation) on results (sorted according to homoionic form)

Test	Type	P-value			
		Ca DR	Mg DR	Na DR	Li DR
Kruskal-Wallis	non-parametric	0.00	0.00	0.00	0.00
Median	non-parametric	0.00	0.00	0.00	0.00
One-way ANOVA	parametric	0.00	0.00	0.00	0.00

Table 5.23 - CaDR samples

	CEC Cu	CEC Ca	CEC uv-vis
CEC Cu		0.00	1.00
CEC Ca	0.00		0.00
CEC uv-vis	1.00	0.00	

Table 5.24 - MgDR samples

	CEC Cu	CEC Mg	CEC uv-vis
CEC Cu		0.00	1.00
CEC Mg	0.00		0.00
CEC uv-vis	1.00	0.00	

Table 5.25 - NaDR samples

	CEC Cu	CEC Na	CEC uv-vis
CEC Cu		0.00	0.92
CEC Na	0.00		0.00
CEC uv-vis	0.92	0.00	

Table 5.26 - LiDR samples

	CEC Cu	CEC Li	CEC uv-vis
CEC Cu		0.00	1.00
CEC Li	0.00		0.00
CEC uv-vis	1.00	0.00	

Influence of ionic form on the CEC results according to the type of CEC calculated are given below. In the group of CEC_{Cu} observations, the Ca^{2+} , Mg^{2+} and Na^{+} homoionic forms are interchangeable (equivalent), no significant influence of form on CEC_{Cu} was found. The Li^{+} -homoionic form significantly differs from the others. Conclusions come from multiple mutual comparisons of p-values of the Kruskal-Wallis test (Table 5.27).

Table 5.27 – Multiple mutual comparison of p-values, investigation of homoionic form influence on CEC_{Cu}

	P-values			
	Ca	Mg	Na	Li
Ca		1.00	1.00	0.00
Mg	1.00		1.00	0.00
Na	1.00	1.00		0.00
Li	0.00	0.00	0.00	

Conclusions of multiple mutual p-values comparison can be seen inamong themselves Fig. 5.56.

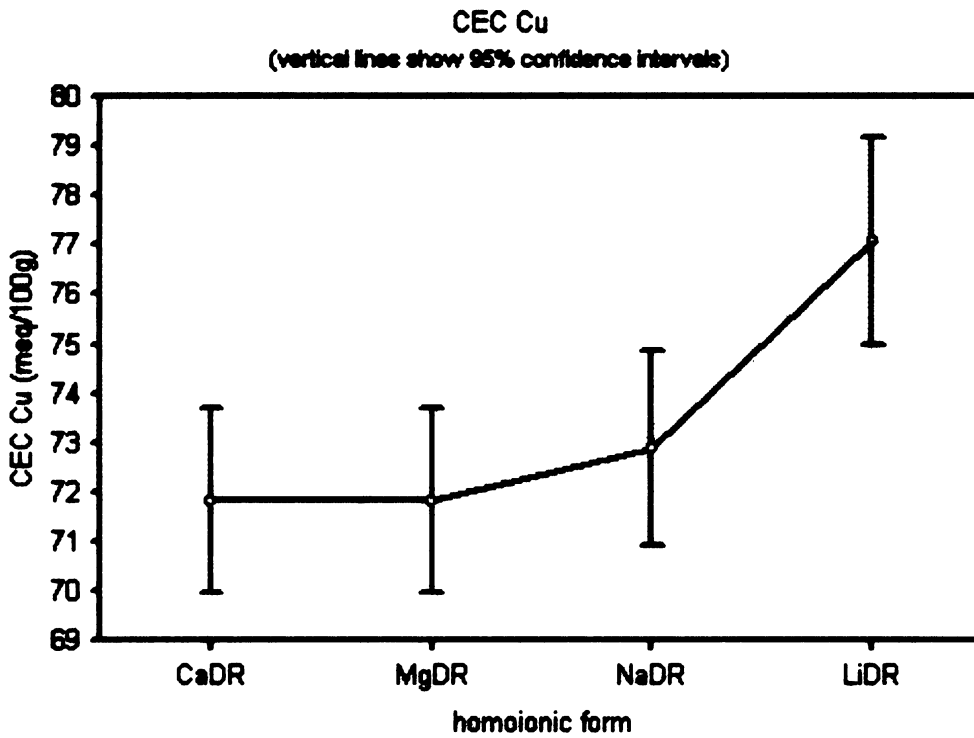


Fig. 5.56 - Influence of homoionic form on CEC_{Cu} values

Multiple mutual comparison of p-values (Kruskal-Wallis test) of $CEC M^{++}$ revealed that only CEC_{Ca} and CEC_{Mg} are similar. The CEC_{Na} and CEC_{Li} differ and they also differ among themselves (see Table 5.28 and Fig. 5.57).

Table 5.28 - Multiple mutual comparison of p-values, investigation of influence of homoionic form on CEC_M

	P-values			
	Ca	Mg	Na	Li
Ca		1.00	0.00	0.00
Mg	1.00		0.00	0.00
Na	0.00	0.00		0.01
Li	0.00	0.00	0.01	

Multiple mutual comparison of CEC_{uv-vis} revealed decreasing similarity in the row $Ca^{2+}-Mg^{2+}-Na^{+}-Li^{+}$ (Table 5.29). Situation is better understood from Fig. 5.58.

Table 5.29 - Multiple mutual comparison of p-values, investigation of influence of homoionic form on CEC_{uv-vis}

	P-values			
	Ca	Mg	Na	Li
Ca		1.00	0.22	0.00
Mg	1.00		0.93	0.00
Na	0.22	0.93		0.05
Li	0.00	0.00	0.05	

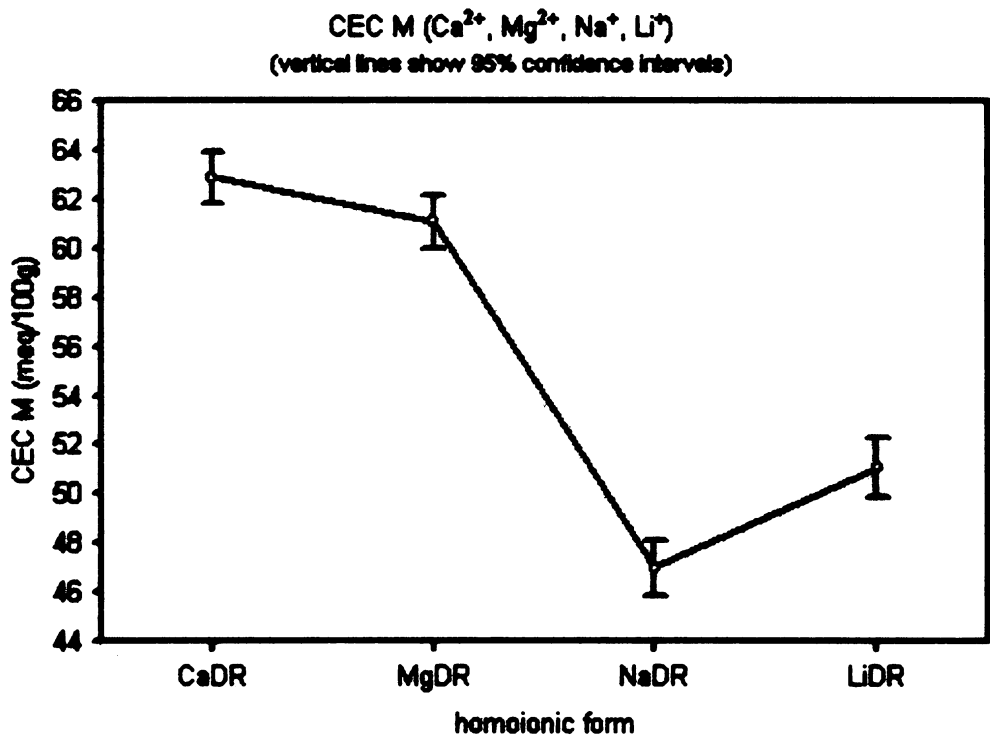


Fig. 5.57 - Investigation of homoionic form influence on CEC_M

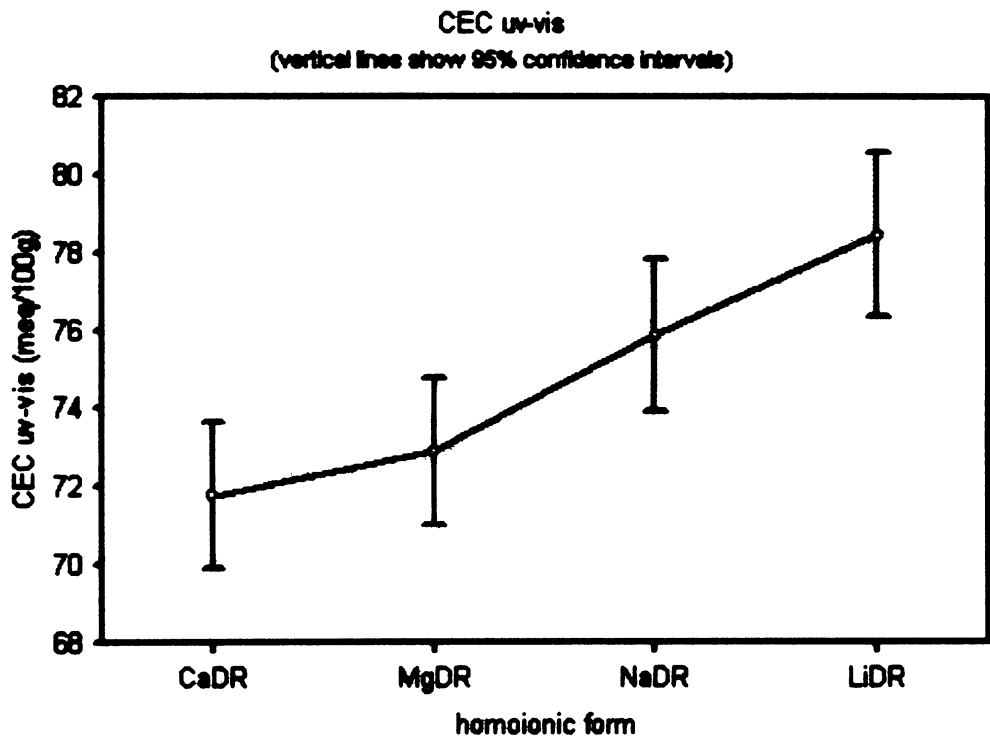


Fig. 5.58 - Investigation of homoionic form influence on $\text{CEC}_{\text{uv-vis}}$

Summary:

Data dispersion of CEC_{Na} and CEC_{Li} is caused by the low number of observations. None of the groups of observations was found to be of other than normal distribution. Tests based on normality condition were of a lower significance and non-parametric

tests were stressed. MANOVA confirmed influence of additon and solution factors (except CEC_{Na} where addition was found to be negligible). An interaction of solution and addition factors was found for CEC_{uv-vis} of monovalent homoionic forms. The CEC_{uv-vis} values were directly related to the concentration of free trien in the stock solution and additon of stock solution. The release of magnesium is related negatively to the free trien concentration in the stock solution and positively to the stock solution addition.

In all homoionic groups the CEC_{Cu} and CEC_{uv-vis} were found to give the same results and CEC_M to differ significantly. The influence of the interlayer cation on CEC showed similar behaviour for CEC_{Cu} and CEC_{uv-vis} confirming their interchangeability. The CEC_{Cu} and CEC_{uv-vis} increase in the $Ca^{2+} < Mg^{2+} < Na^+ < Li^+$ order.

5.5. Comparison of Cu-trien, ammonium acetate and AgTU method

For comparison of Cu-trien, ammonium acetate and AgTU methods, the collected clays were used. Characterization of samples revealed the presence of five smectite-rich samples (CV1BE, CV2BE, CV3BE, HAJBE, STSTBE) and two samples of low expandability containing partially expandable structures (Illite Füz and ME82). The selection itself is neither random nor homogeneous (bentonites prevail). The data dispersion can be seen on a box plot (Fig. 5.59). The data distributions are most probably of other than normal distribution. Normality testing is excluded and non-parametric tests are stressed.

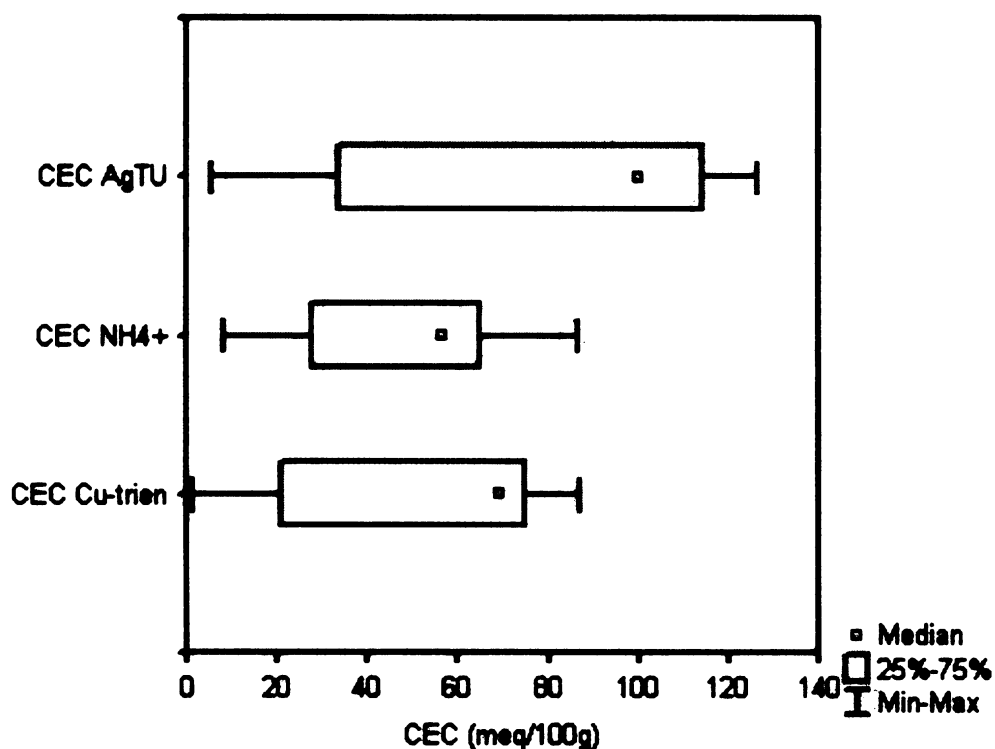


Fig. 5.59 - Box plot, data dispersion of various methods for CEC determination

The CEC results of collected clays, obtained using Cu-trien, ammonium acetate and AgTU method are given in Fig. 5.60.

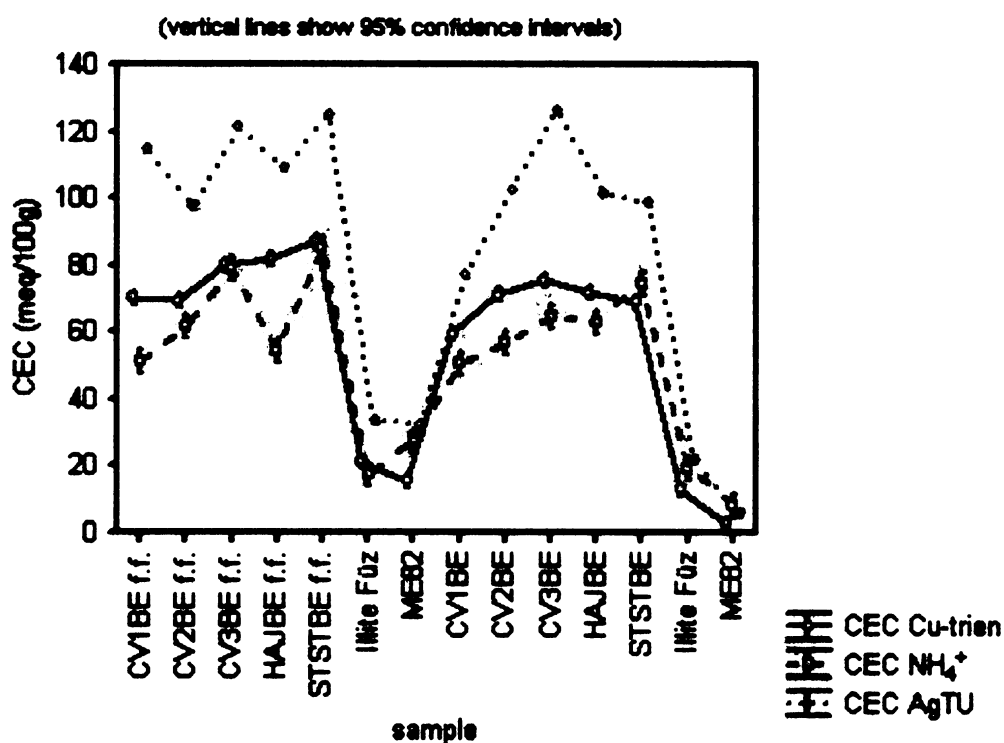


Fig. 5.60 - Results of CEC determination, collected clays, carbonates removed in all samples of $CEC_{NH_4^+}$ and CEC_{AgTU} and fine fractions of $CEC_{Cu-trien}$ (note: f.f. means fine fraction of given sample)

Evaluation of *influence of the method* was performed using one parametric and two non-parametric test (Table 5.30). All the tests revealed significance of the method used. For finer resolution, the multiple mutual comparisons of p-values of Kruskal-Wallis test were performed. No significant differences were found between Cu-trien method and ammonium acetate method. The silver thiourea method differs from the two other methods (see also Fig. 5.61).

Table 5.30 - Testing influence of method for CEC determination

Test	Type	P-value
Kruskal-Wallis	non-parametric	0.00
Median	non-parametric	0.00
One-way ANOVA	parametric	0.00

Table 5.31 - Multiple mutual comparison of p-values, investigation of methods relations

	$CEC_{Cu-trien}$	$CEC_{NH_4^+}$	CEC_{AgTU}
$CEC_{Cu-trien}$		0.85	0.00
$CEC_{NH_4^+}$	0.85		0.00
CEC_{AgTU}	0.00	0.00	

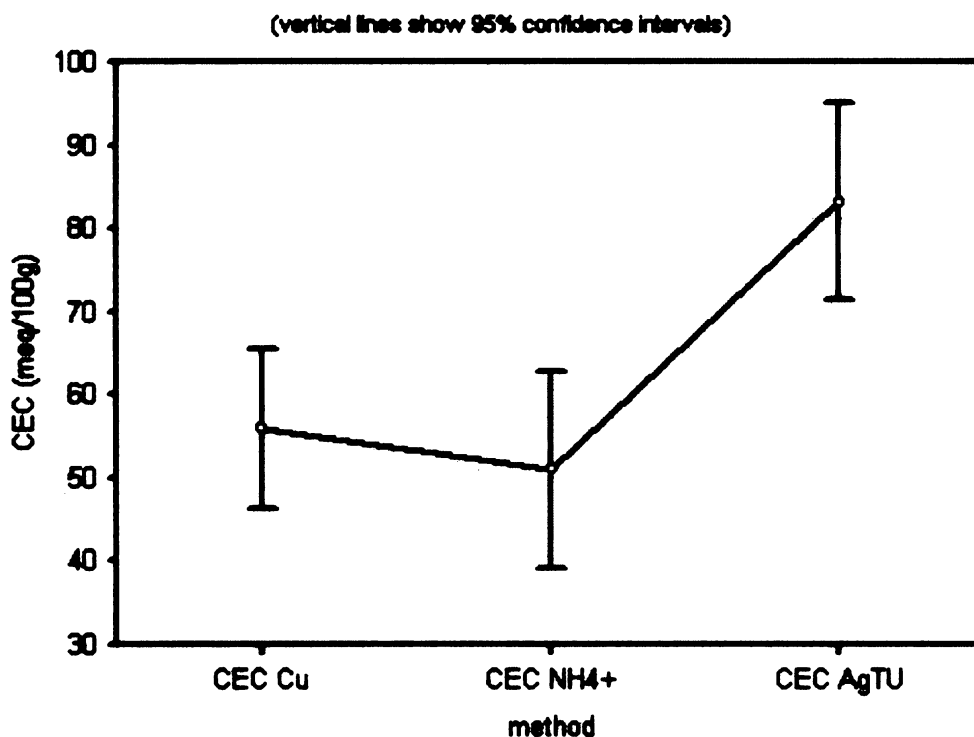


Fig. 5.61 - Comparison of different methods for CEC determination

Summary:

Using seven natural samples and their fine fraction (14 samples), no significant difference was found between CEC determined by Cu-trien and ammonium acetate. The significantly different result of AgTU method originates from application of this method (designed for soils) to bentonites. This is also confirmed by investigation of CEC of samples with low contents of expandable structures (Illite Füz and ME82). In these cases, the difference compared to the ammonium acetate result is significantly smaller than in the case of bentonites.

5.6. Application of Rietveld method

A study of the Rietveld method application was performed in order to inspect a possibility of calculating the layer charge and comparison with CEC determined by Cu-trien method. The Rietveld method was performed using RTS method for sample preparation. The samples were measured using PANalytical X'PertPRO device with X'Celerator detector (Faculty of Science, University of Zagreb) and evaluated using X'Pert HighScore Plus equipped with a Rietveld fitting module.

Calculations were run for all the bentonites of collected clays. Plate structures caused preferred orientation and lowered the Rietveld fit. The second problem was caused by unknown structures of smectites (variation in parameters due to structural substitutions). The Rietveld evaluation was impossible due to the absence of structure models for samples containing specific mixed layered structures (sample Illite Füz, ME82). An example of the results of CV1BE Rietveld analysis is shown below.

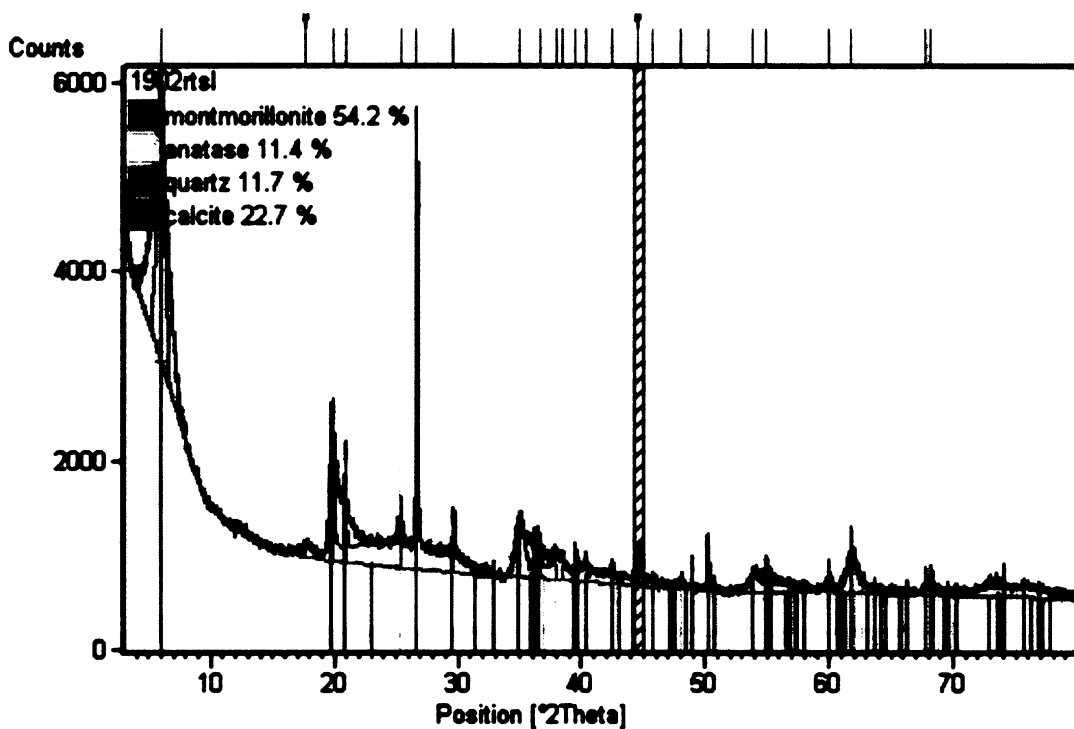


Fig. 5.62 - CV1BE XRD pattern before Rietveld refinement, left upper corner contains fitted minerals and their appropriate content derived from structure models inserted for refinement run. The dashed vertical line defines the interval excluded from fitting because of the presence of support alumina diffraction

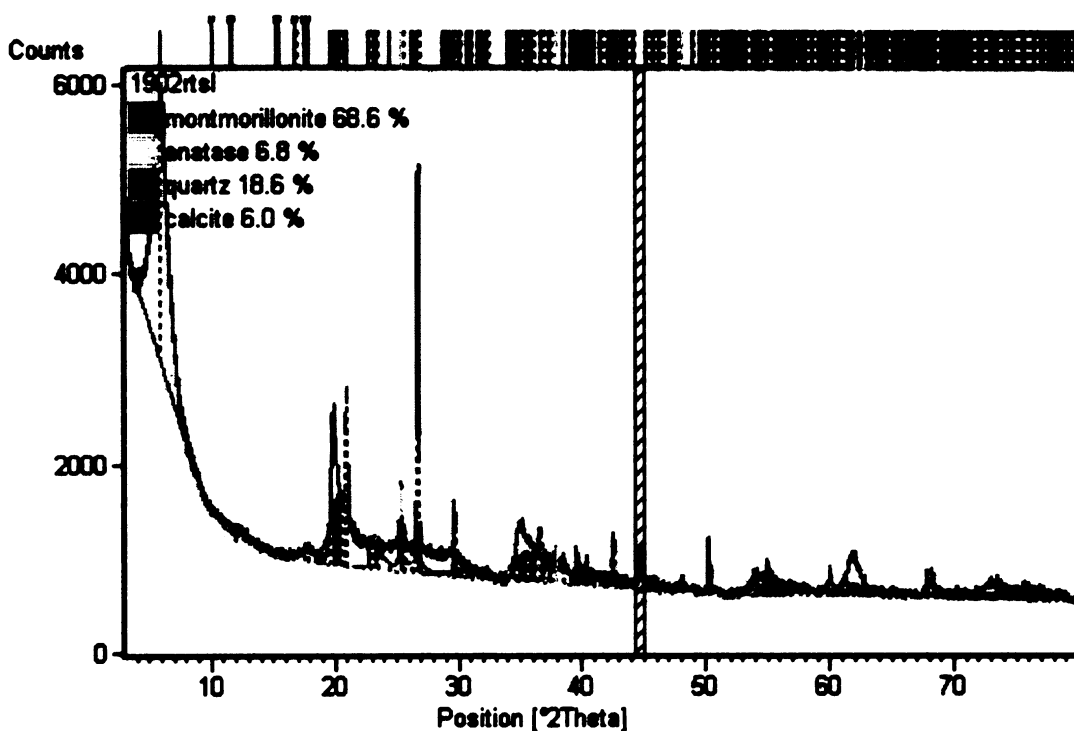


Fig. 5.63 - CV1BE XRD pattern after Rietveld refinement, models are refined, content of mineral phases is recalculated. Shape of blue line area below represents the theoretical XRD pattern of a sample containing refined minerals

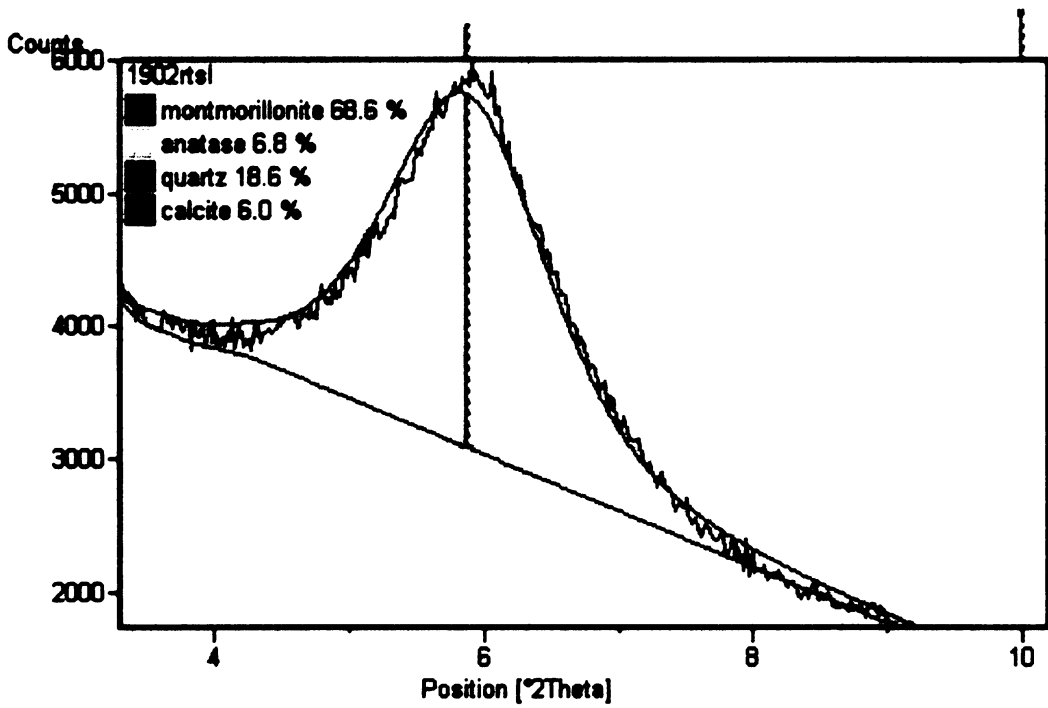


Fig. 5.64 - Zoom of smectitic 001 diffraction after Rietveld refinement. The fit is rather poor concerning the position

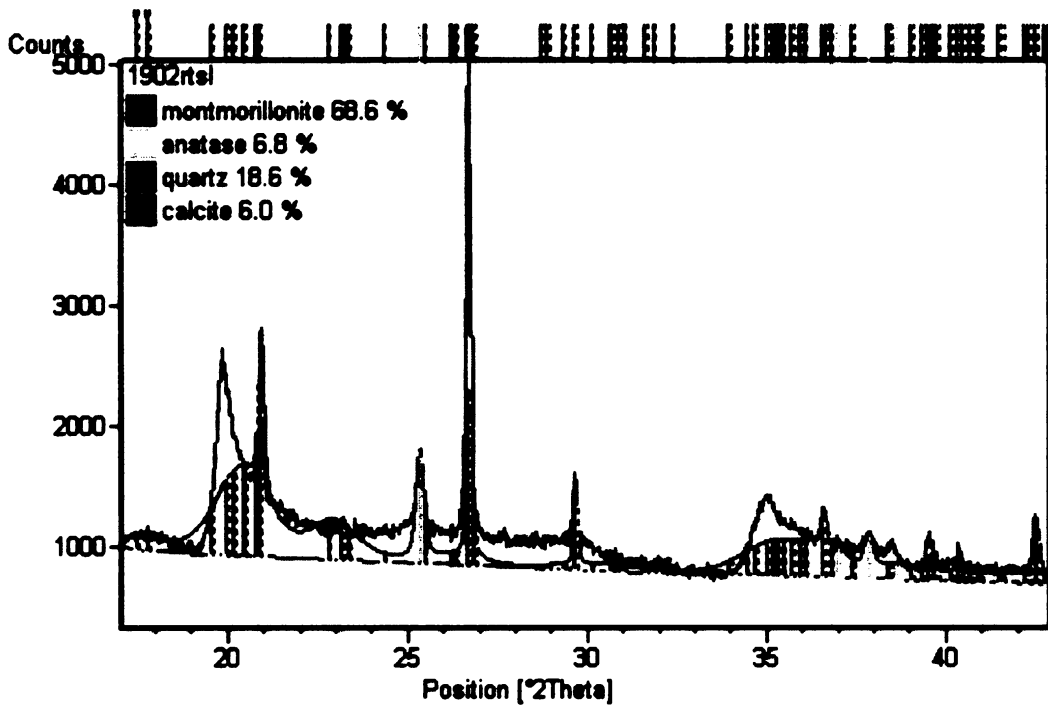


Fig. 5.65 - Zoom of middle-angle region, goodness of fit is significantly influenced by plate structure of minerals, preferred orientation and low crystallinity

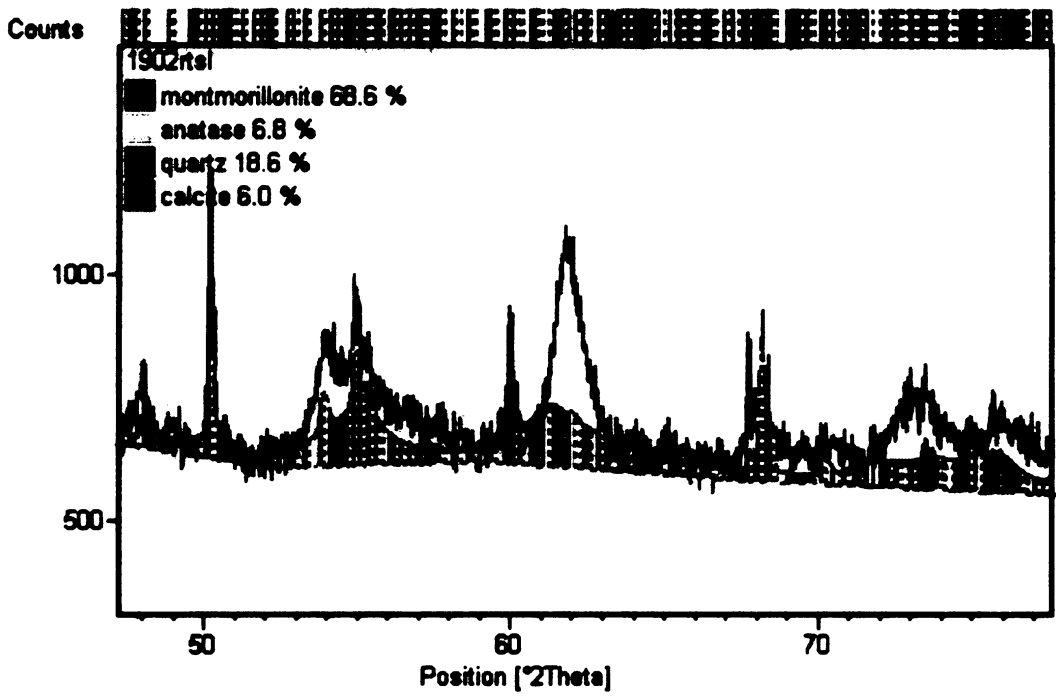


Fig. 5.66 - Zoom of 060 diffraction region, influence of plate minerals is profound

6. Conclusions

The questions asked in Chapter 2 have been answered on the basis of the experiments performed as follows:

Are the results affected by the composition of the stock solution, by the way of its addition and by the sample preparation procedure?

The Cu-trien method is sensitive to the stock solution preparation and to the addition of the stock solution. In the case of charge-reduction or other sample treatment (in order to change its properties), the use of one solution and one addition is highly advised. The influence of the solution and addition factors has been observed for both the Source Clays Standards and homoionic DR forms. Source Clays Standard SWy-2 pointed to problems with dissolution of admixtures and growing difference related to non-equivalent exchange (concerning the valence of a native ion in the interlayer space). Filtration was found to be a faster procedure of sample preparation with a small influence on CEC_{Cu} (calculated from AAS measurement of Cu^{2+} in the supernatant) and CEC_{uv-vis} (calculated from the Cu-trien complex in the supernatant measured by colorimetry). The CEC_{sum} determined as the sum of the released cations has been found to be of lower significance (dependent on the supernatant acquisition procedure, influenced by dissolution of admixtures, time consuming, offers information on the cations in the interlayer space).

Does the type of the interlayer cation influence the results?

Concerning CEC_{Cu} and CEC_{uv-vis} , there were no differences found in relation to the type of homoionic form (DR samples). The interlayer cation influenced CEC_{Cu} and CEC_{uv-vis} in the same manner confirming the interchangeability of the methods. The results of CEC_{Cu} and CEC_{uv-vis} were increased due to the interlayer cation in the $Ca^{2+} < Mg^{2+} < Na^{+} < Li^{+}$ order. The CEC_M differed significantly, due to an inhomogeneous extent of ionic replacement in the interlayer space.

Investigation of the homoionic form revealed an influence of the sample preparation on monovalent cations (Na^{+} and Li^{+}) using CEC_{uv-vis} . The CEC results increased with increasing addition of the stock solution and with increasing content of free trien in the stock solution. The influence was also found for CEC_{Mg} . The magnesium concentration in the supernatant is negatively related to the concentration of free trien in the stock solution and positively to the amount of the stock solution added.

What is the reliability of the Cu-trien method when using atomic absorption/emission spectroscopy and how much the results differ from those obtained by colorimetry?

The comparison of the methods for the reference samples (STx-1 and SWy-2) was unclear. Filtered samples of STx-1 showed similarity of CEC_{Cu} and CEC_{sum} while SWy-2 displayed no relation. The AAS/AES and UV-Vis results for homoionic samples (DR) revealed no statistical difference between the methods. The atomic absorption of cupric ions is equivalent to colorimetry.

How much the results differ from those obtained by the classical NH_4^+ HAc method?

The Cu-trien method was compared with the ammonium acetate and the silver thiourea methods using collected clays. There was no significant difference found concerning the ammonium acetate method. Taking into account the time consumption, the Cu-trien method is incomparably faster. The silver thiourea method was found to be significantly different from the two other methods. The most probable source of error lies in the application of this method to bentonitic samples.

Summarizing all the above conclusions, the cation exchange capacity determined using the Cu-trien complex is not robust. Application of this method requires the same experimental settings within the set of the similar samples. The Cu-trien method is fast and the results are in good agreement with those obtained using the standard ammonium acetate method.

Rietveld refinement

The semiquantitative Rietveld refinement has been found to be difficult to apply to samples containing clay minerals. The results obtained by refinement were unsatisfactory.

7. Literature

1. Paama, L., Pitkänen, I., Perämäki, P.: Analysis of archaeological samples and local clays using ICP-AES, TG-DTG and FTIR techniques. *Talanta*, 2000, 51, 349-357
2. Bergaya, F, Vayer, M.: CEC of clays: measurement by adsorption of copper ethylenediamine complex. *Applied Clay Science* 1997, , 12, 275-280
3. Meier, L. P., Kahr, G.: Determination of the cation exchange capacity (CEC) of clay minerals using the complexes of copper (II) ion with triethylenetetramine and tetraethylenepentamine. *Clays and Clay Minerals*, 47, 386-388
4. Ammann, L., Bergaya, F., Lagaly, G.: Determination of the cation exchange capacity of clays with copper complexes revisited. 2005, 40, 441-453
5. Kawano, M., Tomita, K.: Mineralogy and genesis of clays in postmagmatic alteration zones, Makurazaki volcanic area, Kagoshima prefecture, Japan. *Clays and Clay Minerals*, 1991, 39, 597-608
6. Moore, D. M., Reynolds Jr., R. C.: X-ray diffraction and the identification and analysis of clay minerals. 2nd edition. Oxford University Press, Inc., New York 1997
7. Schwertmann, U., Friedl, J., Stanjek, H., Schulze, D.G: The effect of clay minerals on the formation of goethite and hematite from ferrihydrite after 16 years' ageing at 25°C and pH 4-7. *Clay Minerals*, 2000, 35, 613-623
8. Jouquet, P, Mamou, L., Lepage, M., Velde, B.: Effect of termites on clay minerals in tropical soils: fungus-growing termites as weathering agents. 2002, *European Journal of Soil Science*, 53, 521-527
9. Bailey, S. W.: Summary of recommendations of the AIPEA nomenclature committee. *Canadian Mineralogist*, 1980, 18, 143-150
10. Guggenheim, S., Martin, R.T.: Definition of clay and clay mineral: joint report of the AIPEA and CMS nomenclature committees. *Clay Minerals*, 1995, 30, 257-259
11. Weiss, Z., Kužvart, M: Jílové minerály, jejich nanostruktura a využití. Karlova Univerzita v Praze, nakladatelství Karolinum 2005
12. Moore, D.M.: Comment on: Definition of clay and clay mineral: join report of the AIPEA nomenclature and CMS nomenclature committees. *Clays and Clay Minerals*, 1996, 44, 710-712
13. Guggenheim, S., Martin, R.T.: Reply to the comment by D. M. Moore on "Definition of clay and clay mineral: joint report of the AIPEA nomenclature and CMS nomenclature committees. *Clays and Clay Minerals*, 1996, 44, 713-715
14. Lagaly, G.: Layer charge determination by alkylammonium ions, in CMS Workshop Lectures, Volume 6, Layer charge characteristics of 2:1 silicate clay minerals. Mermut, A. R., ed., The Clay Minerals Society, Boulder, CO, USA, 1994, ISBN-1-881208-07-9
15. Mermut, A., Lagaly, G.: Baseline studies of the Clay Minerals Society Source Clays: Layer-charge determination and characteristics of those minerals containing 2:1 layers. *Clays and Clay Minerals*, 2001, 49, 393-397

16. Komadel, P., Čížel, B.: Structural Formulae of Layer Silicates, in Quantitative Methods in Soil Mineralogy. Dahlgren, R.A., Amonette, J.E., Zelazny, L.W., Soil Science Society of America, Madison, WI, USA, 1994
17. Lagaly, G.: Layer charge heterogeneity in vermiculites. *Clays and Clay Minerals*, 1982, 30, 215-222
18. Lagaly, G., Fernandez Gonzalez, M., Weiss, A.: Problems in layer-charge determination of montmorillonites. *Clay Minerals*, 1976, 11, 173-187
19. Stanjek, H., Friedrich, R.: The determination of layer charge by curve-fitting of Lorentz- and polarization-corrected X-ray diagrams. *Clay Minerals*, 1986, 21, 183-190
20. Janek, M., Smrčok, L.: Application of an internal standard technique by transmission X-ray diffraction to assess layer charge of a montmorillonite by using the alkylammonium method. *Clays and Clay Minerals*, 1999, 47, 113-118
21. Laird, D.A.: Evaluation of the structural formula and alkylammonium methods of determining layer charge, in CMS Workshop Lectures, Volume 6, Layer charge characteristics of 2:1 silicate clay minerals. Mermut, A. R., ed., The Clay Minerals Society, Boulder, CO, USA, 1994, ISBN-1-881208-07-9
22. Laird, D.A., Scott, A.D., Fenton, T.E.: Evaluation of the alkylammonium method of determining layer charge. *Clays and Clay Minerals*, 1989, 37, 41-46
23. Christidis, G.E., Eberl, D.D.: Determination of layer-charge characteristics of smectites. *Clays and Clay Minerals*, 2003, 51, 644-655
24. Margulies, L., Rozen, H., Nir, S.: Model for competitive adsorption of organic cations on clays. *Clays and Clay Minerals*, 1988, 36, 270-276
25. Shariatmadari, H., Mermut, A.R., Benke, M.B.: Sorption of selected cationic and neutral organic molecules on palygorskite and sepiolite. *Clays and Clay Minerals*, 1999, 47, 44-53
26. Cenens, J., Schooneheydt, R.A.: Visible spectroscopy of methylene blue on hectorite, laponite B, and barasym in aqueous suspension. *Clays and Clay Minerals*, 1988, 36, 214-224
27. Bujdák, J., Komadel, P.: Interaction of methylene blue with reduced charge montmorillonite. *J. Phys. Chem. B*, 1997, 101, 9065-9068
28. Bujdák, J., Janek, M., Madejová, J., Komadel, P.: The influence of the layer charge density of smectites on the interaction with methylene blue. *J. Chem. Soc, Faraday Trans.*, 1998, 94, 3487-3492
29. Czímerová, A., Jankovič, L., Bujdák, J.: Effect of the exchangeable cations on the spectral properties of methylene blue in clay dispersions. *Journal of Colloid and Interface Science*, 2004, 274, 126-132
30. Czímerová, A., Bujdák, J., Gáplovský, A.: The aggregation of thionine and methylene blue dye in smectite dispersion. *Colloids and Surfaces A: Physicochem. Eng. Aspects*, 2004, 243, 89-96
31. Kaneko, Y., Nobuo, I., Bujdák, J., Sasai, R., Fujita, T.: Effect of layer charge density on orientation and aggregation of a cationic laser dye incorporated in the interlayer space of montmorillonites. *Journal of Colloid and Interface Science*, 2004, 269, 22-25

32. Bujdák, J.: Effect of the layer charge of clay minerals on optical properties of organic dyes. A review, *Applied Clay Science*, 2006, 34, 58-73
33. Czímerová, A., Bujdák, J., Dohrmann, R.: Traditional and novel methods for estimating the layer charge of smectites. *Applied Clay Science*, 2006, 34, 2-13
34. Maes, A., Stul, M.S., Cremers, A.: Layer charge-cation-exchange capacity relationships in montmorillonite. *Clays and Clay Minerals*, 1979, 27, 387-392
35. Lagaly, G., Ziesmer, S.: Colloid chemistry of clay minerals: the coagulation of montmorillonite dispersions. *Advances in Colloid and Interface Science*, 2003, 100-102, 105-128
36. Bérend, I., Cases, J.M., François, M., Uriot, J.P., Michot, L., Masion, A., Thomas, F.: Mechanism of adsorption and desorption of water vapour by homoionic montmorillonites: 2. The Li^+ , Na^+ , K^+ , Rb^+ and Cs^+ -exchanged forms. *Clays and Clay Minerals*, 1995, 43, 324-336
37. Cases, J.M., Bérend, I., François, M., Uriot, J.P., Michot, L.J., Thomas, F.: Mechanism of adsorption and desorption of water vapour by homoionic montmorillonite: 3. The Mg^{2+} , Ca^{2+} , Sr^{2+} and Ba^{2+} exchanged forms. *Clays and Clay Minerals*, 1997, 45, 8-22
38. Verburg, K., Baveye, P.: Hysteresis in the binary exchange of cations on 2:1 clay minerals: a critical review. *Clays and Clay Minerals*, 1994, 42, 207-220
39. Verburg, K., Baveye, P.: Cation exchange hysteresis scanning curves: mathematical description and interpretation. *European Journal of Soil Science*, 1996, 47, 345-356
40. Fu, M.H., Zhang, Z.Z., Low, P.F.: Changes in the properties of a montmorillonite-water system during the adsorption and desorption of water: hysteresis. *Clays and Clay Minerals*, 1990, 38, 485-492
41. Shang, J.Q., Lo, K.Y., Quigley, R.M.: Quantitative determination of potential distribution in Stern-Gouy double-layer model. *Can. Geotech. J.*, 1994, 31, 624-636
42. Eberl, D.: Alkali cation selectivity and fixation by clay minerals. *Clays and Clay Minerals*, 1980, 28, 161-172
43. Xu, S., Harsh, J.B.: Alkali cation selectivity and surface charge of 2:1 clay minerals. *Clays and Clay Minerals*, 1992, 40, 567-574
44. McLean, E.O., Bittencourt, V.C.: Complementary ion effects on potassium and calcium displacement from tri-ionic bentonite and illite systems as affected by pH-dependent charges. *Soil Science*, 1974, 117, 103-109
45. Rytwo, G., Banin, A., Nir, S.: Exchange reactions in the Ca-Mg-Na montmorillonite system. *Clays and Clay Minerals*, 1996, 44, 276-285
46. Suquet, H., Pézerat, H.: Comments on the classification of trioctahedral 2:1 phyllosilicates. *Clays and Clay Minerals*, 1988, 36, 184-186
47. Malla, P.B., Douglas, L.A.: Problems in identification of montmorillonite and beidellite. *Clays and Clay Minerals*, 1987, 35, 232-236
48. Bailey, S.W.: Nomenclature for regular interstratifications. *Clay Minerals*, 1982, 17, 243-248
49. Guggenheim, S., Alietti, A., Drits, V.A., Formoso, M.L.L., Galán, E., Köster, H.M., Paquet, H., Watanabe, T, Bain, D.C., Hudnall, W.H.: Report of the association internationale pour l'études des argyles (AIPEA)

- nomenclature committee for 1996. *Clays and Clay Minerals*, 1997, 45, 298-300
50. Cox, L., Hermosín, M.C., Celis, R., Cornejo, J.: Sorption of two polar herbicides in soils and soil clays suspensions. *Wat. Res.* 1997, 31, 1309-1316
 51. Rytwo, G., Tropp, D.: Improved efficiency of a divalent herbicide in the presence of clay, by addition of monovalent organocations. *Applied Clay Science*, 2001, 18, 327-333
 52. Konta, J.: Clay and man: Clay raw materials in the service of man. *Applied Clay Science*, 1995, 10, 275-335
 53. Pacáková, V. Počkevičiute, D., Armalis, S., Štulík, K., Li, J., Veselý, J.: A study of the distribution of lead, cadmium and copper between water and kaolin, bentonite and river sediment. *J. Environ. Monit.*, 2000, 2, 187-191
 54. Önal, M., Sarikaya, Y., Alemdaroğlu, T., Bodoğan, I.: The effect of acid activation on some physicochemical properties of a bentonite. *Turk J Chem*, 2002, 409-416
 55. Bhattacharyya, K.G., Gupta, S.S.: Kaolinite, montmorillonite, and their modified derivatives as sorbents for removal of Cu(II) from aqueous solution. *Separation and Purification Technology*, 2006, 50, 388-397
 56. Matthes, W., Madsen, F.T., Kahr, G.: Sorption of heavy-metal cations by Al and Zr-hydroxy-intercalated and pillared bentonite. *Clays and Clay Minerals*, 1999, 47, 617-629
 57. Abollino, O., Aceto, M., Malandrino, M, Sarzanini, C., Mentasti, E.: Adsorption of heavy metals on Na-montmorillonite. Effect of pH and organic substances. *Water Research*, 2003, 37, 1619-1627
 58. Manning, B.A., Goldberg, S.: Modeling arsenite competitive adsorption on kaolinite, montmorillonite and illite. *Clays and Clay Minerals*, 1996, 44, 609-623
 59. Ferrell, R.E, Aagaard, P., Forsman, J., Greenwood, L., Zheng, Z.: Application of a geochemical transport model to predict heavy metal retention (Pb) by clay liners. *Applied Clay Science*, 2002, 21, 59-66
 60. Osmanlioglu, A.E.: Immobilization of radioactive waste by cementation with purified kaolin clay. *Waste Management*, 2002, 22, 481-483
 61. Madsen, F.T.: Clay mineralogical investigations related to nuclear waste disposal. *Clay Minerals*, 1998, 33, 109-129
 62. Bruno, G., Decarreau, A., Proust, D., Lajudie, A.: Clay mineral transformations in static hydrothermal conditions within a simulated engineered barrier for nuclear waste disposal. *Applied Clay Science*, 1992, 7, 169-178
 63. Bonin, B., Colin, M., Dutfoy, A.: Pressure building during the early stages of gas production in a radioactive waste repository. *Journal of Nuclear Materials*, 2000, 281, 1-14
 64. Gens, A., Guimaraes, L.N., Garcia-Molina, A., Alonso, E.E.: Factors controlling rock-clay buffer interaction in a radioactive waste repository. *Engineering Geology*, 2002, 64, 297-308
 65. Annabi-Bergaya, F.: Layered clay minerals. Basic research and innovative composite applications. *Microporous and Mesoporous Materials*, 2007, doi:10.1016/j.micromeso.2007.05.064

66. Handbook of Biodegradable Polymeric Materials and Their Applications. Ed.: Mallapragada, S., Narasimhan, B., American Scientific Publishers, California USA 2005, ISBN: 1-58883-053-5, chapter 8 – Biodegradable Polymer/Layered Silicate Nanocomposites: A Review by Okamoto, M.
67. Sondi, I. Stubičar, M, Pravdić, V: Surface properties of ripidolite and beidellite clays modified by high-energy ball milling. *Colloids and Surfaces*, 1997, 127, 141-149
68. Šucha, V. et al.: *Laboratorne metódy výskumu nerudných surovín*. Univerzita Komenského, Bratislava 1996
69. Weiszburg, T.G., Nagy, T., Tóth, E., Mizák, J., Varga, Z., Lovas, G.A, Váczi, T.: A laboratory procedure for separating micas from quartz in clay-sized materials. *Acta Mineralogica-Petrographica*, 2004, 45/1, 133-139
70. Bache, B.W.: The role of calcium in buffering soils. *Plant, Cell and Environment*, 1984, vol 7, 391-395
71. Pokrovsky, O.S., Golubev, S.V., Schott, J.: Dissolution kinetics of calcite, dolomite and magnesite at 25 °C and 0 to 50 atm $p\text{CO}_2$. *Chemical Geology* 2005, vol 217, 239-255
72. Alkattan, M., Oelkers, E.H., Dandurand, J.L., Schott, J.: An experimental study of calcite and limestone dissolution rates as a function of pH from – 1 to 3 and temperature from 25 to 80 °C. *Chemical Geology*, 1998, 151, 199-214
73. Cubillas, P., Köhler, S., Prieto, M., Chaïrat, C., Oelkers, E.H.: Experimental determination of the dissolution rates of calcite, aragonite, and bivalves. *Chemical Geology*, 2005, 216, 59-77
74. Jeschke, A.A., Vosbeck, K., Dreybrodt, W.: Surface controlled dissolution rates of gypsum in aqueous solution exhibit nonlinear dissolution kinetics. *Geochimica et Cosmochimica Acta*, 2001, 65, 27-34
75. Kuechler, R., Noack, K., Zorn, T.: Investigation of gypsum dissolution under saturated and unsaturated water conditions. *Ecological Modelling*, 2004, 176, 1-14
76. Bodine, M. W., Fernald, T. H.: EDTA dissolution of gypsum, anhydrite, and Ca-Mg carbonates. *Journal of sedimentary research*, 1973, 43, 1152-1156
77. Mehra, O.P., Jackson, M.L.: Iron oxide removal from soils and clays by a dithionite-citrate system buffered with sodium bicarbonate. *Clays and Clay Minerals*, 1960, vol 7, 317-327
78. Manceau, A., Drits, V.A., Lanson, B., Chateigner, D, Wu, J., Huo, D., Gates, W.P., Stucki, J.W.: Oxidation-reduction mechanism of iron in dioctahedral smectites:II.Crystal chemistry of reduced Garfield nontronite. *American Mineralogist*, 2000, vol.85, 153-172
79. Drits, V.A., Manceau, A.: A model for the mechanism of Fe^{3+} to Fe^{2+} reduction in dioctahedral smectites. *Clays and Clay Minerals*, 2000, 48, 185-195
80. Fialips, C.I, Huo, D, Yan, L., Wu, J., Stucki, J.W.: Effect of Fe oxidation state on the IR spectra of Garfield nontronite. 2002, vol 87, 630-641
81. Schuette, R., Goodman, B.A., Stucki, J.W.: Magnetic properties of oxidized and reduced smectites. *Phys Chem Minerals*, 2000, vol 27, 251-257

82. Stucki, J.W., Lee, K., Zhang, L., Larson, R.A.: Effect of iron oxidation state on the surface properties of smectites. *Pure Appl. Chem.*, 2002, vol 74, 2145-2158
83. Varadachari, C., Mondal, A.H, Ghosh, K.: Some aspects of clay-humus complexation: effect of exchangeable cations and lattice charge. *Soil Science*, 1991, vol 151, 220-227
84. Anderson, J.U.: An improved pre-treatment for mineralogical analysis of samples containing organic matter. *Clays and Clay Minerals*, 1961, vol 10, 380-388
85. Meier, L.P., Menegatti, A.P.: A new, efficient, one-step method for the removal of organic matter from clay-containing sediments. *Clay Minerals*, 1997, vol 32, 557-563
86. Follett, E.A.C, McHardy, W.J., Mitchell, B.D., Smith, B.F.L.: Chemical dissolution techniques in the study of soil clays: Part I. *Clay Minerals*, 1965, 6, 23-34
87. Follett, E.A.C., McHardy, W.J., Mitchell, B.D., Smith, B.F.L.: Chemical dissolution techniques in the study of soil clays: Part II. *Clay Minerals*, 1965, 6, 35-43
88. Inczédy, J., Lengyel, T., Ure, A.M.: *Compendium of Analytical Nomenclature, Definitive Rules 1997*, third edition, web edition: http://www.iupac.org/publications/analytical_compendium/, chapter 10.3.4.8
89. Zhang, G., Germaine, J. T., Martin, R. T., Whittle, A. J: A simple sample-mounting method for random powder X-ray diffraction. *Clays and Clay minerals*, 2003, Vol. 51, 21 –225
90. Gates, W.P, Komadel, P. Madejová, J., Bujdák, J. Stucki, J.W., Kirkpatrick, R.J.: Electronic and structural properties of reduced-charge montmorillonites. *Applied Clay Science*, 2000, vol 16, 257-271
91. Internal laboratory guide, Faculty of Mining, Geology and Petroleum Engineering, University of Zagreb
92. Šucha, V.: *Íly v geologických procesoch*. Univerzita Komenského, Bratislava 2001
93. Ortiz, A.L., Cumbreira, F.L., Sánchez-Bajo, F., Guiberteau, F., Caruso, R.: Fundamental parameters approach in the Rietveld method: a study of the stability of results versus the accuracy of the instrumental profile. *Journal of the European Ceramic Society*, 2000, 20, 1845-1851
94. Dollase, W.A.: Correction of intensities for preferred orientation in powder diffractometry: application of the March model. *Journal of Applied Crystallography* 1986, 19, 267-272
95. Bish, D.L. (1993): in *CMS Workshop Lectures, Vol. 5, Computer Applications of X-ray Powder Diffraction Analysis of Clay Minerals*, Reynolds, R.C., Jr., Walker, J.R., Eds., The Clay Minerals Society, Boulder, CO. ISBN-1-881208-06-0
96. Bish, D.L., Howard, S.A.: Quantitative phase analysis using the Rietveld method. *Journal of Applied Crystallography*, 1988, 21, 86-91
97. Chung, H.F.: Quantitative interpretation of X-ray diffraction patterns of mixtures. I. Matrix-flushing method for Quantitative multicomponent analysis. *Journal of Applied Crystallography*, 1974, 7, 519-525

98. Chung, F.H.: Quantitative interpretation of X-ray diffraction patterns of mixtures. II. Adiabatic principle of X-ray diffraction analysis of mixtures. *Journal of Applied Crystallography*, 1974, 7, 526-531
99. Środoń, J, Drits, V.A., CcCarty, D.K., Hsieh, J.C.C., Eberl, D.D.: Quantitative X-ray diffraction analysis of clay-bearing rocks from random preparations. *Clays and Clay Minerals*, 2001, 49, 514-528
100. Batchelder, M, Cressey, G.: Rapid, accurate phase quantification of clay-bearing samples using a position-sensitive X-ray detector. *Clays and Clay Minerals*, 1998, 46, 183-194
101. *Spectroscopic methods in mineralogy*, ed. Beran, A., Libowitzky, E., European mineralogical union notes in mineralogy, volume 6, Eötvös University Press, Budapest, 2004, ISBN 9634636624
102. Rintoul, L, Panayiotou, H., Kokot, S., George, G., Cash, G., Frost, R., Bui, T., Fredericks, P: Fourier transform infrared spectrometry: a versatile technique for real world samples. *The Analyst*, 1998, 123, 571-577
103. Sposito, G., Prost, R.: Structure of water adsorbed on smectites. *Chemical Reviews*, 82, 1982, 554-573
104. Yan, L, Roth, C.B., Low, P.F.: Effects of monovalent, exchangeable cations and electrolytes on the infrared vibrations of smectite layers and interlayer water. *Journal of Colloid and Interface Science*, 1996, 184, 663-670
105. Madejová, J., Bujdák, J., Janek, M., Komadel, P.: Comparative FT-IR study of structural modifications during acid treatment of dioctahedral smectites and hectorite. *Spectrochimica Acta Part A*, 1998, 54, 1397-1406
106. Madejová, J., Arvaiová, B, Komadel, P.: FTIR spectroscopic characterization of thermally treated Cu²⁺, Cd²⁺, and Li⁺ montmorillonites. *Spectrochimica Acta Part A*, 1999, 55, 2467-2476
107. Alvero, R. Alba, M.D., Castro, M.A., Trillo, J.M.: Reversible migration of lithium in montmorillonites. *J. Phys. Chem.*, 1994, 98, 7848-7853
108. Klopogge, J.T., Mahmutagic, E., Frost, R.L.: Mid-infrared and infrared emission spectroscopy of Cu-exchanged montmorillonite. *Journal of Colloid and Interface Science*, 2006, 296, 640-646
109. Madejová, J., Janek, M., Komadel, P., Herbert, H.J., Moog, H.C.: FTIR analyses of water in MX-80 bentonite compacted from high salinary salt solution systems. *Applied Clay Science*, 2002, 20, 255-271
110. Madejová, J.: FTIR techniques in clay mineral studies. *Vibrational Spectroscopy*, 2003, 31, 1-10
111. Bracke, G., Satir, M., Krauß, P.: The cryptand [222] for exchanging cations of micas. *Clays and Clay Minerals*, 1995, 43, 732-737
112. Rytwo, G., Nir, S., Margulies, L.: Interactions of monovalent organic cations with montmorillonite: adsorption studies and model calculations. *Soil Sci. Soc. Am. J.*, 1995, 59, 554 – 564
113. Narine, D.R., Guy, R.D.: Interactions of some large organic cations with bentonite in dilute aqueous systems. *Clays and Clay Minerals*, 1981, 29, 205-212
114. Nir, S., Rytwo, G., Yermiyahu, U., Margulies, L.: A model for cation adsorption to clays and membranes. *Colloid and Polymer Science*, 1994, 272, 619-632

115. Tournassat, C., Greneche, J.M., Tisserand, D., Charlet, L.: The titration of clay minerals I. Discontinuous backtitration technique combined with CEC measurements. *Journal of Colloid and Interface Science*, 2004, 224-233
116. Tournassat, C., Ferrage, E., Poinsignon, C., Charlet, L.: The titration of clay minerals II. Structure-based model and implication for clay reactivity. *Journal of Colloid and Interface Science*, 2004, 273, 234-246
117. Dohrmann, R.: Cation exchange capacity methodology I: An efficient model for the detection of incorrect cation exchange capacity and exchangeable cation results. *Applied Clay Science*, 2006, 34, 31-37
118. Mackenzie, R. C.: A micromethod for determination of cation exchange capacity of clay. *Journal of colloid science*, 1951, 6, 219 – 222
119. Dohrmann, R.: Problems in CEC determination of calcareous clayey sediments using the ammonium acetate method. *J. Plant Nutr. Soil Sci.*, 2006, 169, 330-334
120. Ciesielski, H., Sterckeman, T.: A comparison between three methods for the determination of cation exchange capacity and exchangeable cations in soils. *Agronomie*, 1997, vol. 17, 9 – 16
121. Van Reeuwijk, L. P.(ed.): Procedures for soil analysis (6th ed.). Tech. Pap. 9, ISRIC, Wageningen, The Netherlands 2002, ISBN: 90-6672-044-1
122. ČSN 72 1076
123. Mulvaney, R. L., Yaremych, S. A., Khan, S. A., Swiader, J. M., Horgan, B. P.: Use of diffusion to determine soil cation-exchange capacity by ammonium saturation. *Communication in Soil Science and Plant Analysis*, 35, 51–67, 2004
124. Busenberg, E., Clemency, C. V.: Determination of the cation exchange capacity of clays and soils using an ammonia electrode. *Clays and Clay minerals*, vol. 21, 213 – 217, 1973
125. Borden, D., Giese, R. F: Baseline studies of the clay minerals society source clays: cation exchange capacity measurements by the ammonia-electrode method. *Clays and Clay Minerals*, vol 49, no. 5, 444 – 445, 2001
126. Santoni, S., Bonifacio, E., Zanini, E.: Indophenol blue colorimetric method for measuring cation exchange capacity in sandy soils. *Commun. Soil. Sci. Plant Anal.*, 2001, 32, 15&16, 2519-2530
127. Cruanas, R., Cardus, J.: Cation exchange capacity determination in soils: study of a new potentiometric method for calcareous, gypsiferous and saline soils. *Soil science*, 1987, vol 144, no. 5, 311-318
128. Son, W.K., Kim, S.H., Kim, T.I.: Calculation on ion exchange capacity for an ion exchanger using the potentiometric titration. *Journal of polymer science, part B polymer physics*, 38 (23), 3181-3188, 2000
129. Hajós, P., Inczédy, J.: Simple method for the determination of low cation-exchange capacity and the titration of cation exchangers by constant-current coulometry. *Journal of Chromatography*, 1980, 201, 193-197
130. Chiu, Y. C., Huang, L. N., Uang, C. M., Huang, J. F.: Determination of cation exchange capacity of clay minerals by potentiometric titration using divalent cation electrodes. *Colloids and Surfaces*, 1990, 46 327 – 337
131. Pleysier, J. L., Juo, A. S. R.: A single-extraction method using silverthiourea for measuring exchangeable cations and effective CEC in soils with variable charges. *Soil Science*, 1980, 129

132. Searle, P.L.: The measurement of soil cation exchange properties using the single extraction, silver thiourea method:an evaluation using a range of New Zealand soils. *Aust.J.Soil Res.*, 1986, 24, 193 – 200
133. Dohrmann, R.: Cation exchange capacity methodology II: A modified silver-thiourea method. *Applied Clay Science*, 2006, 34, 38-46
134. Dohrmann, R.: Cation exchange capacity methodology III: Correct exchangeable calcium determination of calcareous clays using a new silver-thiourea method. *Applied Clay Science*, 2006, 34, 47-57
135. Francis, C. W.: Rapid and simple procedure using Sr^{85} for determining cation exchange capacities of soils and clays. *Soil Science*, 1971, 112
136. Routson, R. C., Wildung, R. E., Serne, R. J.: A column cation-exchange-capacity procedure for low-exchange-capacity sands. *Soil Science*, 1973, 115, 107-112
137. Liu, C.L., Wang, K.M., Yang, C.C.: Determination of cation exchange capacity by one-step soil leaching column method. *Commun. Soil Sci. Plant Anal.*, 2001, 32, 2359-2372
138. Cornell, R. M., Aksoyoglu, E. S.: Simultaneous determination of the cation exchange capacity and the exchangeable cations on marl. *Clay Minerals*, 1991, vol 26, 567 – 570
139. Ciesielski, H., Sterckeman, T.: Determination of cation exchange capacity and exchangeable cations in soils by means of cobalt hexamine trichloride. Effects of experimental conditions. *Agronomie*, 1997, 17, 1 – 7
140. Ed.: Bardon, Ch.: Recommendations for the experimental determination of the cation exchange capacity of clay minerals. *Revue de l'Institut Francais du Petrole*, 1983, 38
141. Ciesielski, H., Sterckeman, T.: A comparison between three methods for the determination of cation exchange capacity and exchangeable cations in soils. *Agronomie*, 1997, 17, 9 – 16
142. Rhodes, C. N., Brown, D. R.: Rapid determination of the cation exchange capacity of clay using Co (II). *Clay Minerals*, 1994, 29, 799 – 801
143. Hang, P.T., Brindley, G.W.: Methylene blue absorption by clay minerals. Determination of surface areas and cation exchange capacities (clay-organic studies XVIII). *Clays and Clay Minerals*, 1970, 18, 203-212
144. Bilgiç, C.: Investigation of the factors affection organic cation adsorption on some silicate minerals. *Journal of Colloid and Interface Science* 2005, 281, 33-38
145. Gürses, A., Karaca, S., Doğar, Ç., Bayrak, R., Açıkyıldız, A., Yalçın, M.: Determination of adsorptive properties of clay/water system: methylene blue sorption. *Journal of Colloid and Interface Science*, 2004, 269, 310-314
146. Ma, Y.L., Xu, Z.R., Guo, T., You, P.: Adsorption of methylene blue on Cu(II)-exchanged montmorillonite. *Journal of Colloid and Interface Science*, 2004, 280, 283-288
147. Neumann, M.G., Gessner, F., Schmitt, C.C., Sartori, R.: Influence of the layer charge and clay particle size on the interactions between the cationic dye methylene blue and clays in an aqueous suspension. *Journal of Colloid and Interface Science*, 2002, 255, 254-259
148. Jacobs, K.Y., Schoonheydt, R.A.: Spectroscopy of methylene blue-smectite suspensions. *Journal of Colloid and Interface Science*, 1999, 220, 103-111

149. Kahr, G., Madsen, F.T.: Determination of the cation exchange capacity and the surface area of bentonite, illite and kaolinite by methylene blue adsorption. *Applied Clay Science*, 1995, 9, 327-336
150. Wang, M. K., Wang S. L., Wang, W. M.: Rapid estimation of cation-exchange capacities of soils and clays with methylene blue exchange. *Soil Sci. Soc. Am. J.*, 1996, 60, note
151. Burrafato, G., Miano, F.: Determination of the cation exchange capacity of clays by surface tension measurements. *Clay Minerals*, 1993, 28, 475 – 481
152. Pan, C., Shen, Y.H.: Estimation of cation exchange capacity of montmorillonite by cationic surfactant adsorption. *Communications in soil science and plant analysis*, 2003, 34, 497-504
153. Jaynes, W.F., Bigham, J.M.: Multiple cation capacity measurements on standard clays using a commercial mechanical extractor. *Clays and Clay Minerals*, 1986, 34, 93-98
154. Barton, C.D., Karathanasis, A.D.: Measuring cation exchange capacity and total exchangeable bases in batch and flow experiments. *Soil Technology*, 1997, 11, 153-162
155. Rytwo, G., Serban, C., Nir, S., Margulies, L.: Use of methylene blue and crystal violet for determination of exchangeable cations in montmorillonite. *Clays and Clay Minerals*, 1991, 39, no.5, 551-555
156. Stadler, M., Schindler, P.W.: Modeling of H⁺ and Cu²⁺ adsorption on calcium-montmorillonite. *Clays and Clay Minerals*, 1993, 41, 288-296
157. Cheng, K.L.: EDTA as masking agent in selective spectrophotometric determination of copper with trethenetetramine (an interpretation of masking). *Analytical chemistry*, 1962, 34, 1392-1395
158. Matter, The University of Liverpool: <http://www.matter.org.uk/tem/> (19.10.2007)
159. Center for Materials Research and Analysis University of Nebraska-Lincoln: <http://www.unl.edu/CMRAcfem/interact.htm> (19.10.2007)
160. Murad, E.: Clays and clay minerals: What can Mössbauer spectroscopy do to help understand them? *Hyperfine Interactions* 1998, 117, 39-70
161. Royal Society of Chemistry, UK: <http://www.rsc.org/Membership/Networking/InterestGroups/MossbauerSpect/intro.asp>, (20.10.2007)
162. Engineering Statistics Handbook, National Institute of Standards and Technology, USA, <http://www.itl.nist.gov/div898/handbook/eda/section3/eda35g.htm> (12.12.2007)
163. Meloun, M., Militký, J.: Chemometrie – zpracování experimentálních dat na IBM-PC. Nakladatelství technické literatury, Praha 1991, ISBN 80-03-00462-4.
164. Zichová, J.: Prezentace výsledků a zpracování experimentálních dat, kap. 4 Analýza rozptylu. <http://www.karlin.mff.cuni.cz/~zichova> (16.12.2007)
165. SISA online statistical analysis, Daan Uitenbroek PhD, Research and Statistical Consultant: <http://home.clara.net/sisa/ordhlp.htm#W-W> (16.12.2007)
166. <http://www-stat.stanford.edu/~susan/courses/b494/index/node87.html> (16.12.2007)

167. Chipera, S. J, Bish, D.: Baseline studies of the clay minerals society source clays: powder X-ray diffraction analyses. *Clays and Clay Minerals*, 2001, 49, 398-409
168. Bartoš, J., Hruška A.: North bohemian foundry bentonites. *Acta Universitatis Carolinae-Geologica*, 2000, 44, 83-89
169. Gates, W.P.: Infrared Spectroscopy and the Chemistry of Dioctahedral Smectites. *CMS Workshop Lectures, Volume 13, The Application of Vibrational Spectroscopy to Clay Minerals and Layered Double Hydroxides*, 2005, ISBN 978-1-881208-14-1

8. Acknowledgements

In this place I would like to express my thanks to all the people who supported me on my way to this page.

I would like to thank my family. You were always right.

I highly acknowledge Prof. Ing. Karel Štulík, DrSc., RNDr. Jitka Zichová, Dr., Dr. David Hradil and RNDr. Petr Bezdička, Dr. for all the help, advices and support. Prof. Štulík is acknowledged for valuable and exhausting help with the English text. RNDr. Jitka Zichová, Dr. is acknowledged for valuable consultation concerning stastic evaluation. I would like to thank Dr. David Hradil for introduction into the marvelous world of clay minerals and investigation of clayey samples. My thanks belong to RNDr. Petr Bezdička, Dr. for kind XRD measurements and consultations as well as technical support. It was pleasure to work at Institute of Inorganic Chemistry, CAS.

I would like to acknowledge RNDr. Janka Hradilová and Doc. RNDr. Pavel Coufal, Ph.D who helped me in the time of need. I appreciate your help and I will never forget it. Thank you.

I would like to thank Prof. Goran Durn, DrSc. for allowing me to take exchange at RGN faculty of University of Zagreb. I acknowledge Dipl. Ing. Marta Mileusnić DrSc. and Dipl. Ing. Neven Tadej, not only for introducing me to new methods of XRD investigation and CEC measurement but also for pleasant stay at RGN.

I acknowledge Prof. Darko Tibljaš DrSc. and Dipl. Ing. Vanja Biševac of Faculty of Science, University of Zagreb, for enabling me to measure on X'PertPRO, explanation of Rietveld method application and nice time at Faculty of Science.

This work was supported by the Grant Agency of the Academy of Sciences of the Czech Republic, project No. IAA3032401.